Sedimentology and Tephrochronology of Last-Glacial and Holocene Lake Sediments and Peat from South Westland, New Zealand

A thesis
submitted in partial fulfilment
of the requirements for the Degree
of
Master of Science in Earth Sciences
at the
University of Waikato

by

JEREMY R. COLE-BAKER

University of Waikato

2006

Abstract

A high resolution study of lake sediments and peat from three ice marginal sites in South Westland was carried out with the aim of determining the nature and timing of abrupt climate change during the last glaciation and the glacial–interglacial transition. The flux and composition of aeolian dust were used as proxies for the extent of exposed outwash surfaces and hence the extent of ice advance in the vicinity of the core sites. Cores were collected from Skiffington Swamp, Galway Tarn, and Okarito Pakihi in South Westland and the sediments characterised by measuring magnetic susceptibility (MS), combustible organic carbon (COC), grain size and mineralogy. Previously analysed pollen assemblages (Vandergoes, 2000; Vandergoes and Fitzsimons, 2003; Vandergoes *et al.*, 2005; M. J. Vandergoes, unpublished data) were correlated with the data from this study to interpret the relationship between climate and glacial extent. Cores from Skiffington Swamp and Galway Tarn contained a visible tephra layer identified as the Kawakawa Tephra (c. 26,500 cal. years B.P.) based on stratigraphic position and glass shard composition. This layer provided an excellent chronostratigraphic reference point.

The results from this study show that between 58,000 and 38,000 cal. years B.P., the climate was cool and variable in South Westland. Minor glacier advances occurred within a few kilometres of the Southern Alps. More significant glacier advance was recorded by MS and COC data at Skiffington Swamp after 38,000 cal. years B.P., which implies that glacial advance occurred earlier than the climate cooling recorded by pollen studies. Data from the most distal site (Galway Tarn, located approximately 10 km to the west of Skiffington Swamp) show that ice advanced near to that site at 32,000 cal. years B.P. This marks the start of maximum post-MIS 4 glacier extent. MS values were lowered at Skiffington Swamp during the interval from 30,000 to 22,000 cal. years B.P., indicating that the glacier margins and outwash plains were located well to the west. A decline in MS values at Galway Tarn and a peak in MS values at Skiffington Swamp occurred at 20,000 cal. years B.P., as glaciers retreated and outwash areas moved closer to the Southern Alps. There is no clear evidence at these three sites for a late glacial ice advance. Any such advance had limited impact 10–20 km from the present ice position.

Acknowledgements

I would like to thank my supervisors Drs Chris Hendy and David Lowe for their guidance and support during the course of this study, and for their enthusiasm for research which has helped to inspire many graduate students.

I would also like to acknowledge and thank Gary Comer and the Comer Foundation for generous funding of research into abrupt climate change.

I would like to say a big 'thank you' to Dr Penny Cooke for a large amount of help and advise with lab work and many discussions of data analysis and interpretation.

I am also indebted to Dr Marcus Vandergoes for his extensive work in South Westland, for allowing me access to various unpublished data, for getting me knee-deep in several bogs collecting core samples and for a great deal of advice and discussion regarding the past climate of the region.

I would like to acknowledge the support of the Department of Conservation for granting access to collect material from the study sites. Thanks are also due to Dr Roger Briggs for help with microscope work and mineral identification, Renat Radosinsky for help with slide preparation and Ritchie Sims at the University of Auckland for electron microprobe analysis. Maria Gehrels (née Ballinger) provided invaluable advice about tephra separation. I would also like to thank B. G. Andersen and colleagues for their excellent mapping work on glacial landforms in the South Island.

I would like to thank all the other staff and graduate students at the Earth Sciences department who have provided support and encouragement over the last two years.

A big thanks to my family for their interest in my work and their ongoing support and encouragement.

Contents

List of Figures

List of Tables

Chapter 1

Introduction

1.1 Why Study Climate Change?

Since classical times, it has been appreciated that the climate of the Earth varies continuously, bringing changes in storm frequency, precipitation and temperature. Although variations during historical times have been relatively minor, advances in geological and climatic science have revealed that large-magnitude changes in the climate have occurred. With the current increase in greenhouse gases entering the atmosphere from human activity, it is very important to learn more about how the climate system works in order to better predict future climate change. Investigations of past climate change, especially in Southern Hemisphere locations, can give essential insight into the mechanisms involved.

1.2 History and Significance of Climate Change Research

In the 18th century, early palaeontologists noted the occurrence of unusual fossils, with species associated with cold climates being found in deposits from areas which are today relatively warm. Geologists were intrigued by 'erratic blocks', large boulders which did not match the local geology and appeared to have been transported many kilometres (Figure 1.1). Scientists of the day generally attributed these phenomena to one or more large flood events, possibly related to the biblical flood of Noah. However, by the 19th century, geologists were recognising the role of expanded glaciers, and hence significant climate change. In the 19th century, Louis Agassiz postulated the existence of a large ice sheet covering much of Europe, during a period he termed the 'ice age'. Although most of Agassiz's contemporaries were initially sceptical, by the end of the 19th century the ice age theory was widely accepted. Ongoing detailed studies and mapping of glacial deposits showed evidence for several periods of glacial expansion, possibly occurring cyclically. However, a lack of accurate dating methods at the time meant that the chronology of

these climate changes was not known. The best geologists could do was estimate ages based on weathering characteristics, which were very vague, and results could not be easily correlated from one region to another. It was not until the discovery of paleomagnetism in 1906, and its eventual application to deep-sea cores in the 1950s and 1960s, that a chronology for climate changes in the Quaternary could be established. In the 1950s, radiometric dating techniques (^{14}C, $^{230}Th/^{234}U$, K/A, etc) also became available and were applied to convert the previously developed relative chronologies into numerical chronologies. Carbon dating in particular was extremely useful for studying the latter part of the most recent ice-age event, although older events were beyond the 55,000 year limit of the technique (Walker, 2005).

Figure 1.1: *An early sketch of an erratic block deposited by a Swiss glacier. Features such as these convinced 19th century geologists that glaciers had expanded at times in the past. From Bard (2004).*

Many mechanisms for driving climate change were examined, including changes in the orbit of the Earth, changes in gas concentrations in the atmosphere, and climate feedback mechanisms. Much pioneering work in the properties of radiation and gases of the atmosphere was carried out in the 19th century. Bard (2004) reviewed early research into the greenhouse effect and climate change. However, a lack of detailed paleoclimate data meant that little was known about the timing or frequency of climate change events, which made it difficult to prove any possible mechanism.

1.3 Long-Term and Abrupt Climate Change

During the latter half of the 20th century, detailed climate records have been recovered which demonstrate cyclic climate change over time periods ranging from millions of years to decades. The development of ocean sediment coring techniques in the 1940s and 1950s revealed multiple past glacial cycles, of which only fragmentary records remained on land. Initially, the ratios of different foram species in sediments were studied to provide an ocean temperature indicator. In the early 1950s, Cesare Emiliani developed a method of determining paleotemperature based on the isotopic composition of foram fossils in the sediment (Imbrie and Imbrie, 1979). This allowed the extension of the paleoclimate record from marine sediments, and revealed prominent cycles of glaciation occurring on time periods of c. 100,000 and 40,000 years. In the last 800,000–900,000 years, a strong 100,000 year signal has predominated, producing the succession of Pleistocene glaciations recorded in both marine and terrestrial records (Zachos *et al.*, 2001).

More sensitive records of climate change have been obtained from high-resolution sources such as ice cores, tree rings, fossil pollen and cave deposits. These records show that during the last glaciation, significant climate changes may have occurred on very short time scales. For example, ice-core records from Greenland show abrupt warm 'interstadial' periods and brief, extremely cold periods (Figure 1.2). They also reveal brief periods when the climate returned to significantly colder conditions after the warming at the end of the last glacial period. These changes have occurred on very rapid time scales, often in the order of decades or less (Taylor *et al.*, 1993).

The discovery of these abrupt climate changes raised important questions about the stability of our current climate. Adams *et al.* (1999) suggested that climate forcing and feedback mechanisms might cause an apparently stable climate to gradually build up to a 'break point', where an abrupt change would occur. Such a change would have a very serious effect on world food production, especially if large-scale climate patterns such as tropical monsoons were disrupted. Predicting future climate change is extremely important, both to prepare for any change occurring naturally and also to know what affect human activity is having on the climate. To do so, a better understanding of the mechanisms which drive climate change, and of the factors that tend to enhance climate stability, is required.

A number of mechanisms for rapid climate change have been proposed. These include changes in ocean circulation and biotic productivity, greenhouse gas concentration and snow and ice cover (Adams *et al.*, 1999). It is well established that ocean circulation changes play a key role in sudden climate changes. However, it is not clear whether the trigger mechanism for such changes lies in the high latitudes or the tropics, or whether it

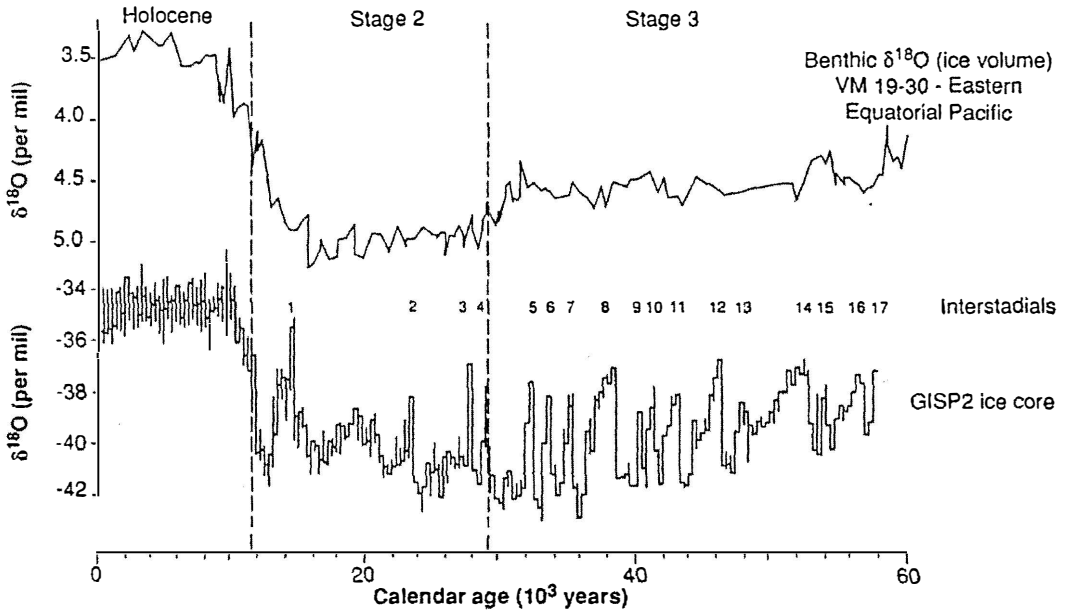

Figure 1.2: *Oxygen isotope data from the GISP2 Greenland ice core compared with a record from a marine core. The ice-core record reveals a number of abrupt climate variations. Numbered interstadial peaks represent brief warm periods. Stage numbers refer to the marine isotope stages (MIS). Modified from Bond et al. (1997).*

involves changes in the ice sheets, precipitation, or atmospheric composition (Broecker, 2000). More evidence is required to determine the role that various mechanisms have played. In particular, it is critical to know the timing of warming and cooling events, and whether such events were synchronous between the Northern and Southern hemispheres (Lowell *et al.*, 1995).

Ample evidence of climate change in New Zealand is provided by sources such as geomorphology (especially glacial landforms), palynology, palaeontology and speleothem geochemistry. A major goal of current research is to improve the chronology and resolution of climate change events in the New Zealand record, and to compare this to the Northern Hemisphere chronology.

1.4 Proxy Records of Climate Change

Evidence of climate change, and especially ice expansion, is seen directly in the moraines, erratic boulders, drop stones and other landforms found in previously glaciated areas. Various other proxy indicators have also been used as evidence of past climate change (Newnham *et al.*, 1999). The following sections describe some important climate proxy indicators and how they have been applied in New Zealand.

1.4.1 Glacial Landforms and Stratigraphy

The most obvious and visually spectacular evidence of climate change is found in the landforms that remain from periods of glaciation in the past. These include moraine ridges, 'U-shaped' valleys, glacial lakes and outwash plains. An examination of landforms is a first step in establishing a chronology of ice advances in an area. However, a stratigraphy derived from moraine deposits is often fragmentary because a large glacial advance, and associated fluvial processes, will tend to obliterate the deposits left by earlier, smaller advances.

New Zealand has a long history of geological investigation, much of which appears to have been undertaken in a detailed and competent manner despite the isolation of the New Zealand islands from major centres of scientific research in Europe. Gage (1985) summarised early work in New Zealand, beginning with the identification of glacial deposits in northwest Nelson made by Dr Ferdinand von Hochstetter and Julius Haast in 1858. Extensive studies of moraine deposits of the Southern Alps were carried out, although correlation with Northern Hemisphere work proved difficult. It was only possible for workers of the time to speculate as to whether New Zealand glaciation occurred simultaneously with that in Europe, which was a critical question when considering possible ice age causes. The advent of aerial photography and good topographical mapping after the Second World War led to great improvements in the mapping of moraine deposits, especially in areas such as South Westland where ground surveying was extremely difficult due to dense vegetation and poor weather. Geoscientists such as R. P. Suggate were able to compile regional overviews of glacial deposits, verifying earlier theories of multiple glacial advances (Gage, 1985). These studies generally involved careful mapping and description of glacial deposits, with relative ages estimated from stratigraphic succession and degree of weathering. Glacial advances were typically named from local features in each study, with tentative correlations between major catchments being made based on weathering, stratigraphy and extent of deposits.

Many good examples exist of geomorphology-based glacial studies. East of the main divide, glacial deposits of the Waimakariri valley were studied by Gage (1958), whereas detailed studies of the Rakaia valley were made by Soons (1963) and Burrows and Russell (1975). Clayton (1968) investigated glaciation of the Waiau valley. Burrows (1975) reported a detailed study of moraines in the Cameron Valley near Lake Heron, including a careful reconstruction of Holocene glacial advances. On the West Coast, Bowen (1965) noted evidence for early Pleistocene glaciations from stratigraphic studies in the Ross area. Suggate (1965) mapped the glacial geology of the upper part of the South Island, including North Westland, and produced a formal framework for the stratigraphy of glacial/interglacial sequences in Westland (Suggate, 1985) (See Chapter 2).

1.4.2 Sedimentology

Evidence of climate change and ice advance is obvious when large moraine systems are preserved. However, in areas where there was no ice cover or where erosion has removed visible glacial landforms, changes in the sedimentology of deposits often show evidence of glaciation. This may range from evidence of cyclic sea-level changes in marine deposits to glacial outwash material found in alluvial deposits.

The earliest direct evidence of glaciation in New Zealand comes from glacial outwash deposits found at Ross, North Westland. These overlie Pliocene marine deposits and represent a late Pliocene glaciation, although the specific age is unknown (Suggate, 1990). In the marine environment, the sedimentology of a core from Deep Sea Drilling Project (DSDP) Site 594 to the east of the South Island was investigated by Nelson *et al.* (1985). A 750,000 year record was recovered, and showed repeated intervals of alternating hemipelagic and pelagic ooze (Figure 1.3). The hemipelagic layers were higher in quartz and feldspar and lower in carbonates, and were interpreted to represent periods of glaciation of the Southern Alps. This core provided a record indicating 12 episodes of expended glaciation of the South Island in the past 730,000 years.

In the North Island, marine sequences now uplifted and exposed in Wanganui, Wairarapa and Hawkes Bay reveal a detailed record of sea-level changes which were primarily driven by changes in global ice volume (Suggate, 1990). Recent work by Naish *et al.* (2005) in the Wanganui basin combined outcrop, borehole and seismic survey data for shallow marine sequences of the last 2.5 million years. These sequences show changes in sedimentation representing as many as 44 cycles of sea-level change, interpreted as a global ice volume signal.

Palmer and Vucetich (1989) investigated river and marine terraces and vegetation history in the Wairarapa Valley. They found that warm climate intervals were represented by marine terraces representing high sea level and lacustrine environments in the Wairarapa Valley. Cold intervals were represented by erosion, fluvial aggradation and loess production. Investigation of river terraces and loess cover beds in the Awatere Valley (South Island) by Eden (1989) showed a similar pattern. Fluvial aggradation was associated with times of colder climate and loess accumulation. More recently, Berryman *et al.* (2000) studied a series of four river terraces in the Waipaoa River, on the east coast of the North Island. The youngest of these was overlain by the 14,700 ^{14}C years B.P. Rerewhakaaitu Tephra, and was interpreted to have stopped aggrading before c. 15,000 ^{14}C years B.P. while the oldest terrace was interpreted to be of MIS 5 or 6 age. This work was later extended by Litchfield and Berryman (2005) and Litchfield and Rieser (2005), with the application of luminescence dating to a number of east coast river terraces. These gave

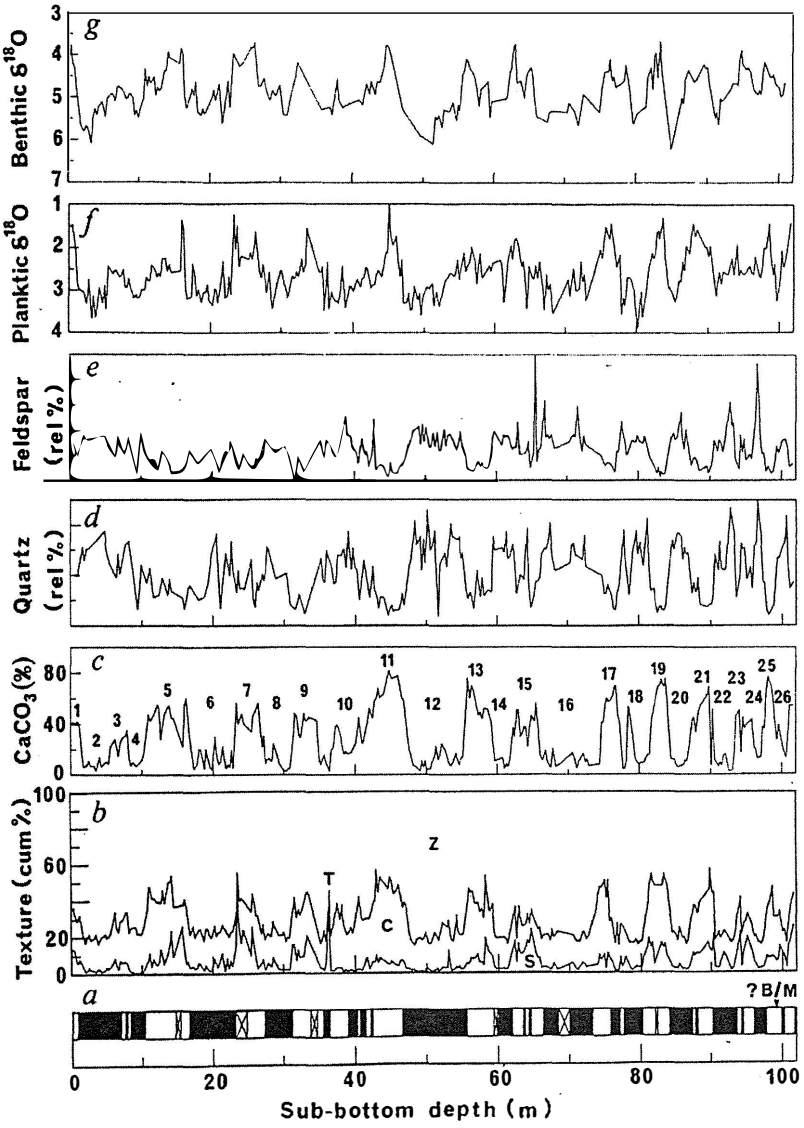

Figure 1.3: *Colour (a), texture (b), calcium carbonate (c), quartz (d), plagioclase feldspar (e) and planktonic and benthic foraminiferal oxygen isotope (f and g) records for the Late Quaternary from DSDP Site 594. The Brunhes-Matuyama boundary (730,000 years B.P.) is marked B/M. For the texture diagram, S represents sand, Z represents silt and C represents clay. Warm interglacials are represented by higher $CaCO_3$ percentage, coarser texture and lower $\delta^{18}O$ values. This record indicates there were at least 12 cycles of glaciation in the last 730,000 years, with glaciation of the Southern Alps of New Zealand (indicated by an inwash of terrigenous sediment and lower $CaCO_3$ percentages) broadly synchronous with increased global ice volume (indicated by enriched $\delta^{18}O$ values). From Nelson et al. (1985).*

ages ranging from 14,800–25,700 calendar (cal.) years B.P. for the youngest terraces, consistent with aggradation during the last glacial period. Various older terrace dates were interpreted to show terrace aggradation at c. 39,700 cal. years B.P. and c. 67,600–75,300 cal. years B.P.

1.4.3 The Marine Oxygen Isotope Record

In 1947, H. C. Urey proposed the use of changes in oxygen isotope abundance ratios to estimate past temperatures (Urey, 1947). Fractionation of isotopes of oxygen occurs when carbonates are precipitated from water, meaning that the isotope ratio of the carbonate is different from that of the source water. This process is dependent on temperature, so small variations in the isotope ratio of carbonates over time may reflect changes in temperature. The ratio is also affected by the isotope ratio of the water, which in the case of sea water is affected by the volume of continental ice. Thus isotope ratios of carbonate foraminifera from marine sediments reflect both local water temperature changes and global ice volume changes (Shackleton and Opdyke, 1973). Emiliani (1955) summarised the various fractionation reactions involved in the ocean and atmosphere system and the resulting variations in isotope ratios, as well as the development of methods for measuring them.

A number of marine cores were analysed in the 1960s, although there was considerable debate at the time as to the relative magnitude of temperature and ice-volume change. For example, Emiliani (1955) presented the results of a very detailed study of oxygen isotopes from Atlantic, Pacific and Caribbean foraminifera, in which he postulated a temperature drop of 6 °C during glacial periods. However, Shackleton (1967) re-examined this finding and stated that the majority of change in the isotope ratios was caused by the build-up of continental ice, and temperature changes in the oceans were significantly less. Emiliani based his calculation of temperature change on a 0.4 ‰ rise in the $^{18}O/^{16}O$ ratio of sea water during glacial periods. Shackleton calculated a change of 1.4–1.6 ‰, and reinterpreted the Pleistocene temperature swings identified by Emiliani as mainly recording changes in global ice volume.

By the 1970s, an isotopic variation of +1.2 ‰ was widely accepted for the oceans at the peak of the last glaciation. Isotopic changes were combined with dating by paleomagnetism for a Pacific core by Shackleton and Opdyke (1973). They presented a detailed record of isotope variations for the last 800,000 years, containing 22 stages which they interpreted as representing fluctuations in Northern Hemisphere ice volume. Chronology was provided by paleomagnetism, with intervening dates estimated from sedimentation rates. The authors showed a close relationship between sea-level changes as recorded in isotope ratios and those derived from other sources for a number of points during the past 120,000 years. This study showed the usefulness of isotope data as an indicator of past ice volume. The authors used the known sea levels to calibrate the

isotope data, allowing a sea-level curve to be produced for the past 800,000 years.

Although isotope data from foraminifera have provided a good overview of past ice volume and climate changes, problems with the technique mean that exact sea-level changes cannot be quantified. Such problems include variations in fractionation between different species of foram and uncertainties about water temperature. A discussion of these problems and methods used to overcome them can be found in Shackleton (1987).

A broad chronology of climate change has been obtained from the paleomagnetism of marine sediments used for oxygen isotope analysis. In the late 1970s, it was noted that the timing of changes in ice volume matched the periods of orbital changes earlier postulated by Milankovitch as a driver for climate change. Hays *et al.* (1976) tested the chronology of several cores from the southern Indian Ocean against the predictions of Milankovitch theory. The chronology of the cores was based on sedimentation rates and some radiometric age determinations. Analysis showed a strong correlation of the oxygen isotope data with Milankovitch cycles. Their conclusion was that the climate signal was driven by orbital changes through a non-linear relationship. This led to the development of orbital tuning, the fine adjustment of the chronology of isotope changes using Milankovitch orbital theory. Figure 1.4 shows oxygen isotope data from benthic foraminifera in the equatorial Atlantic, showing a succession of glacial cycles during the last 3 million years.

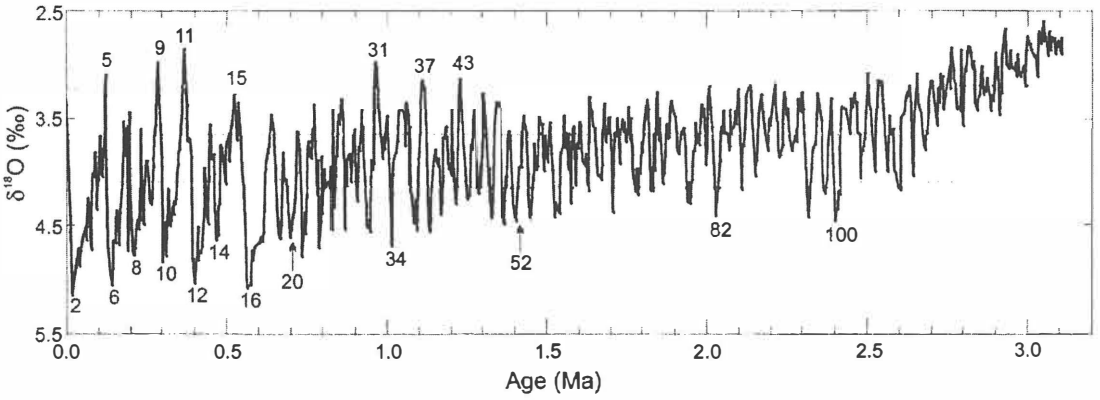

Figure 1.4: *Oxygen isotope record for the last c. 3 million years from an equatorial Atlantic core. Numbers refer to marine isotope stages (MIS). Greater enrichment in $\delta^{18}O$ is a proxy for increased global ice volume. From Bradley (1999).*

With respect to New Zealand glaciations, Nelson *et al.* (1985) examined oxygen isotopes and carbonates from DSDP site 594, recovered east of New Zealand. They showed a close correlation between ^{18}O enrichment (representing global ice volume increases and cooler water temperatures) and carbonate-poor layers (representing an increase in the inwash of terrigenous sediment from the Southern Alps during glacial periods). This relationship indicated a broad synchroniety between northern and southern glaciations. However, the resolution provided by this study was low, so variations in timing on a millennial scale were generally not visible.

1.4.4 Ice Cores

Drilling of ice cores from the Greenland and Antarctic ice sheets has been carried out since the 1970s. Early work such as that by Johnsen *et al.* (1972) focussed on oxygen isotope changes recorded in ice cores, and their relationship to temperatures. A chronology was derived by noting annual layers in the upper part of the ice core (as recorded by seasonal isotope variations), along with tie-points from known historical eruptions. Annual layer variations were not preserved beyond about 8,300 cal. years B.P., and sampling of every annual layer for isotope changes was considered impractical, so the authors used a mathematical calculation to determine a chronology based on core depth. A detailed record of temperature change spanning the last glaciation was presented, which revealed numerous high frequency temperature fluctuations. Figure 1.5 shows an oxygen isotope record from the GRIP ice core.

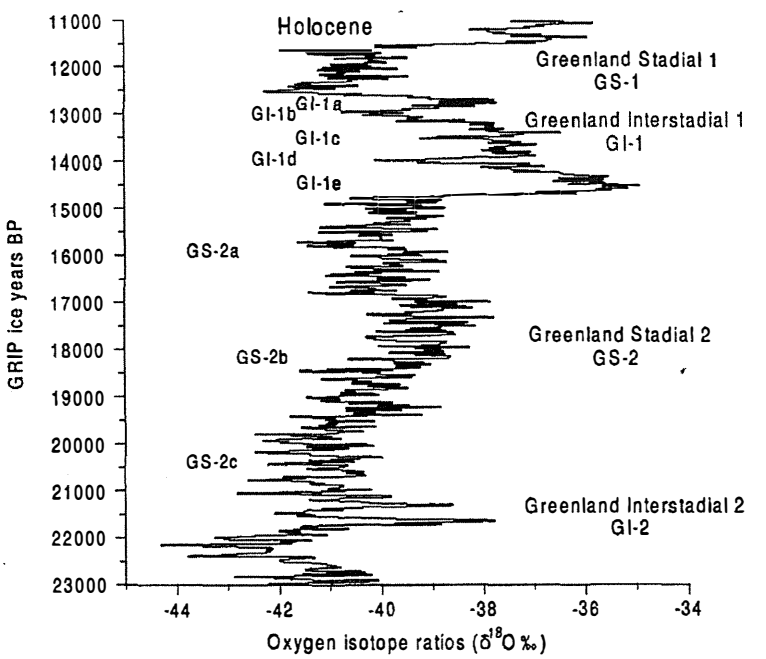

Figure 1.5: *Ice core $\delta^{18}O$ record from the GRIP ice core recovered from Greenland. This illustrates the high resolution available. More negative values represent colder temperatures. From Björck et al. (1998).*

More recently, a number of other climate proxy records from ice cores have been derived. The GRIP and GISP2 cores, drilled from the summit of the Greenland ice sheet, have provided a continuous record of climate back as far as the last interglacial. The chronology for these cores has been established by direct counting of layers (using visual, electrical conductivity and particulate measurements) (Taylor *et al.*, 1993). Such counts provide an independent chronology of events for the last glaciation. Climate proxy records extracted from these ice cores include snow accumulation rates, dust content, electrical conductivity and oxygen isotope profiles (Björck *et al.*, 1998).

Taylor *et al.* (1993) carried out a high resolution study of electrical conductivity measurement

(ECM) for the GISP2 ice core. ECM is an indicator of the continental dust flux into the Greenland ice sheet, which increased by a factor of at least 40 during the last glacial period. From rapid changes in the ECM and hence dust flux, the authors identified a number of very rapid climate changes.

Recent drilling and recovery of deep ice cores from Antarctica has provided a basis for comparison of Northern and Southern Hemisphere climate changes. The European Project for Ice Coring in Antarctica (EPICA) has recovered a core which contains a record extending back 740,000 years, spanning 8 glacial/interglacial cycles. Their analysis has included the greenhouse gases CO_2 and CH_4 as well as electrical characteristics, isotope changes and dust flux (EPICA community members, 2004). More detailed analysis of dust flux in the EPICA core, and a comparison with the shorter Vostok core, can be found in Delmonte *et al.* (2004).

1.4.5 Speleothems

Speleothems, or cave calcites, is the collective term given to the stalactites, stalagmites and other precipitated calcite deposits found in limestone cave systems. These deposits record a wealth of useful scientific information about the period during which they grew. Cave calcites are formed by the precipitation of calcium carbonate from supersaturated groundwater which enters a cave. Trace elements, isotope ratios, pollen and dust may be sealed in place in calcite on the surface of a growing deposit. Growth rates of cave calcite formations, determined by direct measurement or by various dating methods, indicate changes in the groundwater regime of the area (Gascoyne, 1992).

Gascoyne (1992) reviewed the recovery of paleoclimate information from speleothems. Early workers focussed on direct measurement of growth rates. Application of ^{14}C dating in the 1960s and uranium series dating in the 1970s confirmed and enhanced earlier work. Later workers have also examined stable isotopes of oxygen, carbon and hydrogen, the concentrations of which reflect changes in the climate. Pollen and soluble organic acids carried down from the surface have been investigated as potential indicators of surface vegetation, and airborne dust, flood debris and iron precipitated from groundwater have been used for measurement of paleomagnetism. Table 1.1 gives a summary of the various climate proxies found in speleothems.

Variations in ^{18}O and ^{13}C stable isotopes are most commonly investigated as these are thought to contain the most detailed paleoclimate information. Care must be taken in interpreting these variations, however, as a number of processed are involved. The ^{18}O isotope ratio is initially determined by the composition of the ocean from which meteoric water was originally evaporated, which is controlled by global ice volume. Other fractionation effects occur during transport so that the final isotopic composition of rainfall at the location of the speleothem is also influenced by distance from source, latitude, altitude and temperature. The temperature signal must therefore be isolated from other factors such as global ice volume.

The $\delta^{13}C$ isotope ratio in cave calcites is affected by the atmospheric $\delta^{13}C$ composition at the

Table 1.1: *Paleoclimate indicators from speleothems.*

Indicator	**Potential use in paleoclimate research**
Growth rate	Low growth indicates more arid surface conditions or less groundwater due to freezing; High growth indicates moister conditions
Internal stratigraphy (e.g. colour, growth hiatus, clastic sediment layer)	May indicate abrupt climate change event
^{18}O variations	Change in ^{18}O of source water and/or temperature of deposition
^{13}C variations	Change in ^{13}C of source water and/or calcite deposition process
^{2}H variations in fluid inclusions	Change in H of source water due to change in climate
Pollen content	Indicates surface vegetation type
Organic content	May indicate surface vegetation type
Trace metal content variation	Indicates change in water composition and/or temperature of deposition

time of formation, plus the effects of various fractionation processes in vegetation and soil. Inorganic carbon from the karst bedrock at the site and degassing of CO_2 during deposition also alter the final $\delta^{13}C$ isotope ratio (Williams *et al.*, 2004).

Speleothems have been studied by various workers in New Zealand. Hendy and Wilson (1968) studied oxygen isotopes from a speleothem recovered from Waitomo Cave in the North Island, and showed a correlation with temperature changes recorded in the tropical Atlantic. Hellstrom *et al.* (1998) investigated ^{18}O and ^{13}C stable isotopes of speleothems from northwest Nelson. Uranium series dating provided age control, and they were able to extract a continuous and detailed record since c. 31,000 years ago, spanning the latter part of the last glaciation. They describe the various factors influencing stable isotope ratios.

Williams *et al.* (2004) investigated stable isotope variations in Holocene age speleothems from Waitomo in the North Island. They included a discussion of the various factors influencing the isotope ratios of deposited calcite and how they can be used for paleoclimate interpretation. Williams *et al.* (2005) investigated speleothems from several areas of northwest Nelson and Westland, providing a composite record of climate change from 23,400 calendar years ago to the present.

1.4.6 Palynology

Palynology, the study of pollen grains and plant spores, was first developed in the early 1900s. Wind-pollinated plants produce large quantities of pollen, and the resistant outer layer of many pollen grains may be preserved for thousands or even millions of years where they fall into lakes and bogs, or similar favourable environments. Thus an analysis of the fossil pollen found at a site can reveal changes in the local and regional vegetation over time. The study of fossil pollen was pioneered by Lennart von Post, who was very interested in bog stratigraphy and the climate history which could be derived from it (Erdtman, 1969).

In New Zealand, pollen studies have been used to reconstruct past climates in a variety of settings. Sandiford *et al.* (2003) investigated cores from Pukaki Crater in South Auckland (northern New Zealand) and found a mix of grassland and beech forest was predominant in the area during the last glaciation. Newnham and Lowe (2000) investigated Kaipo bog, a peat bog in eastern North Island. The site was located at 980 m altitude, and vegetation changes were interpreted to provide a record of temperature changes. Age control for the pollen analysis was provided by radiocarbon dating and tephrochronology from independently dated tephra layers. The site yielded a record of climate change spanning the late glacial period from 17,600 cal. years B.P.

Extensive pollen analysis has been carried out in South Westland by M. J. Vandergoes and others (Vandergoes, 2000; Vandergoes and Fitzsimons, 2003; Vandergoes *et al.*, 2005). They recovered cores from peat bogs located on moraine deposits near to the maximum extent of ice advance during the Last Glacial Maximum (LGM). Several sites contained continuous records spanning the last glaciation, with one site (Okarito Pakihi) containing a record of the last c. 130,000 years, including the last interglacial period and the end of the penultimate glaciation in MIS 6. These sites all showed a common pattern of expanded grasslands during the LGM between c. 25,000–18,000 cal. years B.P., with grasslands replaced by tall forest as the climate warmed at the end of the glacial period.

1.4.7 Loess Sequences

Loess is a deposit (generally of fine silt) formed by the deposition of airborne particles, typically between 10 μm and 60 μm in size. Many early geoscientists defined loess as a calcareous silt, being a mixture of quartz, carbonates, some clay minerals, and traces of heavier minerals such as hornblende and garnet. However, the mineralogy is dependent on the source from which airborne dust was derived. In areas where carbonate source rocks are rare, or where carbonates are leached by high rainfall, carbonate is absent. Volcanic glass shards may also be present in volcanic regions, either entering the deposit directly from tephra fallout, or through aeolian reworking of existing tephra deposits (Pye, 1987).

Studies of dust entrainment and transport have often focussed on arid or semi-arid environments,

as these were considered to be the main source of aeolian dust. However, a study by Marx and McGowan (2005) showed that dust deposition rates in the modern, super-humid environment of the West Coast were relatively high, comparable with those found in many studies of semi-arid environments. The authors concluded that the main control on dust deposition was abundance of source material, which in the West Coast environment was supplied by braided rivers flowing from the Southern Alps. However, loess production was not strongly active because of the high rates of biological activity and soil formation in the humid environment of the West Coast.

Extensive loess deposits are found in mid-latitude regions (both globally and in New Zealand) associated with glacial periods. Several factors favoured loess production at these times. Glacial outwash surfaces and braided rivers provided a supply of loose, poorly sorted sediments with high proportions of silt, while a higher frequency of strong, turbulent winds enhanced dust transport. In warm interglacial or interstadial periods, aeolian dust transport tends to be significantly reduced as ice sheets retreat and vegetation covers outwash areas. Soil pedogenesis may occur in warmer conditions, producing a sequence of loess and paleosol layers representing changes in the climate (Pye, 1987).

Loess deposits of last glacial age have been widely documented in New Zealand, especially in the southern part of the North Island and the South Island (Newnham *et al.*, 1999). For example, Palmer and Vucetich (1989) described the relationship between loess, river terraces and marine terraces in the Wairarapa Valley. Similarly, loess units were associated with river terrace aggradation during glacial times in rivers of the east coast, North Island, by Berryman *et al.* (2000), Litchfield and Berryman (2005), and Litchfield and Reiser (2005). In the South Island, loess was described on river terraces in the Awatere valley by Eden (1989). More recently, Berger *et al.* (2002) applied luminescence dating to thick loess deposits from the south of the South Island. Although the results of this dating were variable, they did indicate that the most recent episode of loess accumulation at the sites they studied began at between c. 31,000 and 64,000 cal. years B.P., overlying older loess deposits. The oldest site studied contained a sequence of loess and paleosols covering the last c. 350,000 years.

On the West Coast of the South Island, the first mapping of loess deposits was carried out by Young (1967), who reported widespread loess from Lake Mapourika northwards, and especially in North Westland. Loess was found to be thickest on the oldest surfaces. A more detailed study of loess deposits from The Lamplough, south of Greymouth, was carried out by Mew *et al.* (1988). They also noted considerably thicker accumulation of loess on the older of the terraces they studied, and documented the presence of brown layers which might be paleosols. However, they lacked any good dating for the sites.

More recently, Almond (1996) examined loess deposits in Salt Water forest, South Westland. A number of moraines and associated outwash terraces were studied, and paleosol horizons in the loess deposits were used to subdivide the loess into cool and warm periods. The oldest moraines, designated M1, were found to be covered in up to 3 m of loess containing four buried soil horizons. Almond interpreted this moraine to be of at least the penultimate (Waimea)

glaciation age, if not older. Five younger moraines were mapped inside this moraine, based on the thickness of loess/paleosol sequences and the occurrence of the Kawakawa Tephra. The stratigraphy and chronology of loess/paleosol sequences was later revised by Almond *et al.* (2001), based on mineral content and phytolith data. In the revised stratigraphy, five loess units (L1a, L1b, L2, L3 and L4) and six moraines (M2, M3, M4a, M4b, M5 and M6) were correlated to the last glaciation, indicating a more complex glacial history than previously identified.

1.5 Chronology of Past Climate Change

Our knowledge of past climate change is based on a variety of climate proxy records. Older proxy records generally have lower resolution, but broad patterns in climate can be discerned. A brief summary of climate modes through the history of the Earth is given below; more attention is given to late Pleistocene and early Holocene climate change since this is the period for which we have the most detailed climate records, and which is most relevant to this study.

1.5.1 Precambrian and Phanerozoic Climate Change

Most of Precambrian time (prior to 600 million years B.P.) is considered to have been warm and ice free. However, evidence of a cool period is seen in the oldest known glacial till deposits, found in North America and dated at about 2300 million years B.P. Widespread evidence of glacial episodes is also found between about 860 and 600 million years B.P.

Figure 1.6 shows a summary of long term climate change for the Phanerozoic eon. During this period (from 600 million years B.P. onwards) four major cool intervals (including the current 'ice age') have been identified in the geological record, during which ice sheets developed at high latitudes. Cool periods were separated by warm intervals where no evidence of ice sheets has been found. Within both warm and cool periods there is evidence of smaller-scale fluctuations, the sequence of glacial and interglacial cycles within the current Pleistocene cool period being the most recent example (Frakes *et al.*, 1992).

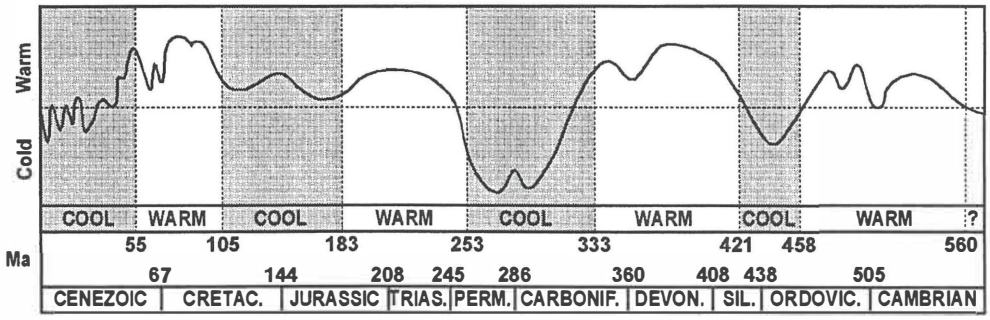

Figure 1.6: *Summary of Phanerozoic climate change. From Frakes et al. (1992).*

The current cool climate mode developed after a significant period of warming in the late

Paleocene and early Eocene, from 59–50 million years B.P. The warming trend peaked during the early Eocene climatic optimum (EECO) at c. 50 million years B.P. The EECO was followed by a long decline in temperatures, culminating in the build-up of ice on Antarctica starting late in the Eocene at c. 34 million years B.P. Antarctic ice was reduced in extent during a warmer phase between c. 26–15 million years B.P., but was probably never ice-free. From c. 15 million years B.P., a significant cooling was once again seen, producing a major expansion of the Antarctic ice sheet (Zachos *et al.*, 2001).

The Northern Hemisphere ice sheets began to grow from about 2.4 million years B.P. Since that time, major glacial-interglacial cycles have intensified, especially in the Northern Hemisphere ice sheets. The early part of this period (prior to about 900,000 years B.P.) was dominated by oscillations with a 40,000 year period; since about 400,000 years B.P., larger magnitude oscillations have been seen with a dominant period of 100,000 years (Frakes *et al.*, 1992).

1.5.2 Late Pleistocene and Holocene Climate Change

The framework for the timing of the last glacial cycle is provided by the marine oxygen isotope (MOI) record (Figure 1.7), which is interpreted to respond to global ice volume changes. The record is divided into marine isotope stages (MIS). MIS 5e represents the last interglacial, when global climate was similar to that of today. The generally accepted age of the start of this warm period is c. 128,000 years B.P., based on the transition seen in the MOI record. The end of stage 5e occurs at c. 116,000 years B.P. in the MOI record; however, the onset of glaciation in the Northern Hemisphere is less distinct (Tzedakis, 2003). Kukla *et al.* (2002) proposed an unstable, deteriorating climate from c. 115,000 years B.P., with evidence of major European glaciation beginning at c. 107,000 years B.P. Tzedakis (2003) identified the influx of ice rafted debris in marine cores at c. 110,000 years B.P. as marking the onset of widespread glaciation.

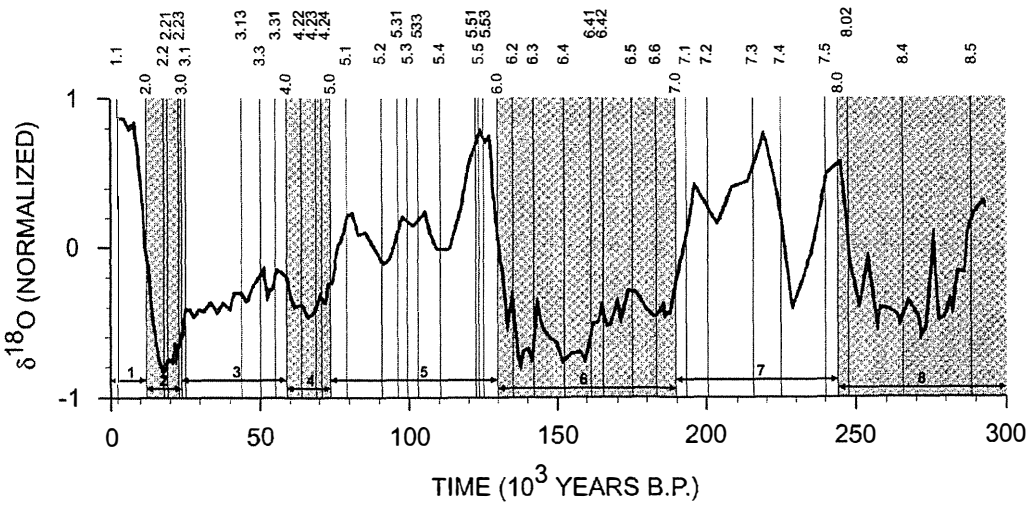

Figure 1.7: *MOI record for the last 150,000 years. Numbers refer to marine isotop stages (MIS). From Bradley (1999).*

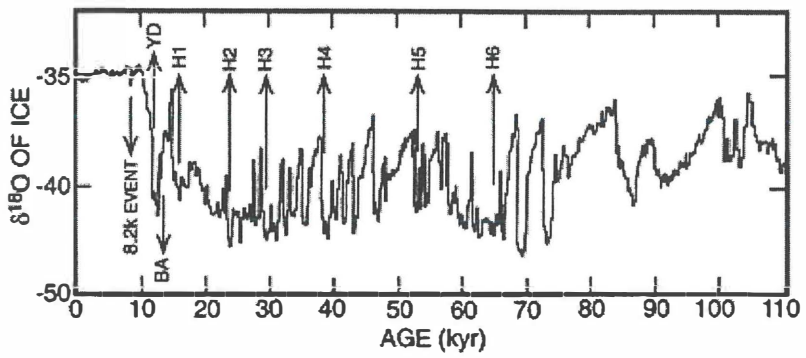

Figure 1.8: *DO and Heinrich events in the oxygen isotope record from the GRIP ice core. Heinrich events are labelled – these are identified by influxes of ice rafted debris into the North Atlantic. Dansgaard-Oeschger events begin with a rapid warming, followed by a more gradual cooling and then a sudden cooling. From Broecker (2000).*

Studies from North America indicate that the northern margins of the Laurentide ice sheet began growing in MIS 5, possibly as early as c. 110,000 years B.P. (MIS 5d). Ice sheet growth was active to the south during the latter parts of MIS 5 and throughout MIS 4. The northern margins were in decline at this time, possibly due to altered precipitation patterns, but the southern margins are known to have expanded at c. 50,000 cal. years B.P. (MIS 3) and reached a maximum extent during the LGM between c. 21,000 cal. years B.P. and 18,000 cal. years B.P. (MIS 2) (Clark *et al.*, 1993).

The temperature record of the last glaciation (as recorded in ice cores from Greenland) was punctuated by repeated brief cycles of warming and cooling. It is likely that similar events occurred during previous glaciations, although paucity of dating and lower resolution of climate proxies available for older records makes them difficult to detect. There were 24 relatively warm interstadial events during the last glaciation (c. 110,000–14,000 years B.P.), each of which typically began with an abrupt warming occurring over a few decades or less and ended with a more gradual and stepwise cooling back to full glacial conditions (Figure 1.8). Known as Dansgaard-Oeschger cycles, these typically lasted c. 1,500 years.

Dansgaard-Oeschger (DO) cycles can be seen in marine sediments from the North Atlantic, although they have proved difficult to detect. The marine sediments also record six pulses of ice rafted debris during the last glacial, interpreted as representing major surges of icebergs into the North Atlantic from the Laurentide ice sheet. Known as Heinrich events, these pulses of ice rafted debris have been correlated with the coldest phase of some (but not all) Dansgaard-Oeschger cycles. They appear to have occurred very abruptly and had a duration of no more than several centuries (Broecker, 2002).

The last glacial period ended with widespread climate warming between c. 15,000 and 12,000 cal. years B.P., and by 9,000 cal. years B.P. the North American ice sheets had disappeared, and sea levels and sea surface temperatures were similar to the present (Frakes *et al.*, 1992).

This warming did not proceed as a smooth trend, however, but rather as a series of rapid warming events interrupted by brief returns to colder climate (Figure 1.9). The Bølling/Allerød interstadial warm period (14,600–12,600 cal. years B.P.) was followed by the Younger Dryas cooling (12,600–11,600 cal. years B.P.), with a return to near glacial conditions (Brauer *et al.*, 1999). Younger Dryas cooling and subsequent warming happened very rapidly, occurring over a space of decades or less. Following the Younger Dryas cooling, temperatures continued to warm rapidly, and conditions similar to the present day were reached by 9,000 cal. years B.P. (Zubakov and Borzenkova, 1990; Walker, 1995).

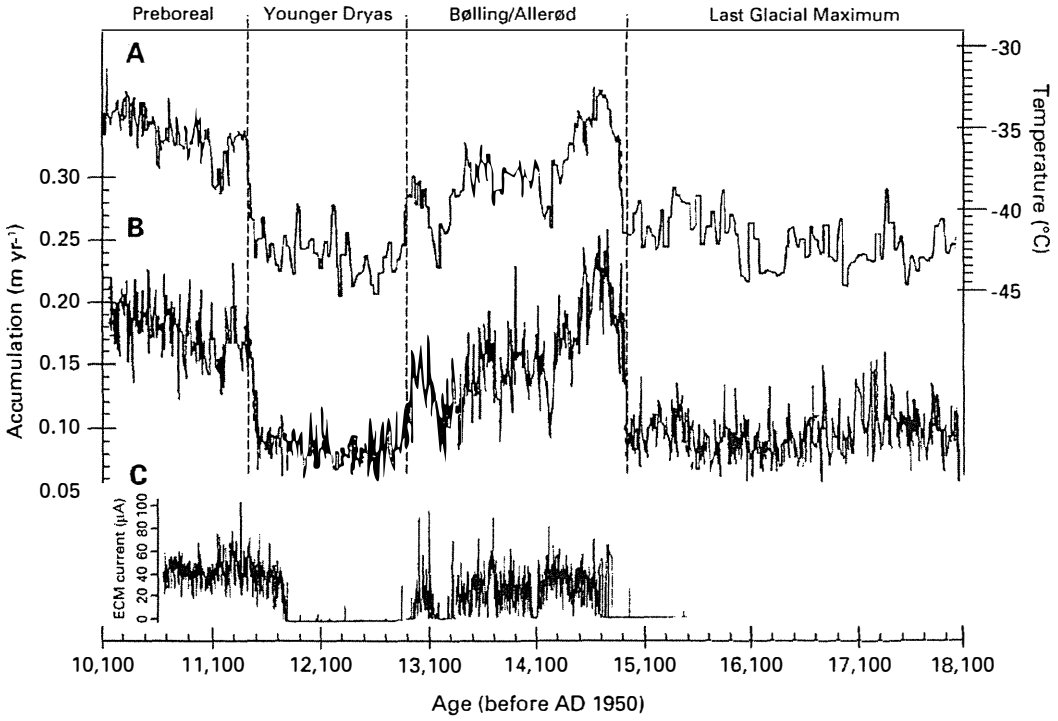

Figure 1.9: *Late glacial climate events from the GISP2 Greenland ice core. Three climate proxies are shown: paleotemperature record based on $\delta^{18}O$ values (A), snow accumulation rate (B) and electrical conductivity (C) which reflects variations in dust content. From Lowe and Walker (1997).*

Ice-core data from Greenland indicate that the Younger Dryas chron was colder, drier and dustier than the earlier warm period. This finding is confirmed by results from other areas such as the Cariaco Basin, Venezuela, where cores showed that windier conditions produced enhanced upwelling and biological productivity during the Younger Dryas (Alley, 2000). The most precise chronologies for late-glacial climate change events are derived from ice-core data and from annually laminated lake sediments. These records generally show good agreement, with small variations being attributed either to lag in response of the climate at different sites, or to small offsets in the time scales (Brauer *et al.*, 1999).

1.6 Causal Mechanisms of Climate Change

The climate system is made up of a number of interacting components, including the ocean, atmosphere, ice sheets, the biosphere and tectonics. These components respond in different ways, have different response times and may be linked in complex ways. External forcing mechanisms are thought to provide the ultimate driver for changes to the climate system, but internal feedback mechanisms and resonances make the resulting change difficult to predict. External forcing mechanisms include changes in the orbit of the Earth and changes in the intensity of solar output. The addition of greenhouse gases to the atmosphere by human activity could also be regarded as an external forcing mechanism, although it will be discussed in the context of naturally occurring greenhouse gas changes, which are better treated as an internal part of the climate system. External forcing mechanisms tend to be small in their relative effect, and significant internal feedback must occur to explain the magnitude and speed of abrupt climate changes seen in climate proxy records (Bard, 2002).

1.6.1 External Climate Forcing Mechanisms

Tectonics and Volcanism

Long term changes in the climate of the Earth are thought to be driven primarily by tectonic activity. Various models have been suggested which include oscillations between a single 'super-continent' and many dispersed continents, occurring on a time scale of 60–500 million years. The super-continent phase of these models is generally associated with a cool 'ice-house' world, where continental relief is higher and more vigorous ocean circulation is possible, mixing more CO_2 into the deep ocean. The development of ice-sheets is thus favoured. Conversely, when continents are fragmented, ocean circulation is reduced and oceans trend to be warmer and more stratified. Higher CO_2 levels in the atmosphere lead to a warmer climate and a 'greenhouse' world. The increased release of CO_2 by the volcanic processes which drive continental fragmentation may also contribute to the warming of the greenhouse world. The current ice-house climate phase, where continental ice sheets occur, resulted from the slowing of sea-floor spreading and reduction of CO_2 release by volcanic processes as the latter phases of continental fragmentation were reached (Veevers, 1990).

Orbital Changes: Milankovitch Climate Forcing

Changes in the Earth's orbit around the Sun affect the distribution and seasonal intensity of incoming solar energy. Changes in the elliptical nature of the Earth's orbit (eccentricity), the amount of tilt of the Earth's axis (obliquity), and the timing of the equinoxes (precession) produce cycles with periods of 100,000 years, 40,000 years and 21,000 years, respectively (Figure 1.10). These cycles change distribution of heat between the hemispheres and between the seasons (Salinger, 2001).

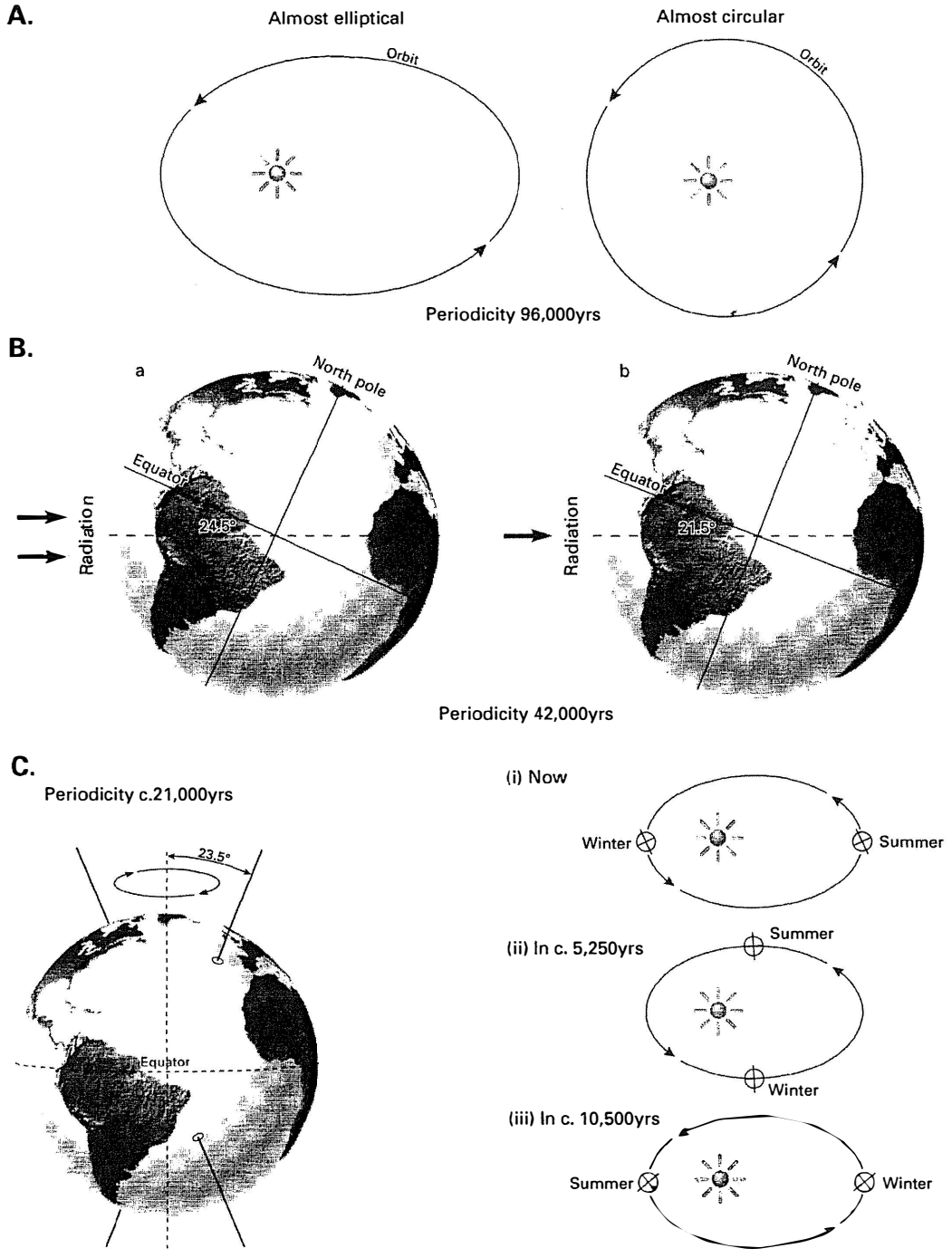

Figure 1.10: *The three orbital variations that drive climate change: Eccentricity (A), Obliquity (B) and Precession (C). From Lowe and Walker (1997).*

As early as the 17th century, some authors had considered the effects of orbital changes on the seasons and hence on changes in the climate. The first detailed discussion of the matter is attributed to James Croll in the 19th century, who theorised that a combination of an elongated orbit and the occurrence of winter solstice near to aphelion (the point at which the Earth is the greatest distance from the sun) would cause an ice age to occur. Orbital variations were studied in greater detail by the mathematician Milutin Milankovitch in the early 20th century, who showed that the effects of eccentricity and precession ought to cause ice sheet expansion and contraction, and that the effect of obliquity changes was much larger than Croll had suggested. Milankovitch suggested that the key factor in ice sheet build up was summer insolation values, since snowfall would be present in winter at high latitudes regardless of winter insolation. The important control on ice-sheet development was therefore the amount of snow melt during summer months (Imbrie and Imbrie, 1979).

Although popular at the time, Croll-Milankovitch climate forcing theories were largely rejected or ignored during the 1950s and 1960s. However, improving resolution of Quaternary climate records from such sources as loess, sea-level records and oxygen-isotope ratios from marine cores in the late 1960s and 1970s brought about a rediscovery of Milankovitch orbital forcing. A common 100,000 year signal of climate change was independently discovered in both terrestrial and marine records, showing that the eccentricity cycle has a strong effect on climate, with ice ages occurring at times of greatest seasonal contrast, as proposed by Croll 100 years earlier. Later and more detailed work, including the use of oxygen isotope analysis on marine cores by Hays *et al.* (1976) noted earlier, has revealed climate change at all frequencies predicted by Milankovitch theory (Huggett, 1991).

Solar Output Changes

Another possible external forcing mechanism is change in the intensity of radiation given off by the Sun itself. Studies of solar activity have shown that the output of the sun varies in a cyclic manner, and investigation of various climate proxies (especially for the Holocene period) has revealed climate changes on timeframes which appear to match variations in solar radiation. The actual variation in solar intensity is small (generally less than 1%) and so would only account for a very small climate change directly. Various mechanisms have been suggested by which solar output changes could indirectly affect the climate. It has been shown that reduced solar output and hence less solar wind would cause an increase in the flux of galactic cosmic rays reaching the atmosphere. This in turn has been shown to lead to increased cloud nucleation, cloud cover and a cooling of the climate (Chambers *et al.*, 1999). In order to test theories of solar forcing of the climate, Turney *et al.* (2005) studied changes in bog tree populations in Ireland during the last 7,468 years. They produced an annually resolved record of tree populations and population age structures which they interpreted to be controlled by changes in precipitation. However, they found no direct link between the timing of these changes and the timing of solar output variations, and concluded that the climate changes they observed were not a linear response to

changes in solar activity. If solar forcing had played a role, it was via an unknown non-linear feedback mechanism.

1.6.2 Feedback Mechanisms

Orbital forcing, on its own, should be expected to produce gradual changes in the climate over long timeframes, and of a fairly low magnitude. Solar output changes, if they do affect the climate, should also have only a small effect. However, paleoclimate records indicate that relatively abrupt, step-wise changes from one state to another are more common. Such changes can be explained by the operation of internal feedback mechanisms that act to enhance small changes in climate or to maintain the climate in one state or another.

Surface Changes: Albedo and Vegetation

The reflectivity (albedo) of the surface of the Earth plays an important role in providing positive feedback in the climate system. Ice and snow cover reflect a large percentage of the solar radiation that reaches the surface, preventing the absorption of heat and thus producing a net cooling of the climate. This acts as a positive feedback to the growth of ice sheets (Bradley, 1999).

The biosphere, and in particular vegetation cover, can exert a variety of feedbacks to the climate system. Different types of vegetation have different albedo values, with grasslands typically absorbing less solar radiation than forests. The biosphere also affects greenhouse gas levels by absorbing or releasing CO_2 and CH_4. Some of these feedback mechanisms may be negative – for example, expanded grasslands, tundra and deserts during glacial times would have led to lower storage of CO_2. However, increased albedo of these areas and reduced production of methane would have provided a positive feedback effect. Loss of vegetation cover also caused a large increase in aeolian dust entrainment during glacial times, which increased the albedo of the atmosphere and also enhanced the absorption of CO_2 by the ocean (see below) (Bradley, 1999).

Greenhouse Gases

Greenhouse gases act to trap heat in the atmosphere by absorbing long-wave radiation released by the surface. Hence, increasing concentration of these gases is associated with warming climate. However, the concentrations of the main greenhouse gases (water vapour, CO_2 and CH_4) also vary in response to changes in the ice sheets and the climate, thereby acting as feedback mechanisms internal to the climate system.

Colder climates and expanded ice sheets are thought to lower CO_2 concentrations in several ways. Greater dust flux into the oceans enhances fertility and ocean biological activity, which absorbs CO_2 and fixes it in the oceans. Cooler water temperatures increase CO_2 solubility and thus more CO_2 is dissolved from the atmosphere, whereas changes in ocean circulation

may change the chemistry of the Southern Ocean, also resulting in absorption of CO_2. CH_4 is also reduced during glaciations because the biological productivity of high latitude continental environments is reduced by cold temperatures and ice cover. Water vapour in the atmosphere is reduced because of cooler sea-surface temperatures and less evaporation (Ruddiman, 2003).

Changes in the quantities of greenhouse gases, especially CO_2 and CH_4, are recorded in gas bubbles recovered from ice cores in Greenland and Antarctica. Such changes are closely linked to changes in ice volume, with periods of glaciation and ice sheet expansion associated with lower levels of these gases. For example, Figure 1.11 shows CO_2 concentration vs. estimated atmospheric temperature for the last glacial cycle (Salinger, 2001). The close relationship between the timing of CO_2 concentration changes and ice volume changes has led to considerable speculation as to the role of CO_2 in climate feedback. In the SPECMAP-group model of glaciation, orbital forcing produced initial changes in the Arctic regions. These changes were propagated to the Southern Hemisphere by the ocean circulation system, and changes in the Southern Ocean then lowered atmospheric CO_2 levels. This in turn provided positive feedback for further cooling and build up of Northern Hemisphere ice (Imbrie *et al.*, 1992, 1993). An improved time scale for changes in greenhouse gas concentrations led Ruddiman (2003) to propose a different model, in which the changes in CO_2 and CH_4 were directly triggered by orbitally forced changes in Northern Hemisphere ice sheets, and provided positive feedback for ice-sheet growth.

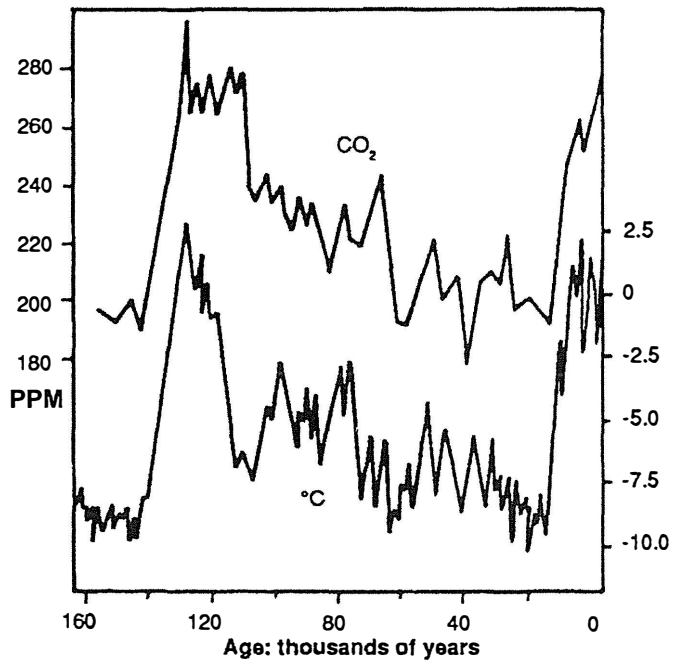

Figure 1.11: *Atmospheric temperature and CO_2 concentration for the last glacial cycle, derived from Vostok ice core data. From Manning (1990).*

The link between greenhouse gas concentrations and global temperature is of great interest given the increase in these gases, especially CO_2, associated with industrialisation and the use of fossil fuels. Climate modelling by Ruddiman (2003) predicted that CO_2 and CH_4 concentrations ought to have peaked in the early Holocene and then declined, whereas both have increased since the

mid-Holocene. Ruddiman considered this trend to be the result of the clearing of forests and the development of agriculture, and theorised that this anthropogenic rise in greenhouse gases may in fact have prevented the renewed growth of ice sheets that his model predicted.

Ocean Circulation

Circulation of water within the oceans exerts a strong influence on climate by redistributing heat from the tropics to the poles. This ocean circulation system is often referred to as the thermohaline conveyor, as it is largely driven by changes in salinity and temperature of sea water. Figure 1.12 shows a simplified map of ocean circulation. Of particular importance is the North Atlantic circulation, which serves to warm the climate of large parts of northern Europe (Lowe and Walker, 1997).

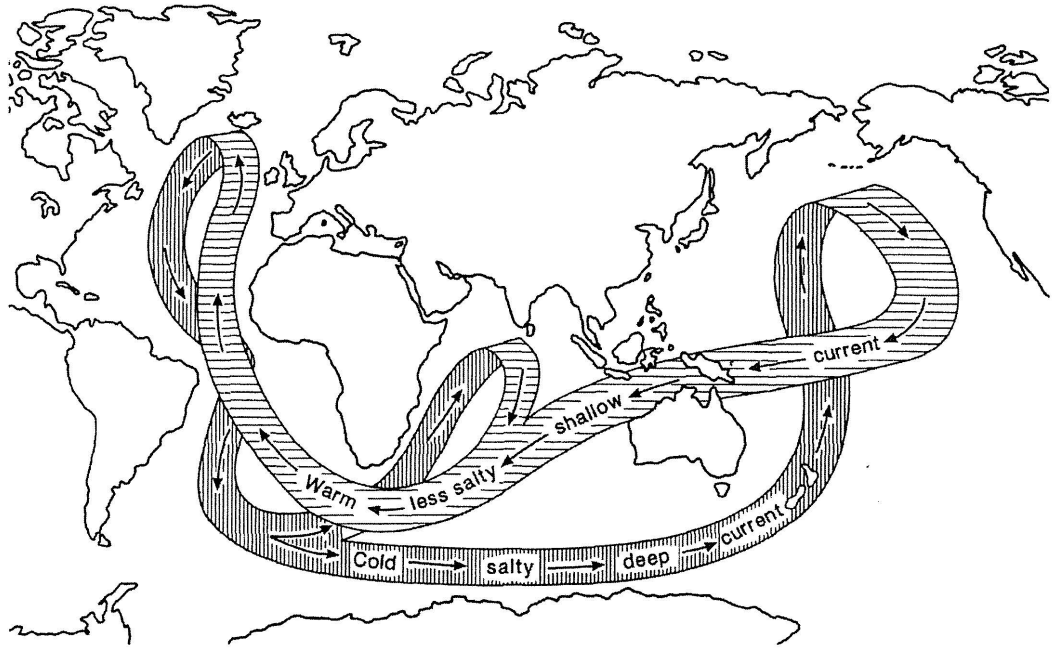

Figure 1.12: *Schematic illustration of the 'thermohaline conveyor'. From Frakes et al. (1992), after Broecker and Denton (1990).*

Thermohaline circulation is driven by the sinking of dense waters in the polar regions. In the North Atlantic, deep water is formed as northward-moving saline surface water becomes more dense due to evaporation, cooling and water removal to sea ice. The increasing density of this water means it eventually sinks (at around latitude 60 °N) to form North Atlantic Deep Water (NADW). NADW travels south along the ocean floor, gradually warming and mixing until it rises again and the cycle repeats (Broecker *et al.*, 1985). The formation of NADW is highly sensitive to the input of fresh water in the North Atlantic. Strong evidence exists that abrupt cooling events during the last glacial period (Heinrich events and the Younger Dryas stadial) were caused by an influx of fresh water which reduced the density of surface waters in the North Atlantic and caused the thermohaline conveyor to shift southwards. This let to an abrupt cooling

of Northern Europe. Resumption of NADW production can also happen quickly, bringing about an abrupt warming of the Northern Hemisphere such as seen at the end of the Younger Dryas (Adams *et al.*, 1999).

Several sources have been suggested for influxes of fresh water into the North Atlantic. Sudden, brief cooling events during Northern Hemisphere de-glaciation, such as the Younger Dryas, may have been caused by the rapid release of melt water from glacial lakes. Such releases are associated with the melting of large ice sheets such as the Laurentide. Another source of fresh water is the sudden release of large flotillas of icebergs due to the gravitational collapse of ice sheets. Denton (2000) suggested the periodic gravitational collapse of unstable marine-based ice sheets grounded on continental shelves as the driving mechanism of millennial-scale Dansgaard-Oeschger and Heinrich cooling events. Denton (2000) also suggested that the 100,000 year glacial cycles of the late Pleistocene are initiated by the collapse of Antarctic marine-based ice sheets, due to interglacial climate warming and rising sea level. The break up of these ice sheets would provide a greater source for deep water production in the marginal seas surrounding Antarctica, which would tend to displace NADW and slow North Atlantic circulation, thereby triggering the development of Northern Hemisphere ice sheets.

1.7 Inter-Hemispheric Synchroneity of Climate Change

At broad time resolutions (greater than a few thousand years), it has been well established that cool climates and ice expansion in the Southern Hemisphere were synchronous with glaciation of the Northern Hemisphere (Nelson *et al.*, 1985). Northern Hemisphere summer insolation is generally considered to be the important trigger for ice sheet growth, because lowered summer insolation reduces the amount of winter snowfall which is melted (Imbrie *et al.*, 1992; Ruddiman, 2003). Kukla and Gavin (2004) placed more emphasis on the role of the tropical oceans and enhanced evaporation and precipitation on ice sheet growth. In either case, most regional records that cover long time scales do not have sufficient temporal resolution to discriminate any lag in response between hemispheres. For example, Nelson *et al.* (1985) showed that terrigenous sediment input to the marine environment from the Southern Alps was high during periods of high global ice volume, and they concluded near-synchronous glaciation of the hemispheres. However, their time resolution was only 3,000 years, meaning that small variations in phase would not have been evident.

Within the broad structure of glacial/interglacial cycles, much more abrupt climate change events have occurred on millennial time scales (Bard, 2002). These changes were too rapid to be driven directly by external forcing such as orbital changes, and were more likely to be responses to instabilities that resulted from various feedback mechanisms within the climate system. There are two main candidates for drivers of these abrupt climate shifts: changes in ocean circulation, and changes in greenhouse gas concentration. In order to better understand the mechanisms involved, a major focus of current research is to compare the timing of millennial scale events

between the hemispheres (Vandergoes, 2000; Vandergoes *et al.*, 2005).

Wunsch (2003) applied frequency domain analysis to ice-core data from Greenland and Antarctica (Figure 1.13). The methane concentrations from each location were used to precisely correlate the records since the atmospheric mixing time of methane is very short (1 year or less). Wunsch (2003) showed that at time periods longer than about 10,000 years the records were coherent, with Antarctica leading the Northern Hemisphere records by 1,000–2,000 years. However, no general correlation was found between records at millennial time scales, and Wunsch concluded that regional processes could govern the timing of millennial scale events. In contrast, Schmittner *et al.* (2003) found that millennial scale events occurred and exhibited an anti-phase relationship between the hemispheres, with temperature changes in Greenland leading changes of the opposite sign in Antarctica by 400–500 years. Wunsch (2006) also suggested that DO cycles seen the Greenland temperature record could have been caused by changes in wind regime rather than shifts in ocean circulation.

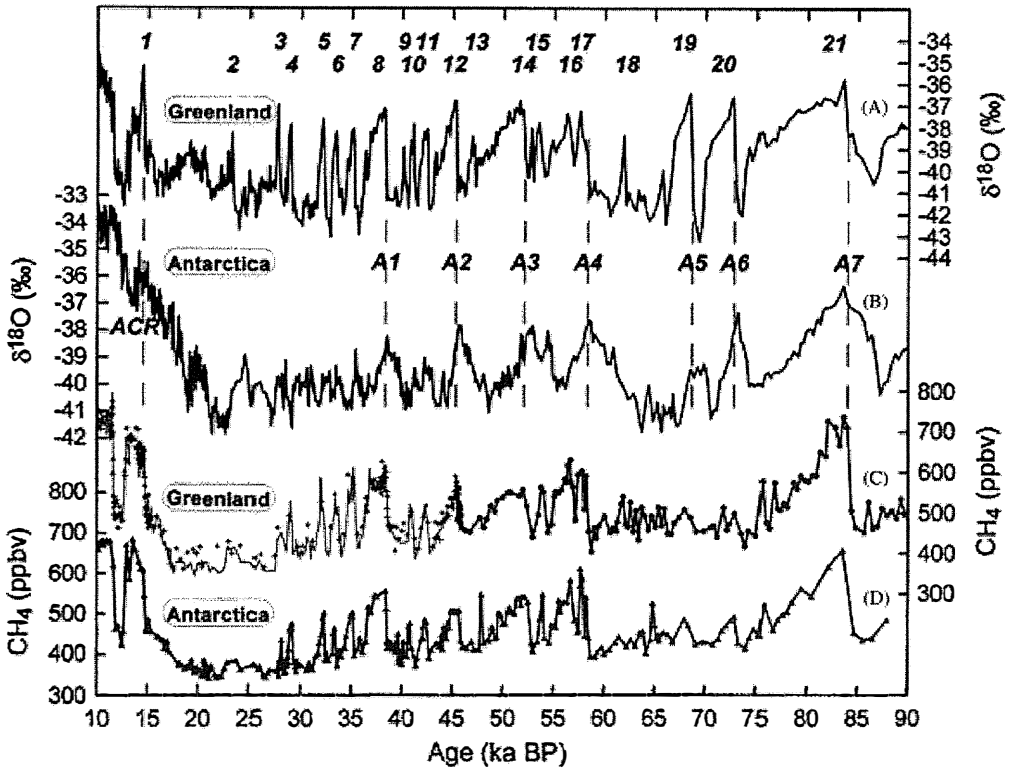

Figure 1.13: *Comparison of ice core $\delta^{18}O$ records (a, b) and CH_4 content (c, d) between Greenland and Antarctic ice cores. The CH_4 values are used to correlate the records because mixing of CH_4 in the atmosphere is very rapid. The $\delta^{18}O$ data show a number of abrupt warming and cooling events in both cores. Numbers above curve (a) are Dansgaard-Oeschger events in the Greenland record, and numbers A1 to A7 above curve (b) represent significant warm intervals in the Antarctic event. From Wunsch (2003).*

Terrestrial records from the Southern Hemisphere have also provided variable results. South American records examined by Denton *et al.* (1999) show similar timing of glaciation to the

Northern Hemisphere records, including late glacial warming and a Younger Dryas age cooling event. This contrasts with results from the southernmost part of South America, where Sugden *et al.* (2005) found that a late glacial advance occurred coincident with the Antarctic Cold Reversal (ACR) between 15,300 and 12,200 cal. years B.P. This is earlier than the Younger Dryas cooling, and significant warming and de-glaciation occurred at the end of the ACR, in the middle of the Younger Dryas interval.

In New Zealand, pollen records from Pukaki Crater in the northern part of the North Island were studied by Sandiford *et al.* (2003). These showed LGM cooling from 28,000 to 18,000 cal. years B.P., with warming conditions from 18,000 cal. years B.P. onwards. No clear evidence of a late glacial climate reversal was seen, although the low altitude of the Pukaki Crater site may have made vegetation at the site complacent to small magnitude climate change. However, a pollen record from Kaipo Bog in the eastern North Island did show a significant late glacial cooling event. Warming at this site was occurring by 16,000 cal. years B.P., and increases in grass and shrub pollen indicated a temporary reversal in this trend between c. 13,600 and 12,600 cal. years B.P., around 600 years earlier than the Younger Dryas cooling and partly overlapping the ACR (Newnham and Lowe, 2000). McGlone *et al.* (2004) produced a detailed record of vegetation and climate change for the Cass Basin, central South Island, based on a number of climate indicators. They showed glacial retreat from the site by 17,000 cal. years B.P., with warming and establishment of forest patches between 16,500 and 14,600 cal. years B.P. From 14,600 to 13,600 cal. years B.P. a cooling trend was seen, roughly coincident with the Antarctic Cold Reversal, and sustained warming was seen during Younger Dryas time. Turney *et al.* (2003) found a similar trend in results from several North Island sites, with post-glacial warming being interrupted by an interval of cooling between 15,000 and 12,900 cal. years B.P. Speleothem isotope data from North Westland show evidence of a reversal in climate warming between 13,530 and 11,140 cal. years B.P. This timing shows cooling occurred later than the cool interval evident in North Island records, but still earlier than the Younger Dryas chron (Williams *et al.*, 2005).

In South Westland, studies of ^{14}C dated pollen sequences from Okarito Pakihi indicated the onset of cooling during the last glaciation at between 28,500 and 30,500 cal. years B.P., earlier than the MIS 2 boundary (see Figure 2.4, Chapter 2). This timing implies that the Southern Hemisphere cooling occurred before the renewed expansion of major Northern Hemisphere ice sheets. The early cooling pattern seen in South Westland is also detected in the Vostok ice core record. Climate warming at the end of the last glacial occurred from 17,300 cal. years B.P. in the Okarito record. The pollen results showed some evidence of a reversal in this warming trend between 14,400 and 11,000 cal. years B.P., which would span both the Antarctic Cold Reversal and the Younger Dryas. Mercer (1988) summarised early dating of wood fragments from Canavan Knob in South Westland. These were recovered from beneath till correlated with a late glacial advance of the Franz Josef glacier. Although there was wide discrepancy in the ages determined, all were earlier than the Younger Dryas chron. However, Denton and Hendy (1994) collected and dated additional wood from the same site and obtained an age

of 11,050 ± 14 ^{14}C years B.P. This age indicated an advance synchronous with the start of the Younger Dryas. Similar results were obtained by Ivy-Ochs *et al.* (1999), who measured exposure ages for moraines in Arthur's Pass in the central Southern Alps using ^{10}Be dating. They determined a mean exposure age of 11,720 ± 320 years B.P., which is also consistent with a Younger Dryas advance.

In contrast, pollen analysis of sites in northwest Nelson by Singer *et al.* (1998) showed no evidence of Younger Dryas cooling, although changes in precipitation patterns were recognised. They suggested that Southern Alps glacial advances seen at Younger Dryas time were variable in regional extent and driven primarily by precipitation rather than temperature changes. However, Newnham (1999) questioned the validity of this conclusion, pointing out the scarcity of dating control for the records used and the difficulties of interpreting some pollen data.

In summary, climate change in the Southern Hemisphere is broadly synchronous with the Northern Hemisphere at time scales greater than a few thousand years, indicating a global response to orbital forcing mechanisms. However, at millennial time scales, abrupt changes of the climate are recorded in both hemispheres, and the exact timing relationship between these changes is contentious. In some cases this reflects difficulties in obtaining exact dating of terrigenous records. In other cases, climate responses may have varied in different regions. However, a number of well-dated records, including pollen, speleothem and marine-based records, have now demonstrated that Southern Hemisphere late-glacial climate changes were not synchronous with Northern Hemisphere events, and that Southern Hemisphere changes may have led Northern Hemisphere changes. In particular, many records show a late-glacial cool phase which occurred significantly earlier than Younger Dryas chron in the Northern Hemisphere.

1.8 Aims of this study

South Westland has proved to be a useful location for the study of mid-latitude Southern Hemisphere climate change. Continuous records encompassing the period from the end of MIS 6 to the present have been recovered from peat bogs and lakes located close to the limits of LGM ice advance. Existing pollen data from these sites show distinct changes in vegetation and climate during the last glacial and the glacial-interglacial transition. ^{14}C dating, luminescence dating and the presence of the Kawakawa Tephra (26,500 cal. years B.P.) provide a chronological framework for this work.

The main aim of this study is to supplement existing pollen studies with high-resolution sedimentology data for cores from sites close to the last glacial ice margins. Sediments were categorised using magnetic susceptibility, combustible organic carbon percentage (using loss-on-ignition), grain size and mineralogy. A second aim is to examine the tephrochronology of the site, including identification of the Kawakawa Tephra and any other tephra layers present in the sediments.

1.8.1 Hypothesis

Lakes and bogs with limited catchment in South Westland receive a significant proportion of non-organic sediment from aeolian dust. The sedimentology of sites close to regions of glacial advance should reflect changes in aeolian dust content which are closely tied to glacial advances. The null hypothesis is that the sedimentology of such sites will not reflect an aeolian dust signal related to ice advance, or such changes will not be detectable.

Chapter 2

Climate Change in South Westland

2.1 Climate Indicators from South Westland

The Southern Alps of New Zealand provide a prime location for the study of climate change in the Southern Hemisphere. New Zealand lies within the Southern Ocean mid-latitudes, the zone of southern westerlies and the oceanic Sub Tropical Convergence Zone (STCZ). Thus the climate of New Zealand is directly influenced by the Southern Ocean, and is sensitive to changes in global atmospheric and oceanic circulation. The mountains of the Southern Alps support glaciers which currently extend to within 150 m of sea level, and which formed a complex system of expanded valley and piedmont ice during glacial periods (Vandergoes and Fitzsimons, 2003). Glacial ice extended beyond the present coastline in parts of South Westland at the peak of the last glaciation. Figure 2.1 shows the location of the study area in South Westland.

Temperate maritime glaciers, such as those of South Westland, have high rates of accumulation and ablation, and respond rapidly to changes in temperature and precipitation. These glaciers have a small time lag between changes in measured weather patterns and the advance or retreat of the glacier terminal position (e.g. 5 to 7 years for Franz Josef Glacier) and are therefore a sensitive indicator of Southern Hemisphere mid-latitude climate (Hooker and Fitzharris, 1999).

Glacial advances tend to override and destroy deposits left by earlier advances, meaning that terrestrial sedimentary records close to areas of major ice advance are often missing or fragmentary, especially for time intervals prior to the last significant advance. In Westland, however, relatively rapid lateral movement of the Alpine Fault continuously displaces the coastal plains northwards. This shifts glacial deposits in South Westland out of the path of subsequent glacial advances and has led to the preservation of a number of sites containing long and continuous paleoclimate records in close proximity to areas of ice advance (C. H. Hendy, personal communication).

Peat bogs and lakes have provided much useful climate proxy information, especially in the form of detailed pollen records. Moar and Suggate (1996) produced a composite pollen record from several sites in North Westland. This showed a general pattern of podocarp forest during warm interglacials and mixed grassland and shrubland during glacial periods. High-resolution studies

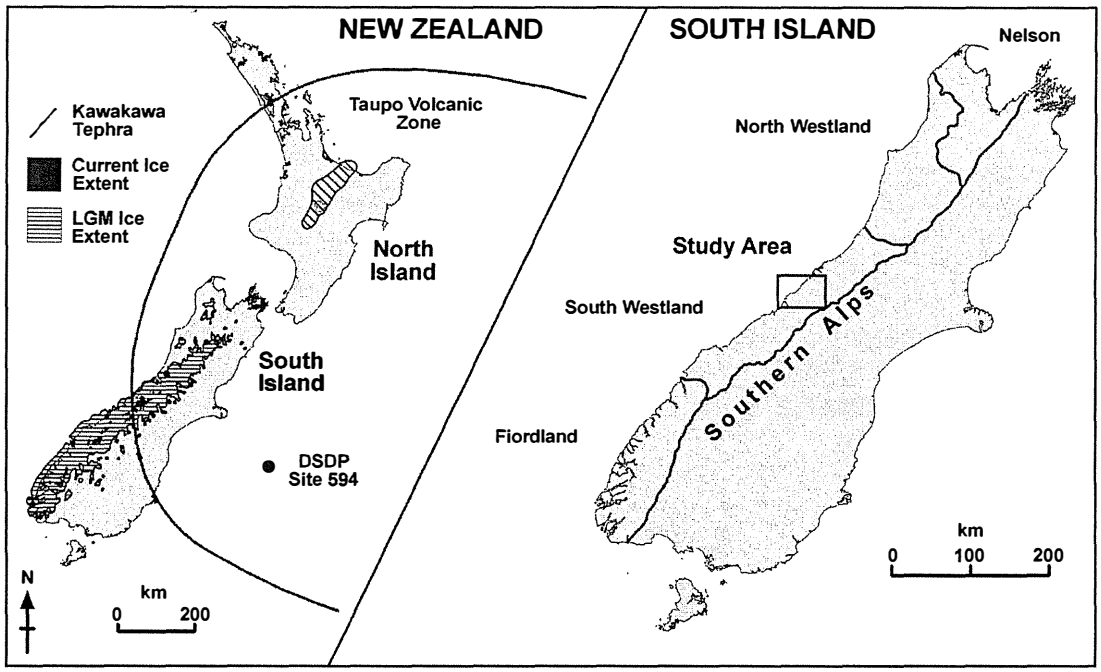

Figure 2.1: *Map of New Zealand and the South Island with South Westland and the study area marked. Last glacial maximum and present-day ice cover from Newnham et al. (1999). The approximate extent of macroscopic deposits of the Kawakawa Tephra is also shown (Shane, 2000).*

of several sites carried out by Vandergoes and Fitzsimons (2003) and Vandergoes *et al.* (2005) provided a much more detailed record of climate change in South Westland, especially during the last glacial. They recovered continuous records from c. 60,000 cal. years B.P. (MIS 4) to the present at several sites, and one site (Okarito Pakihi) was found to contain a record beginning in MIS 6, at least 130,000 cal. years B.P. (Vandergoes, 2000; Vandergoes *et al.*, 2005).

Loess accumulation in the Westland environment has been investigated by several studies, including Eden and Hammond (2003). Almond (1996) correlated loess deposits in the South Westland region with glacial advances, showing that loess accumulation was significant during glacial times. Marx and McGowan (2005) showed that aeolian dust entrainment and deposition is also active in South Westland despite the current warm and wet climate, but the rate is too low to form loess deposits. The main source for aeolian dust is the braided river channels which flow from the Southern Alps and provide abundant fine material which is readily entrained by winds (Figure 2.2). During times of glacial advance, large outwash plains would have provided an increased source area for aeolian dust entrainment (Figure 2.3). Thus, loess deposition should have been enhanced in areas close to the margins of ice expansion during times of glacial advance. Windier conditions during glacial times may also have enhanced aeolian dust entrainment.

The wet climate of South Westland means that exposed outwash areas are quickly colonised by vegetation once glaciers retreat. This would lead to a reduction in the source area available for aeolian dust entrainment (C. H. Hendy, personal communication). The relationships between

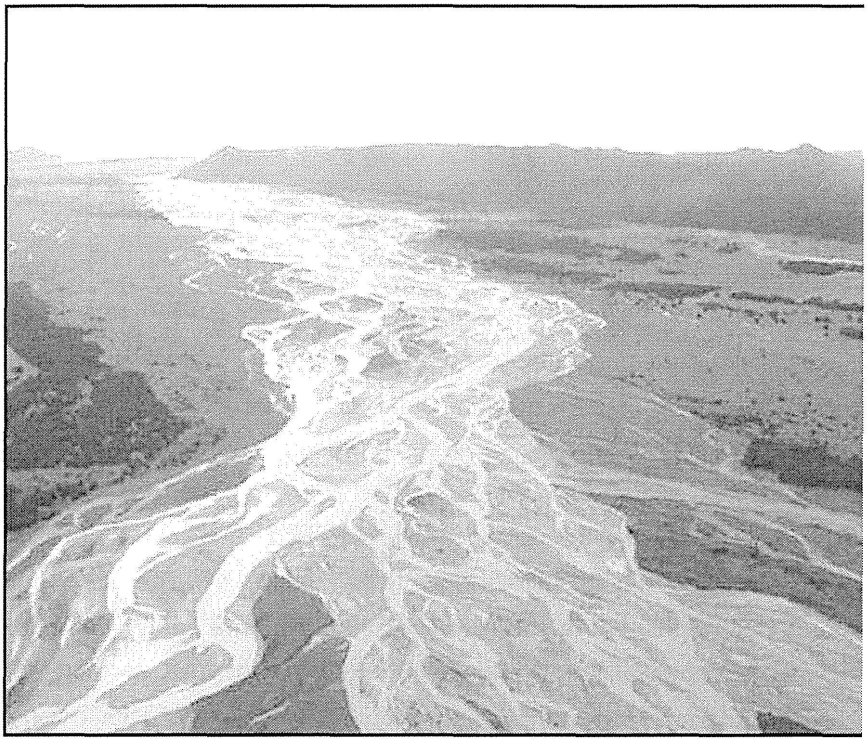

Figure 2.2: *Braided river channel of the Cook River (South Westland). These areas provide the main source for modern aeolian dust.*

Figure 2.3: *Outwash from the current termination of the Franz Josef Glacier (South Westland). Large outwash areas would have provided an increased source of aeolian dust during glacial advances. Vegetation quickly stabilises outwash areas when glaciers retreat, reducing the source area for aeolian dust.*

loess accretion and soil formation were described by Almond and Tonkin (1999).

2.2 Glaciations of South Westland

The stratigraphic nomenclature of Westland glacial deposits was developed from North Westland by Suggate (1965) and revised by Suggate (1985). The timing of glacial advances in the later part of the Otiran glacial has been constrained by ^{14}C dating. An independent chronology was developed from cave sediments and speleothems in Fiordland by Williams (1996), and correlation with this record has been used to infer ages for older advances. Preusser *et al.* (2005) produced a chronology based on luminescence dating of glacial deposits in North Westland.

Table 2.1 shows a summary of the glacial/interglacial sequences in Westland and the associated nomenclature. Evidence is seen for several episodes of glaciation older than the last (Otiran) glacial, but these are not well dated. A glacial advance at c. 227,000 cal. years B.P. (Aurora 7) in Fiordland has been correlated with the Waimea glacial deposits, which would indicate an advance during MIS 6 (Vandergoes, 2000).

Table 2.1: *Glacial/interglacial sequences and nomenclature for Westland, adapted from Suggate (1990).*

Years [1] BP	MIS [1]	Glacial / *Interglacial*	Age [2] (k yrs BP)	Moraine [2]	Formation [3]	Age [4] (k yrs BP)	Ice [4] Advance
0							
	1	*Aranui*					
12,000						11 - 14	Aurora 1
	2	Otira	19 - 20.5	M6	Moana	15 - 17	Aurora 2
						18 - 20	Aurora 3
			21.5 - 24.5	$M5_2$			
24,000					Larrikins		
			28 - 34	$M5_1$			
	3					40 - 41	Aurora 4
			45 - 50	M4	?	46 - 48	Aurora 5
59,000							
	4		~60	M3	Loopline		
				M2			
74,000						67 - 91	Aurora 6
	5	*Kaihinu*					
130,000							
	6	Waimea	?	M1	Waimea	?	Aurora 7

[1] MIS boundaries and boundary ages (Bradley, 1999)
[2] South Westland glacial chronology (Suggate and Almond, 2005)
[3] Moraine formations (Suggate, 1985)
[4] Fiordland speleothem/cave sediment record (Williams, 1996)

Six ice advances are recognised by Suggate and Almond (2005) for the Otira glacial interval. The oldest of these, relating to the Loopline Formation, are beyond the range of ^{14}C dating.

Preusser *et al.* (2005) dated various deposits associated with the Loopline Formation, and reported evidence for several small glacial advances in MIS 5d and MIS 5b (c. 111,000 and 85,000 cal. years B.P. respectively), and a significant advance in MIS 4 (c. 64,000 cal. years B.P.). The later advances of the Loopline Formation probably correlate with the Aurora 6 advance in Fiordland, dated at 67,000–91,000 cal. years B.P. This was followed by a relatively warm period during MIS 3, although Suggate and Almond (2005) found evidence for an ice advance at c. 50,000–45,000 cal. Years B.P. Two advances occurred during this time in the Aurora Cave record (Aurora 4 and 5, c. 40,000 and 47,000 cal. years B.P. respectively). Preusser *et al.* (2005) dated an ice advance which occurred sometime after 32,000 cal. years B.P.

Suggate (1985) identified moraine deposits representing two ice advances during MIS 2 (the Larrikins and Moana formations), considered to correspond to the peak of glaciation locally. Suggate and Almond (2005) produced a chronology of the last glacial in Westland based on ^{14}C dating. The older and slightly more extensive Larrikins Formation moraines were subdivided into two glacial advances of similar extent, occurring at c. 34,000–28,000 and 24,500–21,500 cal. years B.P. The younger Moana Formation was dated at 20,500–19,000 cal. years B.P. The Moana Formation may correlate with the Aurora 3 advance in Fiordland, dated at c. 19,000 cal. years B.P.

Almond *et al.* (2001) studied loess accumulation, soil stratigraphy, mineralogy and phytoliths from moraines in Saltwater Forest and Okarito Forest in South Westland. Five loess sheets were correlated to glacial advances that occurred during the Otira glaciation. The associated moraine deposits (M2 to M6) were identified, whereas an older moraine (M1) was correlated to the previous Waimea glaciation.

A chronology of climatic events during the last glacial and the last glacial to interglacial transition (LGIT) has been developed from pollen records recovered from lake and peat bog cores in South Westland (Vandergoes, 2000; Vandergoes and Fitzsimons, 2003; Vandergoes *et al.*, 2005). The dating used for this chronology has been established from numerous ^{14}C dates, supported by luminescence dating and tephrochronology. One site studied (Okarito Pakihi) contained a basal silty layer correlated to the latter stages of MIS 6, and an uninterrupted record of pollen from the last interglacial (MIS 5e) through to the present (Figure 2.4). Several other sites provided shorter records beginning from MIS 4 and encompassing the last glacial maximum (LGM) and LGIT.

Analysis of the Okarito Pakihi pollen data shows that the latter stages of MIS 6 were cool, with two distinct grass pollen peaks suggesting that at least two ice advances occurred. The end of the penultimate glaciation is marked by a major expansion of podocarp/hardwood forest, producing a dominance of forest pollen in the Okarito record. Grass pollen remains rare during MIS 5, indicating a generally warm climate throughout this period. However, the amounts of forest and montane-subalpine shrub pollen vary, suggesting some degree of climate change during MIS 5. Such an interpretation is consistent with variations seen in the marine oxygen isotope record and the subdivision of MIS 5 into sub-stages 5a–5e.

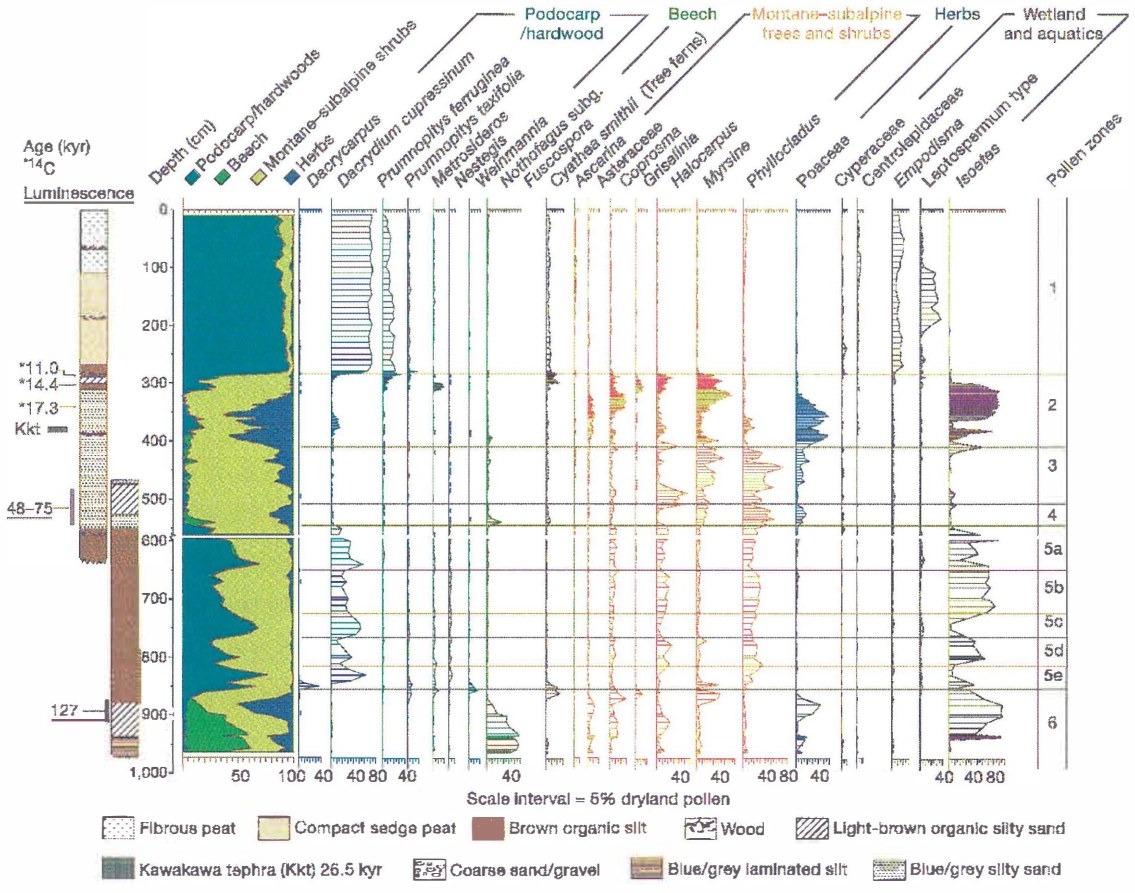

Figure 2.4: *Okarito pollen record, from Vandergoes (2000).*

Climate cooling is indicated by a distinct grass pollen peak and a reduction in forest pollen, dated at 48,000–75,000 cal. years B.P. (luminescence dating). This first cooling probably correlates with MIS 4, and the ice advance associated with the Loopline moraine deposits. The subsequent MIS 3 remained cool, dominated by shrub and grass pollen, although no direct evidence of further ice advance is seen until the end of MIS 3. Major grass peaks show that significant climate cooling began at the end of MIS 3 and continued through MIS 2, representing the LGM in South Westland. The Kawakawa tephra (c. 26,500 cal. years B.P.) provides a well dated chrono-stratigraphic marker (Wilson *et al.*, 1988), and occurs at the end of the first LGM grass peak. This shows that LGM cooling in the Southern Hemisphere mid-latitudes began at c. 28,500–30,500 cal. years B.P. This is earlier than the MIS 2/3 boundary, which is interpreted to represent major Northern Hemisphere ice accumulation.

Expansion of montane-subalpine shrubland and a corresponding reduction in grass pollen began at c. 17,300 cal. years B.P. This change indicates significant climate warming, and is coincident with rapid glacial retreat in South Westland. There is some evidence for a late glacial reversal of this warming trend occurring between 14,000 and 11,400 cal. years B.P., beginning earlier than the Younger Dryas event in the Northern Hemisphere (12,600–11,600 cal. years B.P.), but approximately coincident with cooling in northwest South Island recorded from speleothems

(Williams *et al.*, 2005). However this change is seen only in the Okarito Pakihi pollen record, and may be associated with stronger westerly circulation and increased precipitation rather than significant cooling. From c. 11,400 cal. years B.P., climate warming led to the establishment of lowland podocarp forest similar to today.

2.3 Dating techniques

2.3.1 ^{14}C Dating

The radioactive carbon isotope ^{14}C is produced as a result of bombardment of nitrogen atoms by cosmic rays in the upper atmosphere. Once produced, ^{14}C atoms quickly form $^{14}CO_2$ and mix with CO_2 in the lower atmosphere. From the atmosphere they are distributed throughout the biosphere by the biological processes of living organisms. After an organism dies, the carbon it contains is isolated from the atmosphere and the radioactive ^{14}C gradually decays. Hence, by measuring the amount of ^{14}C present, the amount of time since the organism died can be determined. The amount of ^{14}C present in the sample eventually becomes too small to detect accurately, meaning that the oldest ages that can be measured are around 55,000 years. Several other difficulties also arise with this technique. The atmospheric ^{14}C content has changed over time, meaning that ^{14}C dates are generally younger than the true age of the sample, and a calibration must be carried out. Also, due to short periods when atmospheric ^{14}C concentration temporarily increased, there are 'dating plateaus' where a particular ^{14}C concentration in a sample could correspond to a range of calendar ages (Bradley, 1999).

Another problem is the potential contamination of a sample by younger or older carbon. For example, the penetration of roots into a peat bog may introduce younger carbon into the older peat material, or inwash of material into a lake may introduce older carbon. Permeation of ground water in high rainfall environments with extreme leaching such as Westland has also been associated with contamination by modern carbon and anomalously young ^{14}C dates. These problems have been well documented in South Westland by Vandergoes and Prior (2003). They found that dates based on concentrated pollen were generally older than other dates, and these were considered to be more reliable. In some instances, however, residual organic material may provide older ages than pollen concentrates (Newnham *et al.*, 2006). Difficulties with contamination in samples from South Westland mean that uncertainties still exist in the dating of last glacial events from the region.

2.3.2 Luminescence Dating

Some minerals (especially quartz and feldspars) exhibit luminescence when exposed to light or subjected to heating. The amount of light emitted is related to the amount of radiation the sample has been exposed to over time. Exposure to heat or (more usually) sunlight prior to

burial resets the luminescence signal in the sample, which then builds up over time as a result of exposure to background radiation. In order to measure the time since the sample was last reset by exposure, the amount of luminescence produced by heating (thermoluminescence, TL) or exposure to light (optically stimulated luminescence, OSL) is measured. The background radiation level and the sample's sensitivity to radiation exposure must also be determined (Bradley, 1999). TL and OSL dating were used to determine ages for clastic-rich sediments from Okarito Pakihi which were beyond the range of ^{14}C dating (Vandergoes *et al.*, 2005). Although there was relatively large uncertainty in the results from this technique, the ages determined give a broad timeframe which allows events to be tentatively correlated with global events seen in the marine oxygen isotope record. Correlation is also possible with the luminescence dates obtained by Preusser *et al.* (2005) in North Westland (see Section 2.2).

2.3.3 Tephrochronology

Tephra layers (unconsolidated pyroclastic material of explosive volcanic origin, including widely dispersed volcanic ash) are emplaced quickly (generally over a matter of a few days to weeks) and may be preserved in a variety of sedimentary environments. Tephra layers can therefore serve as isochronous geological marker horizons allowing correlation across many sites (Shane, 2000).

In New Zealand, the volcanoes in the Taupo Volcanic Zone in the central North Island, and Mt Taranaki and Mayor Island (Tuhua), have produced numerous large-scale rhyolitic and andesitic eruptions. Deposits from these have been extensively studied, resulting in the development of a good stratigraphy of late Quaternary eruptions. Many of these eruptions have been accurately dated, allowing them to supplement the chronology of sites where they are found (Shane, 2000).

In South Westland, the only late Quaternary tephra identified so far is the Aokautere Ash member of the Kawakawa Tephra, the distal fall product of the Kawakawa (or Oruanui) eruption from Taupo volcano (Froggatt and Lowe, 1990). This large scale eruption, which released over 530 $km^3$of magma and formed the caldera of Lake Taupo, has an age estimated at 26,500 cal. years B.P. (Wilson *et al.*, 1988; Wilson, 2001; Manville and Wilson, 2004). Macroscopic deposits of the Kawakawa Tephra have been identified in many parts of New Zealand and are also seen on Chatham Island and in deep sea cores 1400 km from the source (Figure 2.5). The distal deposits in northern South Island were mapped by Wilson (2001) as fall deposits 9 and 10 of the Oruanui eruption (using Wilson's 2001 nomenclature).

Kawakawa tephra has been identified in various studies from the South Island. In studies of loess from South Westland, Almond (1996) found widespread glass shards but no macroscopic tephra layer. Glass shards were identified as Aokautere Ash (Kawakawa Tephra) using geochemical techniques, and the stratigraphic location of the tephra was placed at the point of maximum glass-shard concentration. The presence of Kawakawa Tephra was used to identify loess which was actively accumulating during the LGM at c. 26,500 cal. years B.P. Loess in southern South

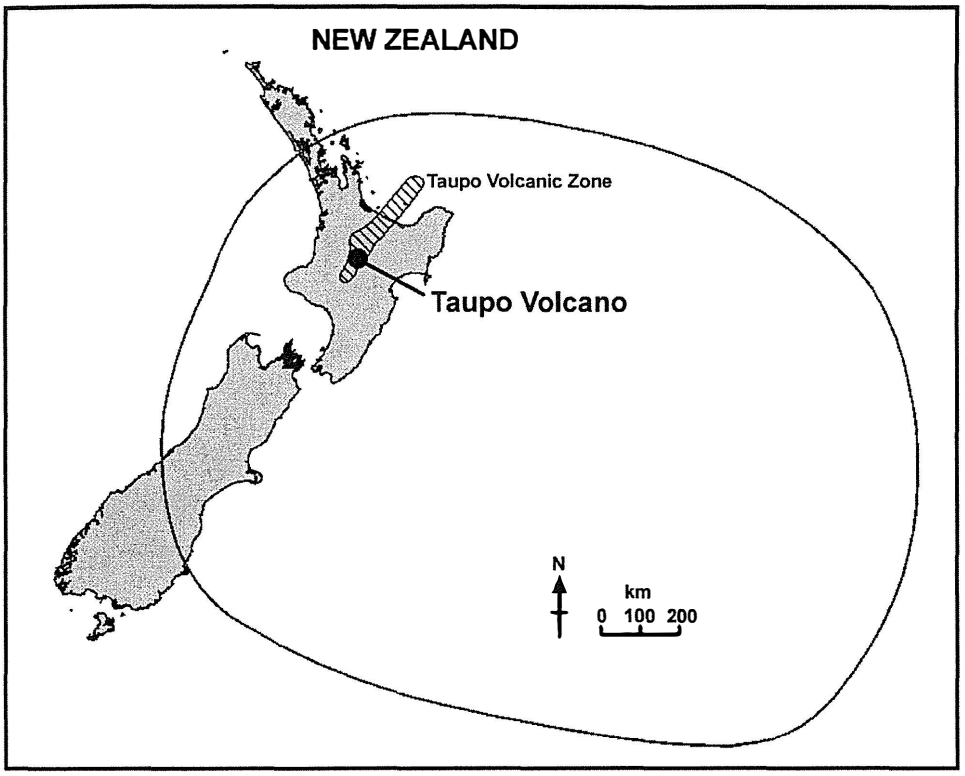

Figure 2.5: *Distribution of macroscopic deposits of the Kawakawa Tephra. The source (Taupo volcano) is also shown. From Shane (2000).*

Island was found to contain glass shards from Kawakawa Tephra and two other older tephras, suggesting significant aeolian reworking (Eden *et al.*, 1992).

A 1–2-cm-thick macroscopic tephra layer is reported in many lake and bog sediment cores from South Westland, and has been identified as the Kawakawa Tephra using glass composition and stratigraphic position. In some cores it is not visible as a macroscopic layer, but can be identified as a 'cryptotephra' by glass-shard counts (Vandergoes *et al.*, 2005; M. J. Vandergoes, unpublished data). This tephra provides a chrono-stratigraphic tie-point to allow correlation of records from different sites.

2.4 Study Area

Sites were selected for this study from the Fox Glacier area of South Westland (see Figure 2.7). The glacial stratigraphy of the area has been formalised by Suggate (1990), as described in Section 2.2 above. Glacial advances out of the valleys of the Southern Alps have produced extensive moraine deposits which form most of the low hills to the west of the Alpine Fault. These were mapped by Warren (1967), who grouped moraines in the region into two main formations, the Okarito (older) and the Moana (younger). Mapping of the moraines is currently being revised by B. G. Andersen and others. The older Okarito Formation (formed during the

Waimea Glacial or earlier) has been subdivided into two units (Tansey, older, and Waimea, younger), while three younger moraines of the Last (Otira) Glacial have been identified and mapped as Loopline, Larrikins and Moana, according to the glacial stratigraphy recognised by Suggate (1990) (Figure 2.6).

2.5 Site Selection

Sites were selected for this study based on the following criteria:

- *LGM/LGIT sedimentary record:* Sites were selected that were known to contain a continuous record of the LGM and the subsequent glacial/interglacial transition.
- *Existing pollen studies:* The aim of this study was to supplement existing pollen studies by adding high resolution sedimentology data for previously studied sites.
- *Sites close to the LGM ice margins:* In order to show maximum sensitivity to changes in ice extent, sites were selected close to the limits of LGM ice advance.
- *Low sediment input from fluvial sources:* Sites were selected which had minimal catchment area and limited stream flow, in order to minimise the terrigenous sediment input from the area surrounding the site. Input of locally-derived aeolian dust to the sites should therefore be easier to detect.

Three sites were used in this investigation. Two of these, Skiffington Swamp and Galway Tarn, were used for detailed sedimentological studies. The third site, Okarito Pakihi, was used in a study of magnetic susceptibility for comparison with the other sites.

2.5.1 Skiffington Swamp

Skiffington Swamp is located 5 km northwest of Fox Glacier township, at 340 m altitude (Figure 2.7 and 2.8). This site consists of a small lake (0.5 km^2) surrounded by swamp, which drains predominantly to the west through the Waihapi Creek. The site formed within lateral moraine deposits mapped as Okarito Formation by Warren (1967). More recent mapping places this site within the Loopline Formation, formed by an early Otira glaciation advance during MIS 4 (see Figure 2.6). This interpretation is consistent with the stratigraphy and palynology of the bog, which records a long period of cool climate at the base of the bog, followed by a deterioration of conditions representing the LGM. Lateral moraines of the Larrikins Formation (early MIS 2 advance) occur adjacent to the site, while moraines of the later Moana Formation occur only a few hundred metres within the Larrikins Moraines. Hence, the margins of LGM ice were very close to the site.

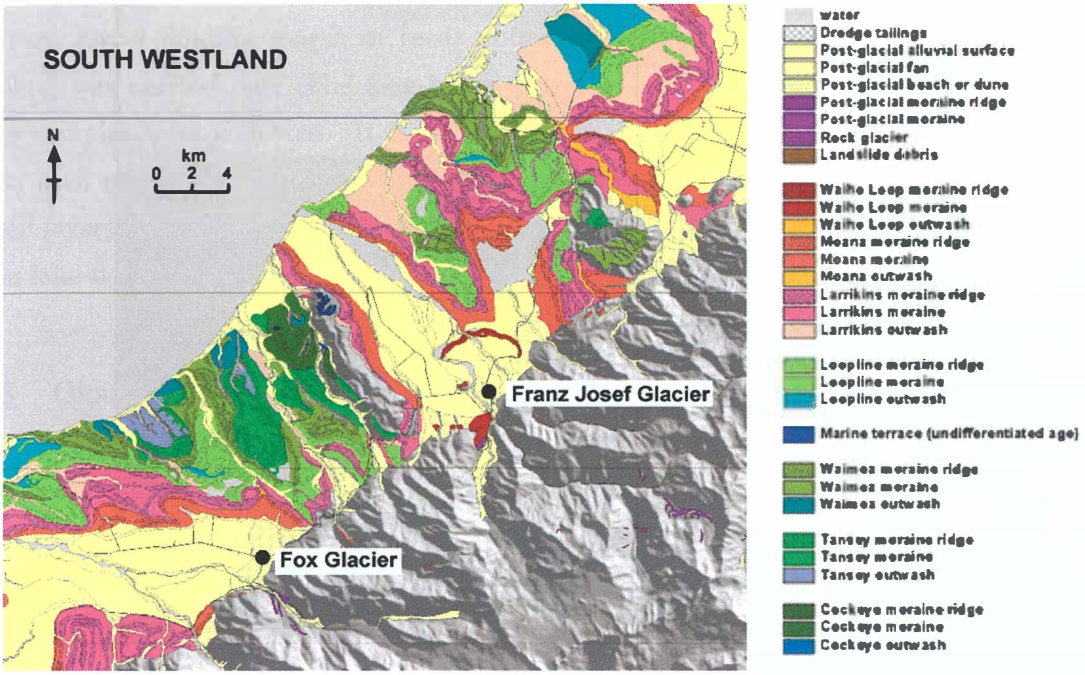

Figure 2.6: *Glacial geomorphology of the Fox Glacier area of South Westland, mapped by B. G. Andersen et al. (draft).*

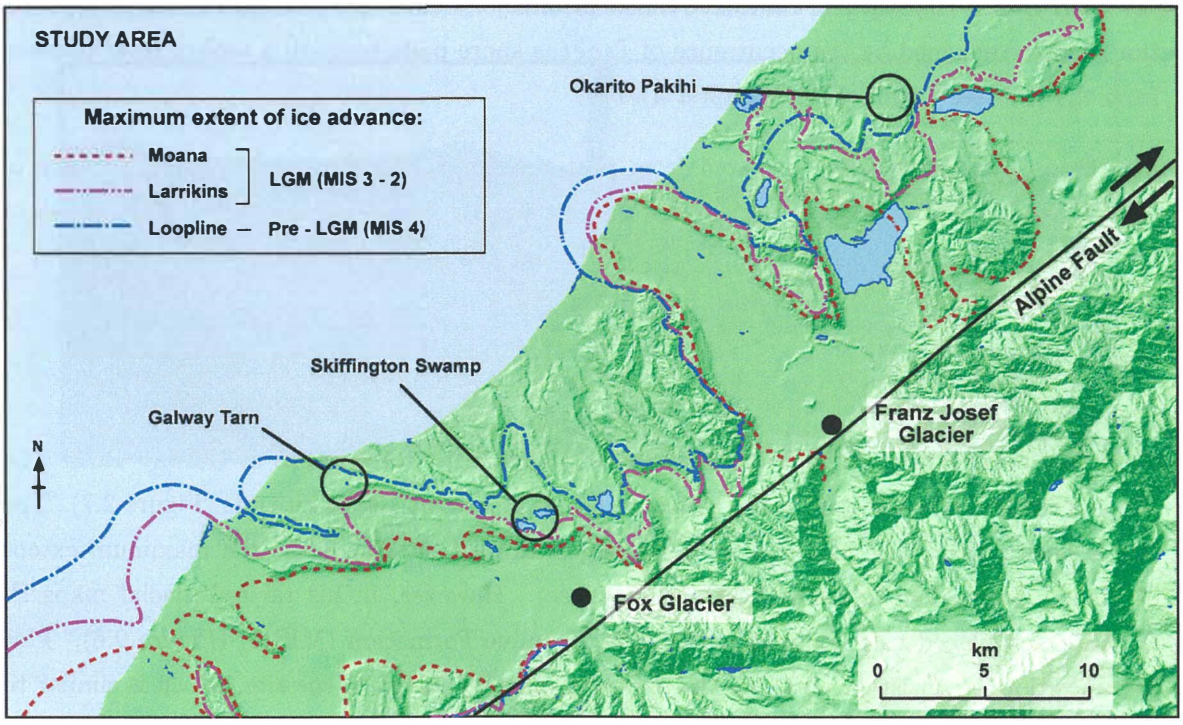

Figure 2.7: *Map of the study area and glacial ice advances in South Westland, from Figure 2.6 above.*

Figure 2.8: *Skiffington Swamp (right) and Lake Gault, looking west. The ridge in the foreground is moraine of the Moana Formation. Photo courtesy of C. H. Hendy.*

The coring site is currently a peat bog. Occurrence of pollen from the aquatic species *Isoetes kirkii* indicates that the site contained a lake prior to c. 14,000 cal. years B.P. This interpretation is also confirmed by the occurrence of *Isoetes* spore pods beneath a tephra layer in cores from the site (see Figure 4.5 in Chapter 4).

Skiffington Swamp is largely isolated from post-glacial fluvial activity, and little evidence of erosion is seen in the small catchment area that feeds the bog and lake. Thus, the inwash of fluvial sediments into the lake is considered to be low (Vandergoes and Fitzsimons, 2003).

2.5.2 Galway Tarn

The second site is an unnamed tarn near Galway Creek, here referred to as Galway Tarn. The site is a small kettle-hole tarn 4 km east of Gillespie Beach, at 130 m altitude (Figure 2.7). The site is positioned at the end of a moraine ridge, mapped by Warren as the maximum extent of Moana Formation deposits (LGM ice advance). However, in his revised glacial maps B. G. Andersen placed this site within the older Loopline Formation (MIS 4) (Figure 2.6). This juxtaposition is consistent with the stratigraphy and palynology of the site, which is similar to that of Skiffington Swamp.

The Galway Tarn site is separated from Larrikins Formation moraines by a low moraine ridge. This indicates that ice advanced close to this site during the earlier part of MIS 2. Unlike Skiffington Swamp, the Moana Formation moraines were mapped by B. G. Andersen as occurring several kilometres to the south east, indicating that the later advance of MIS 2 did not reach as

close to this site.

The tarn has a floating marsh of reeds and small shrubs at the southwest side, where core sampling was carried out. The lake below this floating mat was 5–6 m deep at the location where samples were collected. It is surrounded with marsh, gentle slopes and dense lowland forest, with no visible surface drainage and very little evidence of inwash of sediment. Sharply defined layers in the recovered cores, including one visible tephra, indicate very little disturbance at the lake bed.

2.5.3 Okarito Pakihi

Okarito Pakihi (Figure 2.9) is a rheotrophic peat bog located approximately 3 km southeast of Okarito Lagoon at an altitude of 70 m. The site is within moraines mapped as Okarito Formation by Warren (1967) and interpreted as having formed during the penultimate (Waimea) glaciation. This interpretation was confirmed by B. G. Andersen who placed the site within Waimea Formation moraines. This site differs from the other two sites studied in that it was not overrun by ice advances during the last (Otira) glaciation, although the three major advances came to within 1–2 km of the site (Figure 2.7). As a result, the site contains a long sequence of sediment which includes the end of the penultimate (Waimea) glaciation (MIS 6), the last interglacial (MIS 5e) and the last (Otira) glaciation. The chronology for this interpretation has been confirmed by luminescence dating of silts recovered from the site (Vandergoes *et al.*, 2005).

Figure 2.9: *Okarito Pakihi. Photo courtesy of C. H. Hendy.*

Chapter 3

Methodology

The laboratory work carried out for this study used cores of peat and sediment collected during several trips to the field area in South Westland. In this chapter the core collection process and the laboratory procedures used are described.

3.1 Core Collection

Three cores were used in this investigation. Two cores, from Skiffington Swamp (Core SS906, archive number W20060041) and Okarito Pakihi (Core OP913) were collected by C. H. Hendy and M. J. Vandergoes. A third core was collected from Galway Tarn (Core GT0507, archive number W20060042) by M. J. Vandergoes and the author. The cores were collected using a 50-mm-diameter rectangular rod corer with a 1-m-long core barrel. Cores were recovered in 1-m long sections, numbered T1, T2, etc, starting from the uppermost section (See Figure 3.1). Core sections were extruded onto a plastic guttering made from a 50-mm-diameter plastic pipe cut in half longitudinally. Core sections were described before being wrapped in plastic film, labelled and packed for transport.

The cores from Skiffington Swamp and Okarito Pakihi were collected in January 1999. Each site was probed along transects to determine the deepest area from which to obtain cores. At Skiffington Swamp (Core SS906), material was recovered from a depth of 52 cm until impenetrable basal gravel of the underlying moraine was reached at a depth of 507 cm. Material was recovered for Okarito Pakihi (Core OP913) from a depth of 100 cm until laminated sand was reached at a depth of 971 cm.

The core from Galway Tarn (Core GT0507) was collected in January 2005. The coring site was close to the site where cores had previously been collected by C. H. Hendy and M. J. Vandergoes. Coring was carried out from a floating weed mat at the southwest side of the lake, approximately 30 m from the lake shore (Figure 3.2). Below this weed mat, the lake-bottom sediment was encountered at a depth of 500 cm, although the uppermost core section comprised unconsolidated material and was not recovered. Core recovery commenced from a depth of

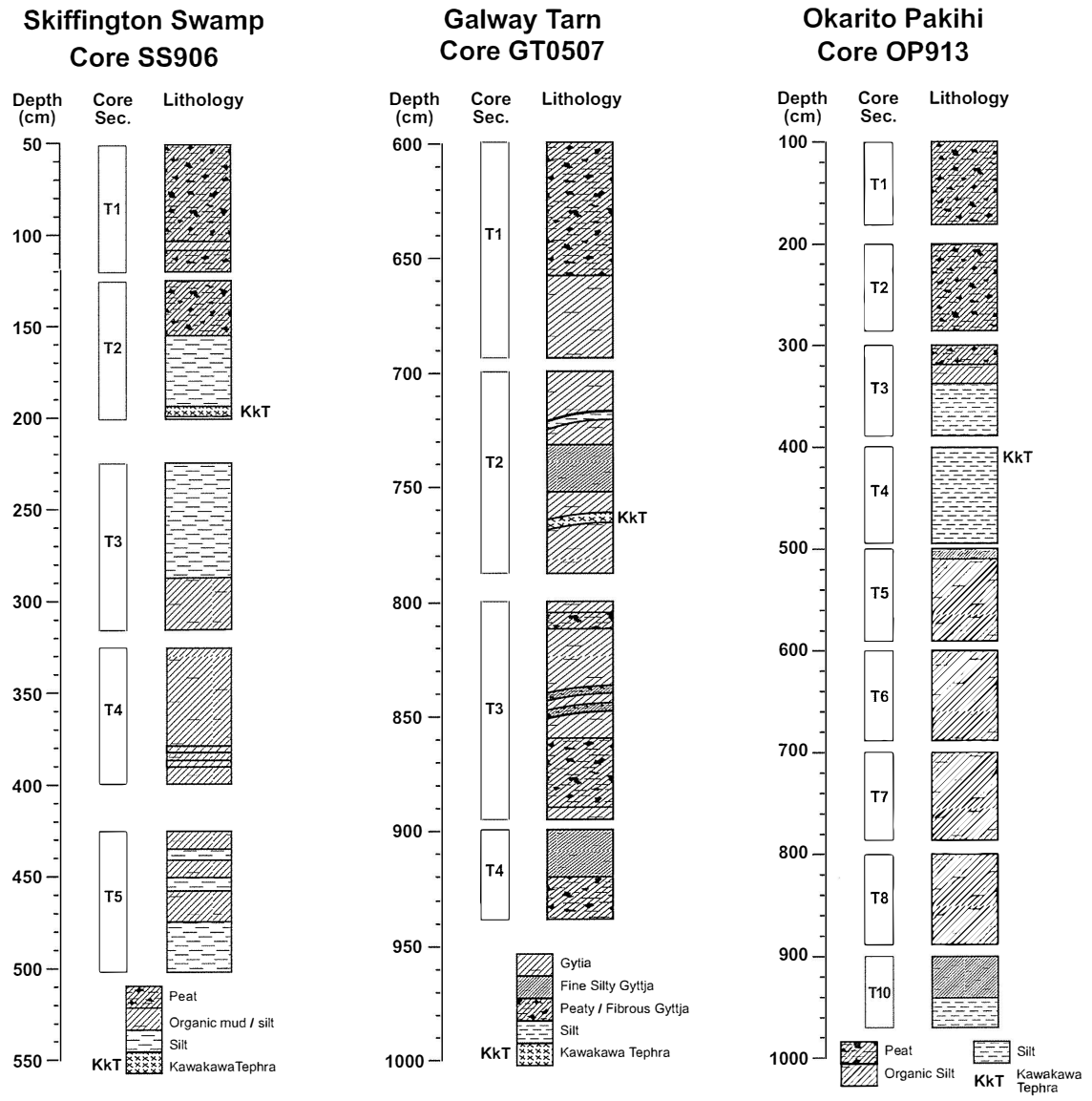

Figure 3.1: *Summary of the core stratigraphy and nomenclature for cores used in this study.*

600 cm until basal material was reached at a depth of 940 cm.

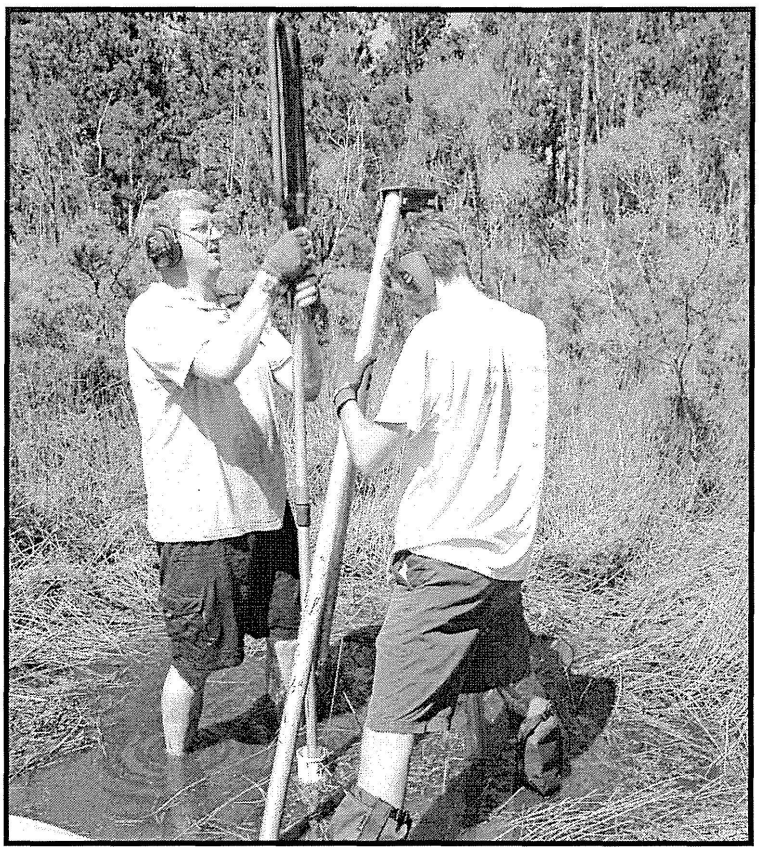

Figure 3.2: *Collecting core samples at Galway Tarn. Photo courtesy of M. J. Vandergoes.*

Cores were stored in a cool-room at the University of Waikato at a temperature of approximately 5 °C. Although wrapped in plastic film, considerable drying and shrinkage of the older cores was noted. Cores SS906 and GT0507 were split longitudinally into archival and working halves. Core OP913 had several split and several intact sections, which were left intact as the only work to be undertaken on this core was a non-destructive survey of magnetic susceptibility. All intact core sections and archival halves were re-wrapped in plastic film and stored in the cool-room when not in use.

3.2 Magnetic Susceptibilty

Magnetic susceptibility (MS) was surveyed in order to obtain an overview of magnetic mineralogy in the core sections. The MS of core sections from Skiffington Swamp and Galway Tarn (Cores SS906 and GT0507, respectively) was measured using a Microkappa hand-held unit manufactured by Geofyzika, and a Bartington MS2 lab meter.

The Microkappa uses the inductive effect of the material being measured as a proxy for MS. The face of the unit (Figure 3.3) contains a coil, which is part of an oscillator circuit operating at approximately 10 kHz. The frequency of oscillation is affected by magnetic minerals of the

nearby material, and slight variations in frequency are used to determine the MS of the material.

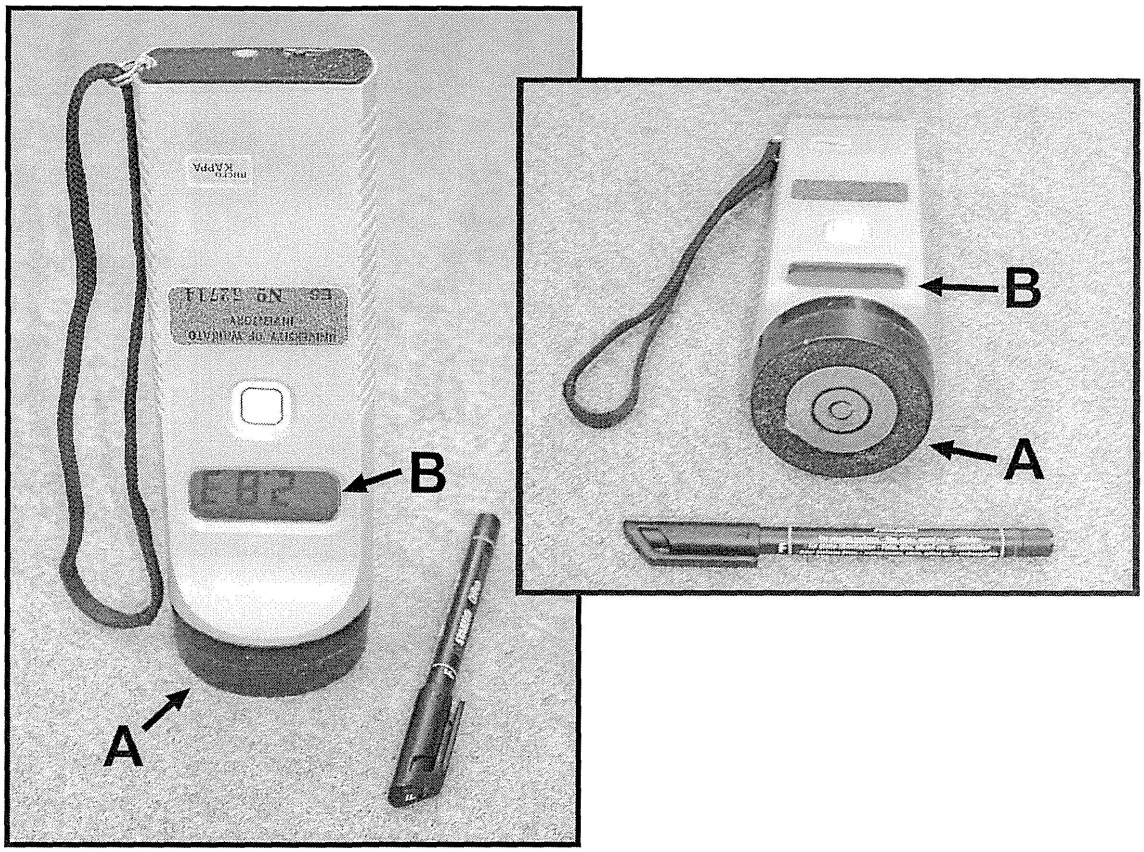

Figure 3.3: *The Microkappa handheld MS meter. The active face (A) of the instrument is placed against the surface to be tested. The MS value (in SI units) is read from the digital display (B).*

The design of the device means that accurate readings are only achieved when applied to an infinitely deep face of infinite extent, which in practice means a body of material at least 50 mm deep with a face area large enough to contain a circle of at least 100 mm diameter (Geofyzika documentation). When applied to sedimentary sections in the field, previous workers have found that the device gives results which correlate very well with those obtained from more accurate laboratory techniques (Horrocks, 2000). Smaller bodies of material (such as split core sections) result in lower than expected readings due to the limited amount of material behind the measuring face. However, the data obtained from split core sections provides a comparative magnetic stratigraphy of the core sections. This technique has the advantages of being fast and non-destructive.

Each core section was wrapped in thin plastic film which was left in place since it has no effect on readings. A variety of measurement techniques and locations was tested. It was found that measurements were near to the lower sensitivity limit of the Microkappa, and that interference from metal and other materials strongly affected the results, making many locations unusable. A location with predominantly wooden desks was eventually chosen. The core section was placed on two cardboard boxes (approximately 25 cm high) to further isolate it from the effects of the

desk and surrounding metal. Figure 3.4 shows the layout of a core section with the Microkappa meter in measuring position.

Figure 3.4: *The Microkappa in measuring position on a core section. Cardboard boxes were used to raise the core above the desk and avoid interference.*

Each core section, still in its plastic storage tube, was placed in the measuring location and a fibreglass tape measure was fixed to the side of the storage tube. Readings of MS were taken at 2 cm intervals, starting at the top of the core. Readings from the beginning and end of the core were discarded due to end effects (the reading obtained was reduced because of the smaller volume of material under the active face of the meter). For each reading, the Microkappa was zeroed while holding it in the air approximately 40 cm from the core section. A reading was then obtained with the face of the meter centred on the core the appropriate distance from the top. The meter was pressed lightly but firmly against the face of the core section. MS readings were obtained working from the top down, and the process was repeated four times for each core section. The values obtained were then averaged to obtain a final magnetic susceptibility profile for each core section.

MS measurements were also made using a Bartington MS2 lab meter manufactured by Bartington Instruments Limited, and fitted with an MS2F probe attachment. This probe uses a sensor which works on a similar principle to the Microkappa handheld meter, but with a sensing coil diameter of 1 cm, making it more suitable for measuring small diameter material such as core sections (Figure 3.5).

Initially, the MS2 meter was zeroed away from the core between readings to remove instrument drift. However, a faster method was later adopted whereby an 'air' measurement was taken every 10 or so readings, and used to correct for drift. Three measurements were carried out for each core section and the results were averaged. The upper section of Core SS906 (peat with very low MS values) was surveyed at 2 cm intervals, and the upper section of Core GT0507 was

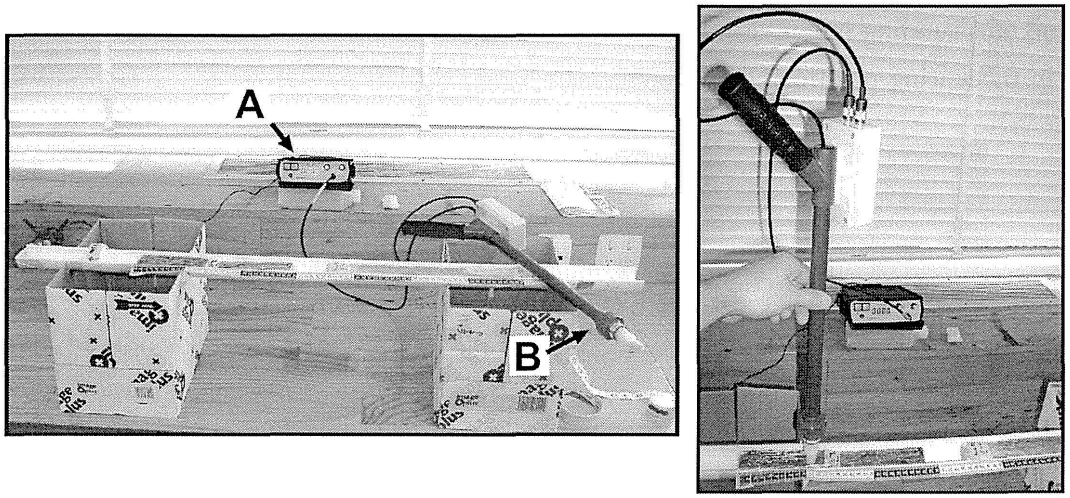

Figure 3.5: *Left: The Bartington MS2 meter (A) and MS2F handheld field probe (B) with a core section set up for measuring. Right: The MS2F probe in use.*

surveyed at 5 cm intervals. All other sections of these cores were surveyed at 1 cm intervals. MS measurements on the Okarito Pakihi core (OP913) were carried out using only the Bartington meter. The upper and lower peaty sections (T1, T2 and T6–T10 in Figure 3.1) were surveyed at 2.5 cm or 5 cm intervals, while sections T3–T6 (containing material from the LGM and LGIT) were surveyed at 1 cm intervals.

The results obtained with the Bartington MS2 meter showed a very similar trend to those obtained with the Microkappa handheld meter (Figure 3.6), but the Microkappa MS values were generally much lower. This was because the diameter of the core half-sections was too low to provide the optimum volume of material for the Microkappa meter. A higher sampling resolution was also possible with the Bartington MS2 meter because of the smaller probe size, so the results from the Bartington MS2 meter were used in this study.

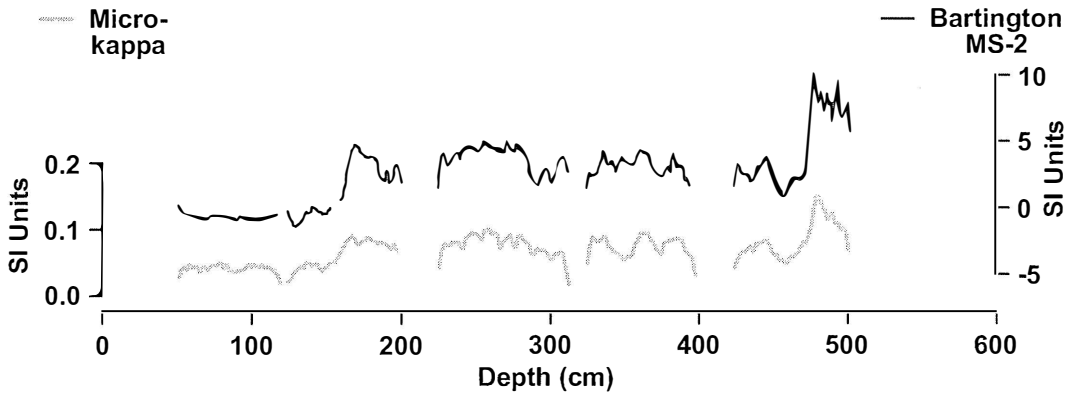

Figure 3.6: *Comparison of the results obtained with the Bartington (top) and Microkappa MS meters. The results shown are for Core SS906. The results from both meters show similar trends, but the Bartington meter had greater resolution and produced higher values.*

3.3 Core Description

Following the completion of MS analysis, the working half of each section from Core SS906 and Core GT0507 was removed from its plastic wrapping and a detailed core description was carried out (see Appendix A), with changes in colour and texture noted along with any other features of interest. The stratigraphy of the cores is described in Chapter 4. A simplified summary of the core stratigraphy and nomenclature is shown in Figure 3.1.

3.4 Sampling for Lab Analysis

The working halves of Core SS906 and Core GT0507 were sliced into 0.5-cm-thick samples and placed in labelled plastic bags. The core was sliced using a craft knife (Figure 3.7). To minimize contamination, any loose material was removed if the source of the material was uncertain. Some sections of the core were difficult to slice cleanly due to fractures in the material nearly coinciding with the cutting point, or because the material was too dry and brittle. Where the core could not be cleanly sliced at the appropriate 0.5 cm interval, the actual cutting point was noted on the bag. In particular, the bottom 10 cm of Core SS906 section T5 was very brittle and fractured, and was cut at 1 cm intervals. Similarly, the bottom 4 cm of Core GT0507 section T3 and the bottom 5 cm of Core GT0507 section T4 were cut at 1 cm intervals.

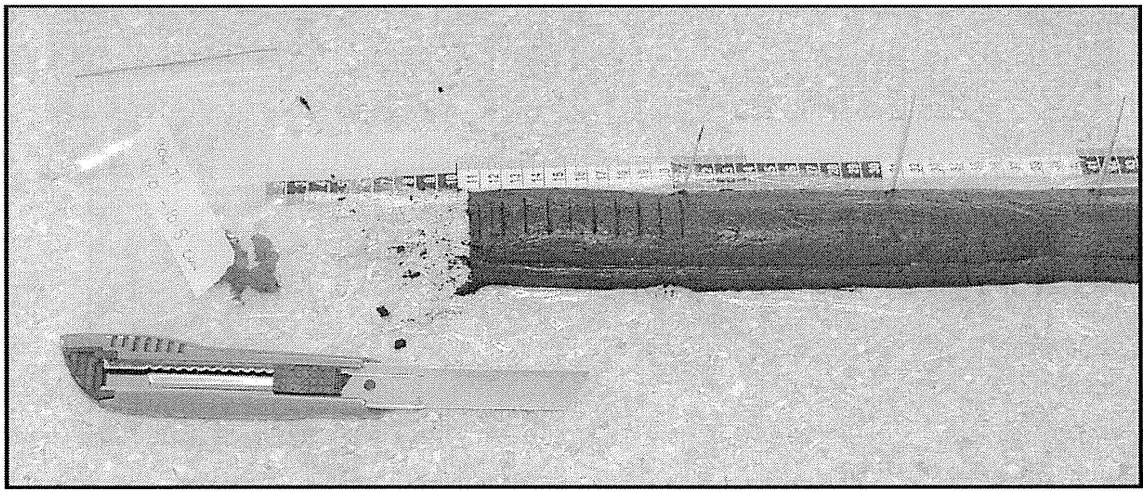

Figure 3.7: *Core sections were sliced into 0.5 cm lengths using a craft knife and placed in labelled sample bags. Toothpicks were placed in the core section at 10 cm intervals so that accurate location of the core relative to the tape measure could be maintained easily.*

3.5 Combustible Organic Carbon Content

The combustible organic carbon (COC) content of cores was determined by a loss-on-ignition (LOI) technique, similar to that used by Ballinger (2003). A scoop was taken from each sample

and placed in a ceramic crucible which had previously been weighed. Crucibles containing the samples were dried overnight in an oven at 105 °C, and cooled in a vacuum desiccator. The cooled crucibles were then weighed again, giving a dry weight for the sample.

The crucibles were placed in a furnace for at least 4 hours to combust the organic matter fully (Figure 3.8). After combustion, crucibles were placed in a desiccator to cool. Once cooled, samples were removed from the desiccator and weighed again, allowing the LOI (indicating organic carbon content) to be calculated from the change in weight. The remaining residue was brushed into a glass vial and stored (Figure 3.9).

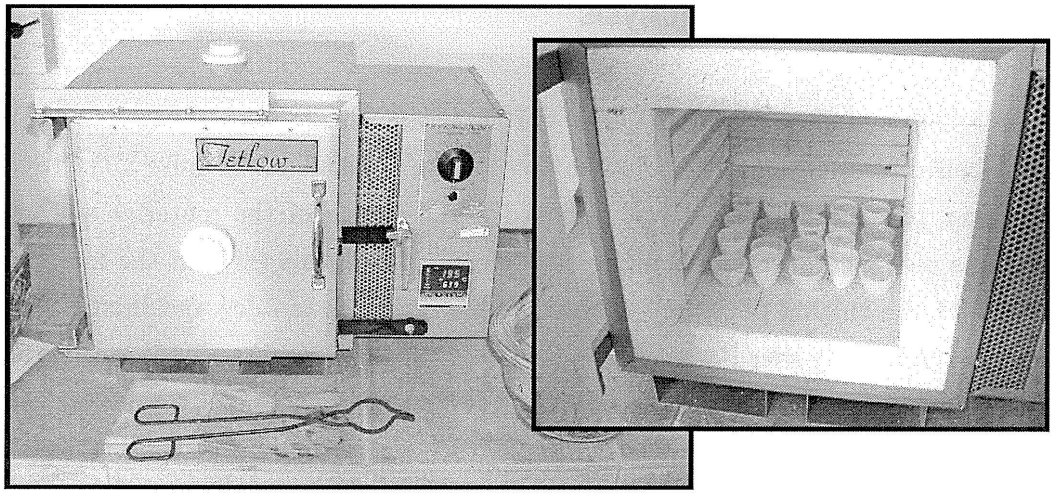

Figure 3.8: *A Jetlow furnace (left) was used to combust samples for measurement of organic carbon content.*

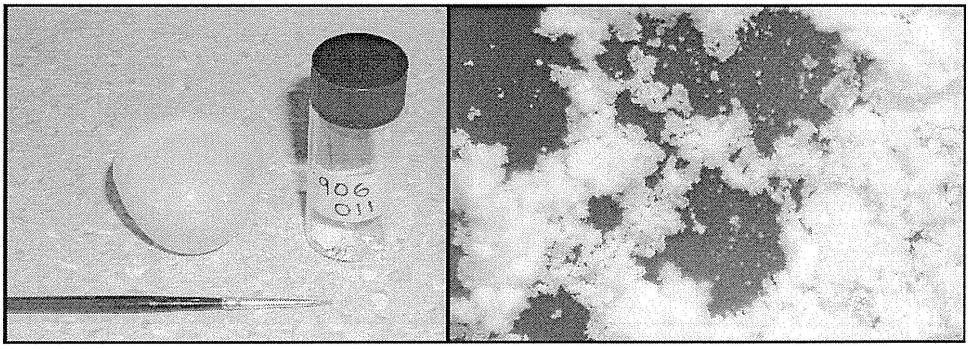

Figure 3.9: *The ash residue from each sample was brushed into a small glass vial (left) for storage. Some residue is also shown (right) magnified 60 times.*

Samples for the first 55 cm of Core SS906 Section T1 were combusted at 700 °C, in accordance with the technique used by Ballinger (2003). Subsequent samples were combusted at 500 °C, which was found to be equally effective. Samples for Core SS906 were processed at 0.5-cm intervals. For Core GT0507, every second sample was used, giving a sampling interval of 1 cm. All weights were recorded using a digital balance to an accuracy of approximately 0.0001 g. Accuracy of the results was limited in the peat-rich parts of the core due to the high moisture

content (80–90 %) and the high organic content (75–90 %) which meant that the resulting residue was very small.

3.6 Particle Size Analysis

Particle size analysis was carried out using a Malvern Mastersizer-S laser particle sizer (Figure 3.10). This technique is based on the principle that suspended particles will diffract light through different angles depending on the particle size. The laser sizer normally measures particles suspended in water, and this model is effective up to 2 mm particle size.

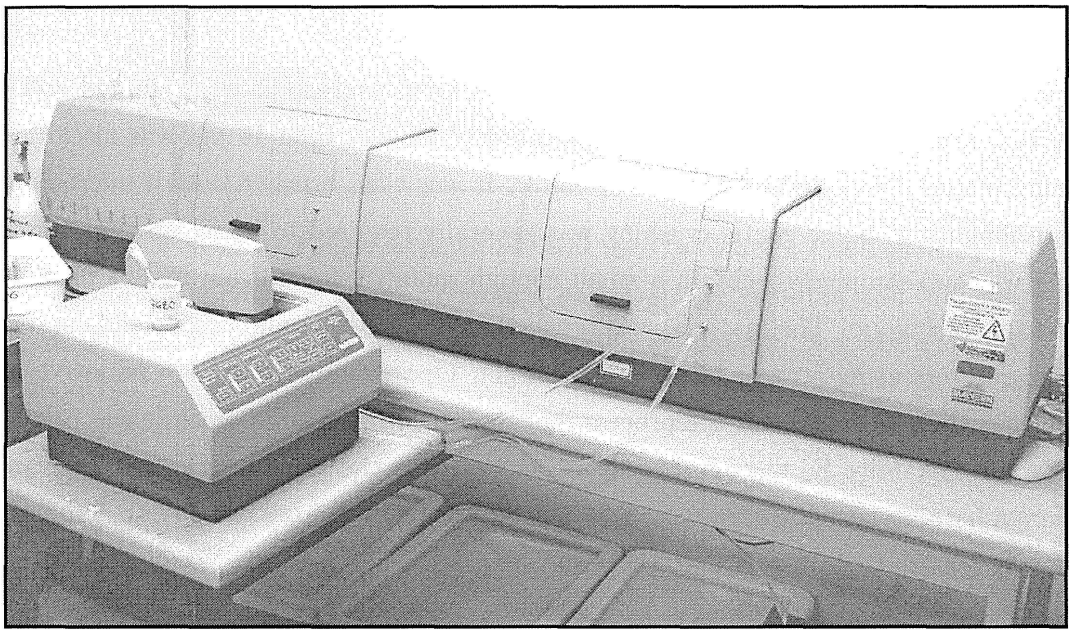

Figure 3.10: *The Malvern Mastersizer-S laser particle sizer.*

A hydrogen peroxide treatment was used to remove organic carbon prior to laser sizer analysis. A small amount of each sample (approximately half a teaspoon) was placed in a labelled beaker and covered in 27% hydrogen peroxide. The beakers were gently heated and stirred, and allowed to react. Further hydrogen peroxide was added and repeated heating and stirring continued over a period of several weeks, until all reaction ceased. The residue was washed through a 2-mm sieve to remove any particles larger than the measuring range of the laser sizer. Samples were then measured and the particle size distribution recorded. The laser sizer required only a small amount of material from the sample, which was sub-sampled using a pipette. The sample was agitated vigorously to ensure mixing as the pipette was filled.

Samples from Core SS906 sections T2–T5 were processed at 1-cm intervals, T1 being primarily Holocene peat with a very low inorganic content. Core GT0507 was also processed from 700–809 cm (section T2 and the upper 10 cm of section T3, containing the Kawakawa Tephra and sediments from the LGM and LGIT).

Examination of the laser sizer results for Core SS906 revealed several significant peaks of coarse grain size occurring in the upper part of the core, at depths of 155 cm and 130 cm. To test the validity of these peaks, the grain size of selected samples was measured independently using an optical microscope. The samples were mounted on slides (see below). To assess the grain size, slides were mounted on an auto-advancing slide holder. For any mineral grains crossed by the horizontal cross-hair of the microscope, the length of the maximum dimension of the grain was estimated using the scale on the cross-hair. The slide was then advanced and the process repeated. 30 grains were measured for each sample, and the mean grain size calculated.

3.7 Microscope Analysis

The fraction of each sample not used in the laser sizer measurement was retained and sieved, first at 25 μm then at 10 μm. The residue of material smaller than 10 μm was discarded. The remaining material was dried overnight at 35 °C. It was then brushed onto a microscope slide for grain mounting. Some gentle crushing was generally required to break up the sample. The material was sub-sampled to obtain a small enough quantity for a grain mount using a 'cone and quarter' technique. The material was brushed onto a labelled microscope slide and divided into four quarters using a razor blade (Figure 3.11). Opposite quarters were removed, and the material was then re-mixed and the process repeated until the desired amount was obtained. A drop of resin (Araldite K142) was added and mixed with the sample, and the slide was then heated on a hotplate at approximately 60 °C to thin the resin and remove any air bubbles. Once heated, a cover slip was pressed onto the resin.

Grain mounts were analysed under a petrographic microscope. A point counting method was used to assess the mineral composition of the sample. The microscope was fitted with an auto-advancing slide holder connected to a point counting machine. This allowed the slide to be scanned on a grid, with grains being counted whenever they were aligned with the crosshairs of the microscope. Where no grain was aligned with the crosshairs, the slide was advanced without any count being incremented. For Core SS906, grains were identified and counted until a total of approximately 300 was reached. Core GT0507 was found to contain a lot of phytoliths and other material of biological origin, which were counted separately from the main count. Because of the very low abundance of mineral grains, counting was continued until a total of approximately 100 mineral grains or glass shards was reached.

3.8 Tephra-Derived Glass Concentration

Examination of microscope slides showed several peaks in the volcanic glass-shard count, other than the visible tephra layer. Tephra extraction techniques were used to extract shards for geochemical investigation using electron microprobing.

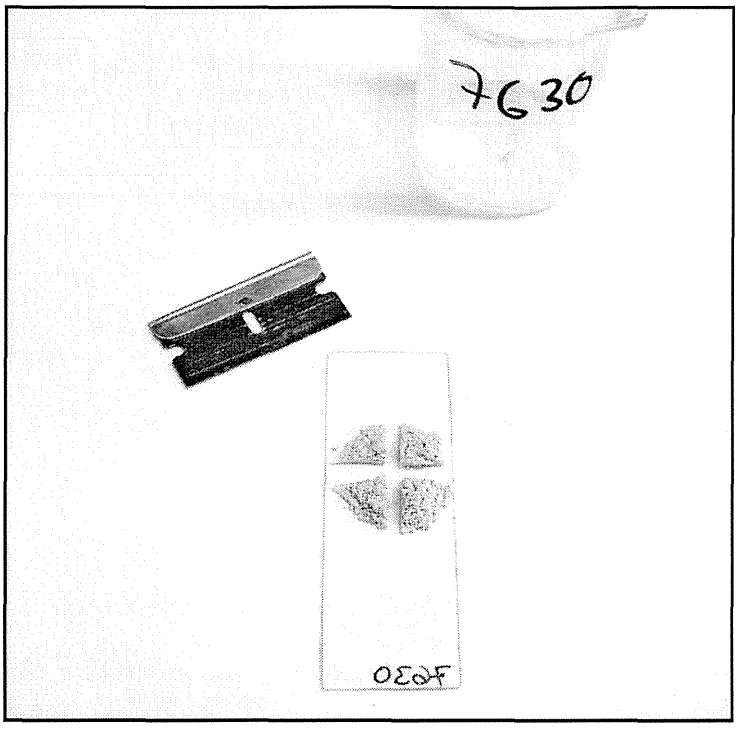

Figure 3.11: *A 'cone and quarter' technique was used to obtain a small quantity of sample for mounting on microscope slides. Opposite quarters were removed and the sample was remixed. This was repeated until the required amount of material had been obtained.*

To concentrate the shards, sodium polytungstate (SPT) heavy liquid solution was used, following a technique modified from Turney (1998). SPT is a dense crystal which can be dissolved in water to produce a solution of any density from that of water to about 3 g cm^{-3}. It has low toxicity and can be recovered and reused by filtration and evaporation. A flowchart illustrating the heavy liquid separation method is shown in Figure 3.12.

SPT solution was diluted with distilled water to obtain a solution with a density of 2.51 g cm^{-3}. Solution density was measured during dilution using a small glass disk of known density. The solution was adjusted until neutral buoyancy was observed. The process shown in Figure 3.12 was then used to separate the sample, resulting in almost all the mineral component being removed in the 'sink' portion. Some mica and a significant quantity of organic remnants (mostly plant silicates) were included in the 'float' portion. In order to further separate the samples, SPT solution with a density of 2.35 g cm^{-3} was mixed, and the process was repeated. For all steps, the 'float' and 'sink' portions were washed as shown in the second stage of Figure 3.12, dried, and checked for tephra-derived glass shards. It was noted that at a density of 2.35 g cm^{-3}, most tephra shards floated, along with some of the organic material, while the majority of the remaining mica was removed in the 'sink' portion.

Glass shards were hand-picked from the separated samples using a needle and a stereoscopic microscope. Shards were collected in water in small plastic sample tubes. For samples 220, 240, 272 and 274, large numbers of shards were present, and picking was done using a bulk technique whereby all shards were collected from a small area of the sample. Samples 164, 166 and 198

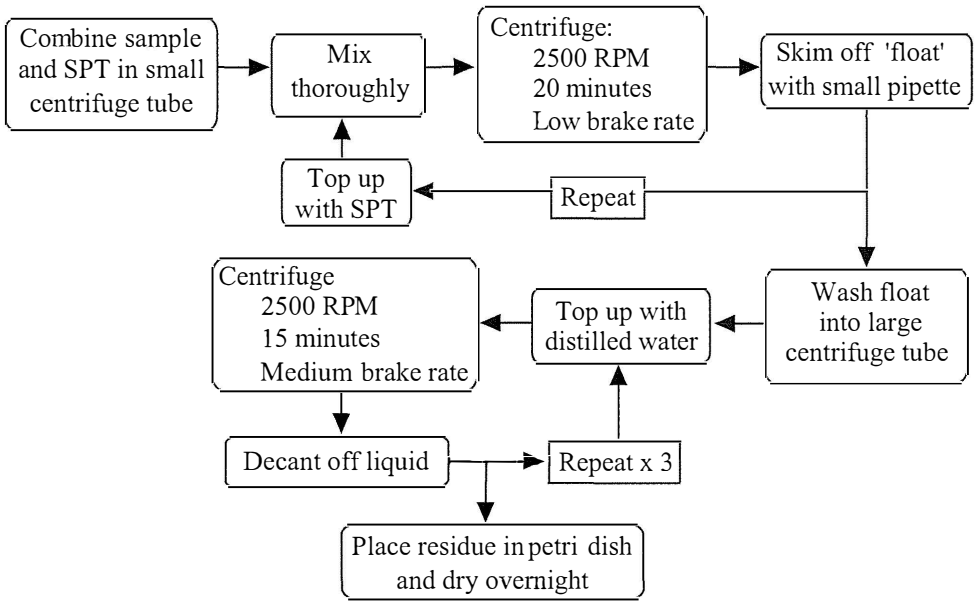

Figure 3.12: *Sodium polytungstate (SPT) heavy liquid separation technique. The initial centrifuge step was repeated twice to ensure good separation. Washing of the 'float' portion in distilled water was repeated three times to remove any SPT residue from the grains. Where retention of the 'sink' portion was required, the same washing technique was employed.*

contained only very rare shards even after separation with SPT, so a thorough search of the concentrated portion was carried out for these samples.

3.9 Electron Microprobe Analysis

Electron microprobe analysis of glass shards was carried out at The University of Auckland, using a converted JEOL JSM-840A SEM. This instrument has been rebuilt to JXA-840A EPMA (electron probe micro-analyser) specifications, with the inclusion of three JEOL WDS X-Ray spectrometers and a Princeton Gamma-Tech Prism 2000 Si(Li) EDS X-Ray detector.

For microprobe analysis of tephra, an accelerating voltage of 15 kV and beam current of 1.5 nA were used. Electron beam analytical spot diameter was approximately 15 microns, and samples were probed for 100 s to determine the concentrations of 14 elements. Samples where the analytical total was less than 90% were rejected, and the results were then normalised to 100%, the missing fraction being attributed to hydration of the glass (Stokes *et al.*, 1992).

Suitable shards were selected using a visual search of the slide, and these were probed. Where possible, 10 or more shards were probed, although the limited number of suitable shards on some slides made this impossible.

Chapter 4

Stratigraphy and Chronology

This chapter presents the stratigraphy and chronology of the cores studied. A detailed stratigraphic description was carried out on split core sections before they were sub-sampled for laboratory analysis. The correlation methods used to match the results of this study with previous dating and pollen data are described. The age model of the sites (based on ^{14}C dating, luminescence dating and tephrochronology) is also given.

4.1 Site Stratigraphy

All three sites studied show distinct bands rich in terrigenous mineral grains, alternating with dark reddish-brown peaty material. Some cores contain fine laminated silts which were probably deposited by direct inwash of melt-water from an adjacent glacier. Changes in the local environment are represented by changes in the rate of organic and terrigenous deposition in the cores. Full core logs are included in Appendix A.

4.1.1 Skiffington Swamp

Figure 4.1 shows a summary of the stratigraphy of Core SS906 (Skiffington Swamp). The lowest 25 cm of material recovered was fine laminated silt with strong light and dark bands, and was interpreted to have originated from direct inwash of melt-water as ice receded from the site (Figure 4.2).

Above the laminated silt there was an abrupt change to dark, organic-rich silt, indicating a lowered rate of terrigenous sediment after ice retreat in the area. Dark brown organic silt continued to a depth of c. 290 cm, above which there was a change to olive-grey silt, representing a significant change in the environment and an increase in the terrigenous sediment input (Figure 4.3).

This olive-grey silt unit contained a macroscopic tephra layer, identified by its yellowish colour (Figure 4.4). The tephra was c. 2 cm thick and the transition from silt to tephra occurred smoothly over about 0.5 cm, indicating some reworking or mixing of tephra with the sediment

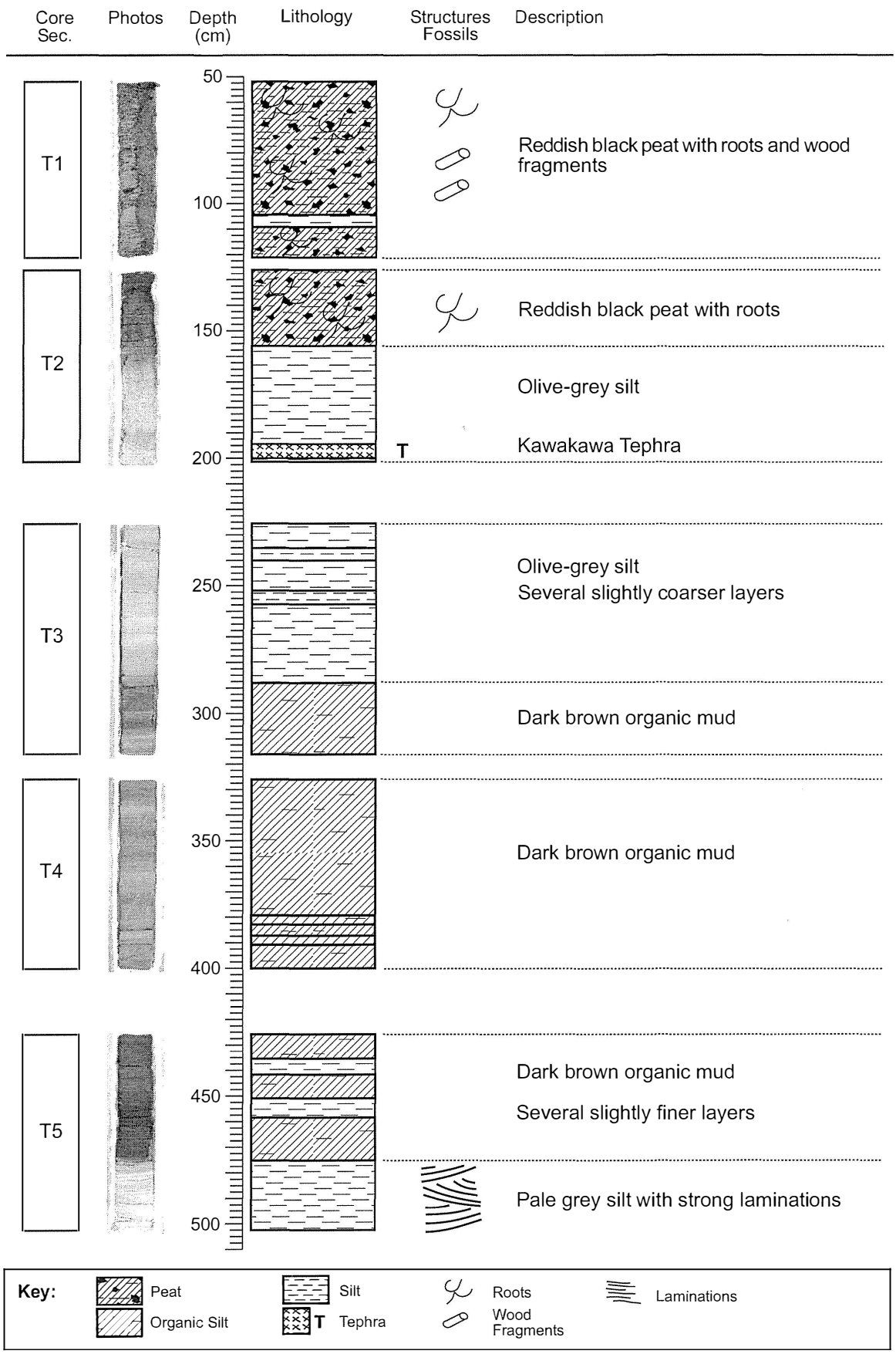

Figure 4.1: *Summary of stratigraphy from Core SS906 (Skiffington Swamp).*

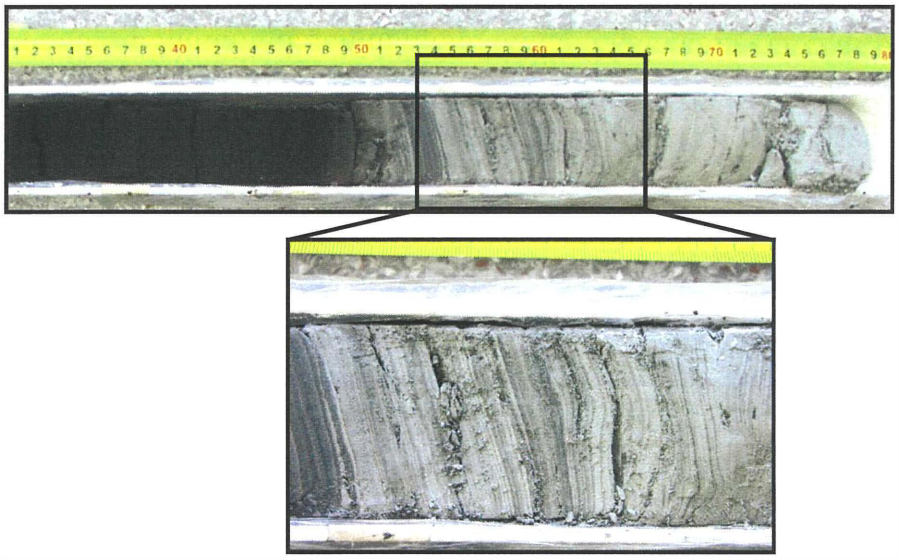

Figure 4.2: *Laminated silt from the bottom of Core SS906. The lower photo illustrates the fine nature of the light and dark bands.*

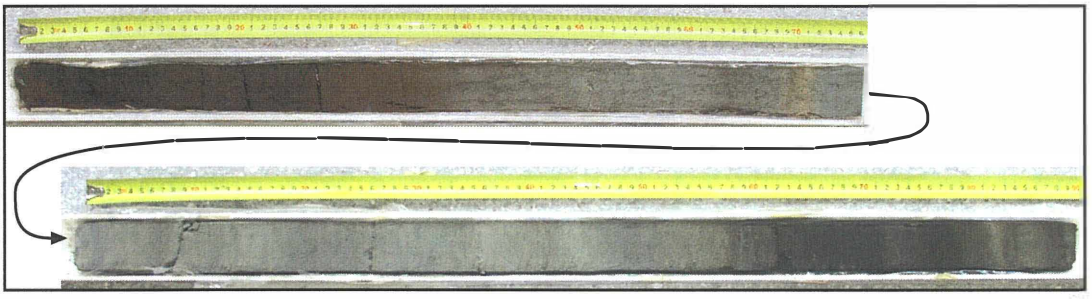

Figure 4.3: *Sections T2 (top) and T3 from Core SS906, showing the olive-grey silt unit between darker organic silt (below) and peat (above). The top of each core section is at the left of the photo. The Kawakawa Tephra occurs at 70 cm depth from the top of section T2, and the olive-grey silt was interpreted as representing the LGM cold period.*

above and below.

Several plant macrofossils (identified as spore pods of the aquatic plant *Isoetes kirkii*) were found directly beneath the tephra (Figure 4.5), and were interpreted to have been trapped and preserved by the tephra fall because they were not observed anywhere else in the core. Based on stratigraphic position and previous studies, the tephra was identified as the Aokautere Ash member of the Kawakawa Tephra (dated at c. 26,500 cal. years B.P.), and is referred to simply as 'Kawakawa Tephra' in this study. This interpretation was confirmed by glass geochemistry (see below). A gradual change from olive-grey silt to reddish-black peat occurred at a depth of c. 160 cm. The upper part of the core was dark, highly organic peat with roots and occasional wood fragments (Figure 4.6).

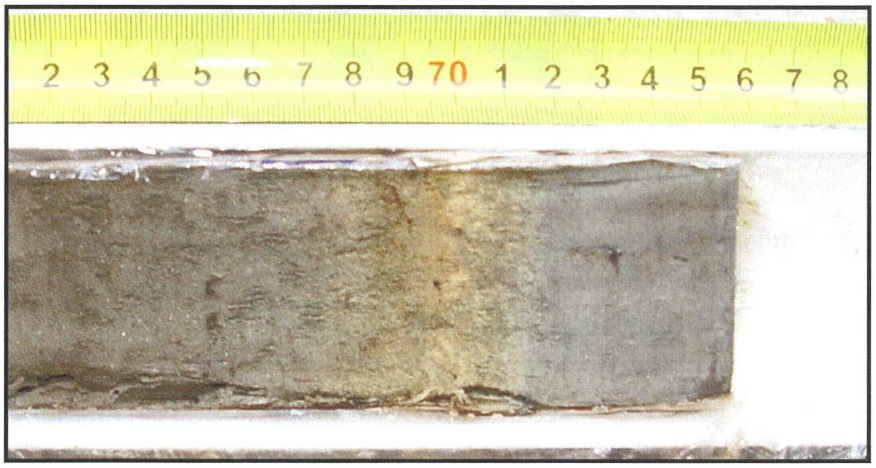

Figure 4.4: *Kawakawa Tephra at the bottom of section T2 in Core SS906 (70–72 cm).*

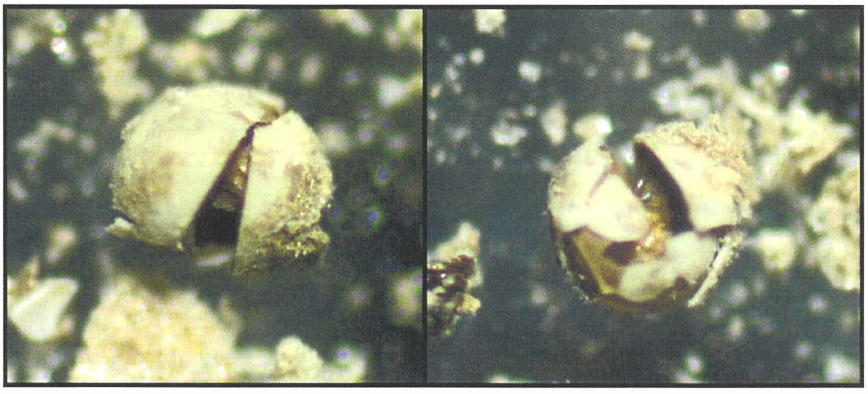

Figure 4.5: *Plant macrofossils recovered from below the Kawakawa Tephra in Core GT0507. The macrofossils are c. 0.5 mm in diameter and have been identified as spore pods of the aquatic plant* Isoetes kirkii. *They were also found in samples from below the tephra in Core SS906, indicating that both sites contained a lake at the time (c. 26,500 cal. years B.P.).*

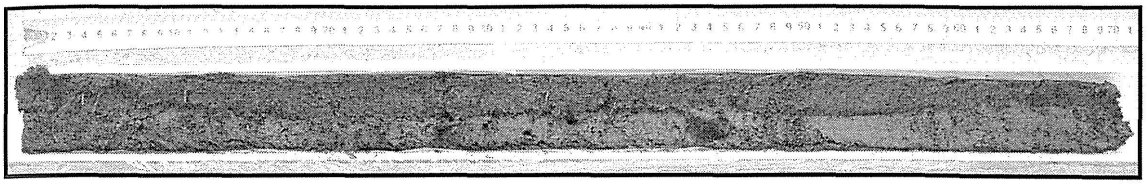

Figure 4.6: *Dark brown peat containing roots and occasional wood fragments, from the top section (T1) of Core SS906.*

4.1.2 Galway Tarn

Figure 4.7 shows a summary of the stratigraphy of Core GT0507 (Galway Tarn). This core did not have any basal laminated silt unit. However, the field notes state "Corer bent; hit base", indicating that impenetrable morainic material was reached. The field notes indicate that some previous cores collected from Galway Tarn did contain a thin basal silt layer, and so some inwash of glacial melt water to the site is likely to have occurred during ice recession.

The lower part of the core (sections T3 and T4) was comprised of dark brown, highly organic gyttja. Within this, slight colour changes were seen, and there were some distinct layers which appeared more 'peaty' and fibrous (Figure 4.8). These were most evident between 810 cm and 860 cm. Above 805 cm, the material recovered was slightly more grey-brown in colour, and lacked the fibrous nature of the gyttja below.

A tephra layer occurred at a depth of 766 cm (Figure 4.9). It was 1 cm thick and had sharp upper and lower contacts. A number of plant macrofossils were found at the bottom contact of the tephra, similar to those found at Skiffington Swamp. Based on stratigraphic position, previous studies and correlation with other sites, the tephra was identified as the Kawakawa Tephra. The increased thickness and less distinct boundaries of the tephra in Core SS906 are likely to have resulted from the reworking of material by lake focussing processes or by inwash of tephra from the surrounding catchment, or both. The small lake size, greater water depth and very small catchment area of Galway Tarn meant that reworking of material on the lake bottom was minimised.

Above the tephra, a layer occurred which was slightly more grey in colour. A very fine grey silt layer was also noted at a depth of 722 cm. There was a noticeable change to a dark reddish-brown peaty gyttja at a depth of 658 cm. In general, the Galway Tarn core had a much higher organic content than the Skiffington Swamp core.

4.1.3 Okarito Pakihi

Cores from Okarito Pakihi were not logged in this study, but the stratigraphy of the bog has been described by Vandergoes (2000). Cores from Okarito Pakihi typically contain a basal laminated silt similar to that seen at Skiffington Swamp, with a silty layer above this. This is generally

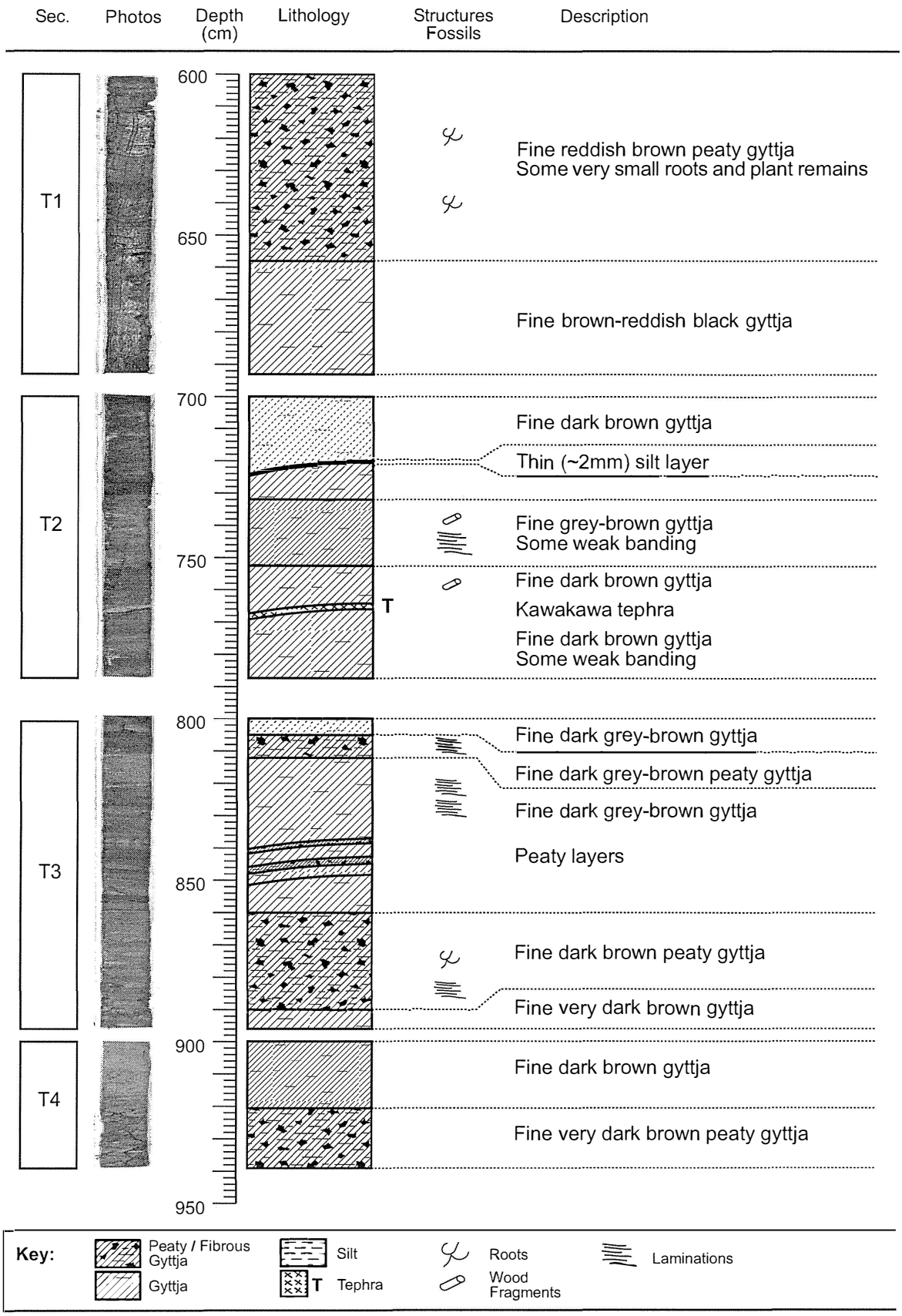

Figure 4.7: *Summary of stratigraphy from Core GT0507 (Galway Tarn).*

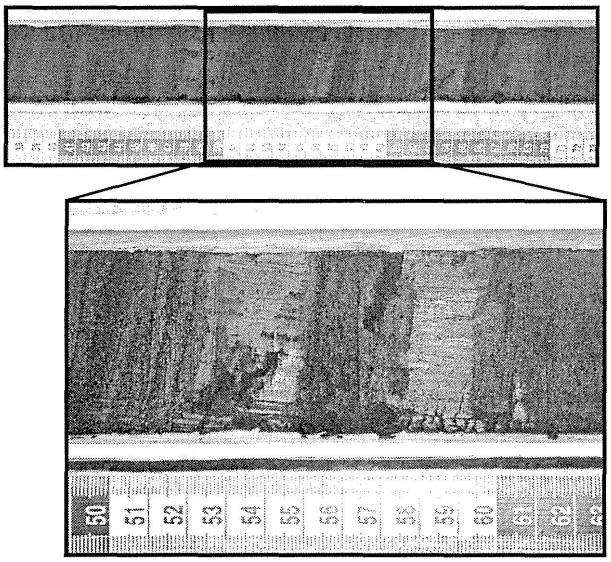

Figure 4.8: *Part of section T3 from Core GT0507, showing peaty gyttja with alternating fibrous layers. The lower photo shows a close-up of the fine layering seen in this core.*

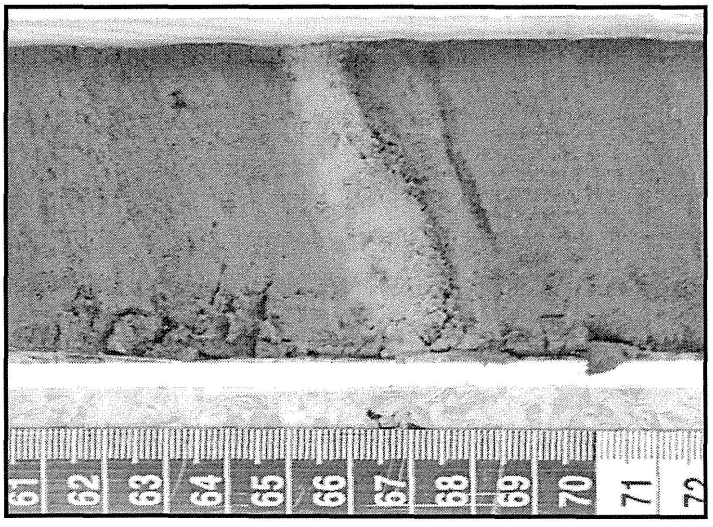

Figure 4.9: *Kawakawa Tephra in Core GT0507. The tephra layer in Core GT0507 is thinner and has sharper contacts with the sediment above and below than in Core SS906.*

followed by a highly organic or peaty layer, then a return to blue-grey or olive-grey silt similar to that seen at Skiffington Swamp, and also containing a tephra layer. However, the tephra layer at Okarito Pakihi is often difficult to see in the field and requires microscope examination to locate. The upper parts of cores from Okarito Pakihi are generally a mix of dark brown organic silt and peat.

4.2 Volcanic Glass Major Element Composition

As previously mentioned, cores collected from Skiffington Swamp and Galway Tarn contained a macroscopic tephra layer. During analysis of the mineralogy for samples from Core SS906 (using a point counting method), a number of small peaks in glass shard concentration were also noted above the macroscopic tephra layer (Figure 4.10).

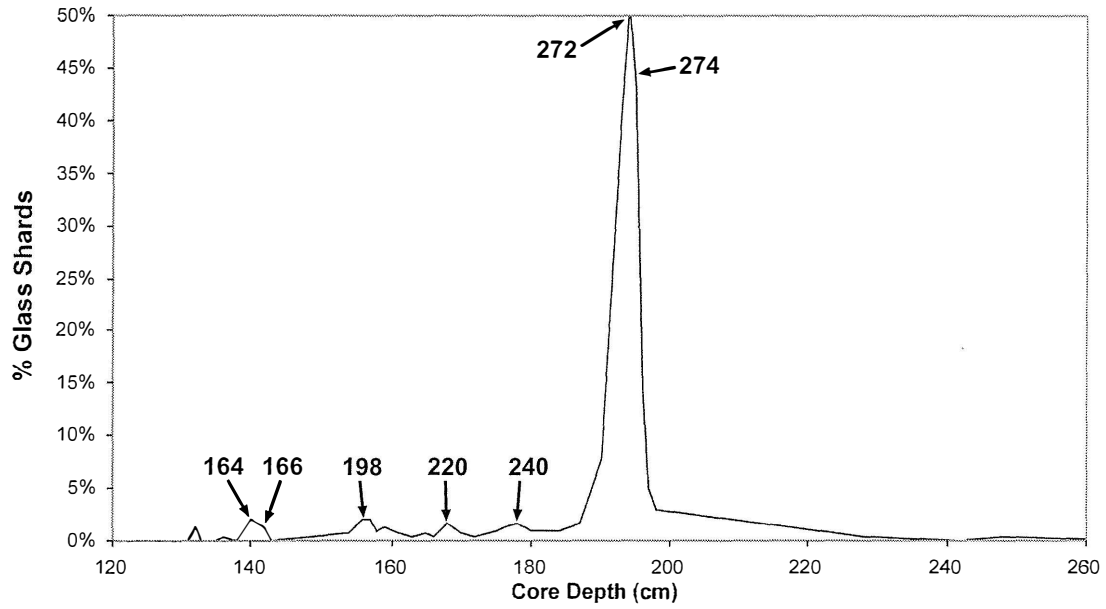

Figure 4.10: *Glass shard counts for Core SS906 (Skiffington Swamp). The shard concentration is expressed as a percentage of the total count of inorganic grains for the sample. The labels identify the location and sample number of samples concentrated for microprobe analysis.*

Other studies have noted the presence of volcanic glass shards from the Kawakawa Tephra (Aokautere Ash member) in North and South Westland. Mew *et al.* (1986) identified Kawakawa Tephra in a loess deposit in the Grey River valley, North Westland, where it was preserved as a macroscopic layer. Identification was by glass major element chemistry and mineralogy. Almond (1996) used the occurrence of glass shards from the Kawakawa Tephra in loess to constrain the age of deposition for loess sheets in South Westland. Vandergoes *et al.* (2005) have previously identified the tephra in cores from the study area as Kawakawa Tephra based on major element chemistry.

Table 4.1: Composition of glass shards recovered from Core SS906 (Skiffington Swamp, South Westland). For each sample, the mean and standard deviation (in brackets) are shown, along with the number of shards probed (n). All values are in weight percent and have been normalised to a total of 100 %. Various other results are also shown for comparison.

	SiO_2	Al_2O_3	TiO_2	FeO†	MnO	MgO	CaO	Na_2O	K_2O	Cl	n
164	77.53	12.35	0.14	1.07	0.04	0.03	1.15	4.60	3.13	0.14	8
	(0.84)	(0.42)	(0.09)	(0.26)	(0.03)	(0.05)	(0.13)	(0.26)	(0.22)	(0.03)	
166	77.30	12.44	0.15	1.07	0.08	0.09	1.14	4.65	3.14	0.17	12
	(0.69)	(0.66)	(0.08)	(0.15)	(0.07)	(0.10)	(0.10)	(0.23)	(0.16)	(0.03)	
198	77.51	12.19	0.19	1.05	0.06	0.09	1.15	4.44	3.31	0.19	3
	(0.37)	(0.09)	(0.04)	(0.16)	(0.07)	(0.11)	(0.20)	(0.14)	(0.43)	(0.03)	
220	77.45	12.40	0.17	1.05	0.07	0.06	1.12	4.59	3.14	0.16	12
	(0.58)	(0.61)	(0.07)	(0.11)	(0.04)	(0.06)	(0.05)	(0.21)	(0.10)	(0.04)	
240	77.59	12.26	0.13	1.04	0.11	0.08	1.05	4.46	3.26	0.18	11
	(0.27)	(0.10)	(0.09)	(0.10)	(0.06)	(0.08)	(0.06)	(0.18)	(0.19)	(0.05)	
272	77.32	12.21	0.15	1.08	0.09	0.05	1.08	4.71	3.28	0.18	12
	(0.27)	(0.14)	(0.04)	(0.09)	(0.06)	(0.08)	(0.09)	(0.20)	(0.11)	(0.03)	
274	77.40	12.22	0.15	1.13	0.06	0.11	1.09	4.60	3.17	0.17	13
	(0.39)	(0.16)	(0.05)	(0.11)	(0.05)	(0.09)	(0.07)	(0.25)	(0.09)	(0.02)	
***1a**	78.04	12.65	0.14	1.13	0.06	0.13	1.02	3.34	3.27	0.20	20
	(0.30)	(0.15)	(0.03)	(0.10)	(0.06)	(0.02)	(0.07)	(0.41)	(0.34)	(0.05)	
***1b**	77.75	12.59	0.13	1.13	0.08	0.13	1.04	3.79	3.06	0.23	20
	(0.36)	(0.16)	(0.03)	(0.13)	(0.05)	(0.03)	(0.06)	(0.24)	(0.11)	(0.16)	
***1c**	77.88	12.55	0.15	1.09	0.09	0.12	1.03	3.75	3.13	0.18	20
	(0.38)	(0.19)	(0.03)	(0.13)	(0.05)	(0.03)	(0.07)	(0.28)	(0.16)	(0.03)	
***2**	78.55	12.03	0.12	1.17	-	0.12	1.09	3.62	3.10	0.21	24
	(0.27)	(0.13)	(0.03)	(0.05)		(0.02)	(0.06)	(0.11)	(0.13)	(0.02)	
***3**	78.69	12.25	0.12	1.17	-	0.12	1.05	3.42	3.05	0.18	275
	(0.46)	(0.23)	(0.03)	(0.10)		(0.02)	(0.09)	(0.29)	(0.20)	(0.04)	
***4**	78.74	12.53	0.10	1.16	-	0.13	1.08	3.76	2.49	-	32
	(0.42)	(0.20)	(0.03)	(0.12)		(0.02)	(0.10)	(0.11)	(0.50)		
***5**	77.89	12.63	0.13	1.19	0.06	0.15	1.23	3.51	3.06	0.16	10
	(0.48)	(0.67)	(0.05)	(0.11)	(0.09)	(0.03)	(0.10)	(0.22)	(0.14)	(0.05)	

†Total Fe expressed as FeO

Results from other studies:

*1a, *1b, *1c: Previous results from Okarito Pakihi, Galway Tarn and Skiffington Swamp, respectively (Newnham *et al.*, 2006)

*2: Type locality for Aokautere Ash, Aokautere (Pillans *et al.*, 1993)

*3: Kawakawa Tephra in various marine cores from the Southwest Pacific (Carter *et al.*, 1995)

*4: Kawakawa Tephra from the Grey River valley, North Westland (Mew *et al.*, 1986)

*5: Kawakawa Tephra in cores from Lake Poukawa, Hawkes Bay (Shane *et al.*, 2002)

In order to positively identify the visible tephra layer, and to determine if other peaks in glass shard concentration were 'cryptic' deposits from other eruptions or reworked material from the same tephra, major element analysis of glass shards was carried out. Shards were concentrated from the macroscopic tephra and from selected samples where a peak in the glass shard concentration had been noted, and electron microprobe (EMP) analysis was used to produce a geochemical 'fingerprint' for the tephra. Table 4.1 shows a summary of glass composition as measured by EMP. Full results are given in Appendix B.

Figure 4.11 shows bivariate plots of several selected oxides. The results for individual shards are displayed, showing the distribution of compositions in relation to the published results from other studies. Figure 4.12 shows the mean values for shards from each sample.

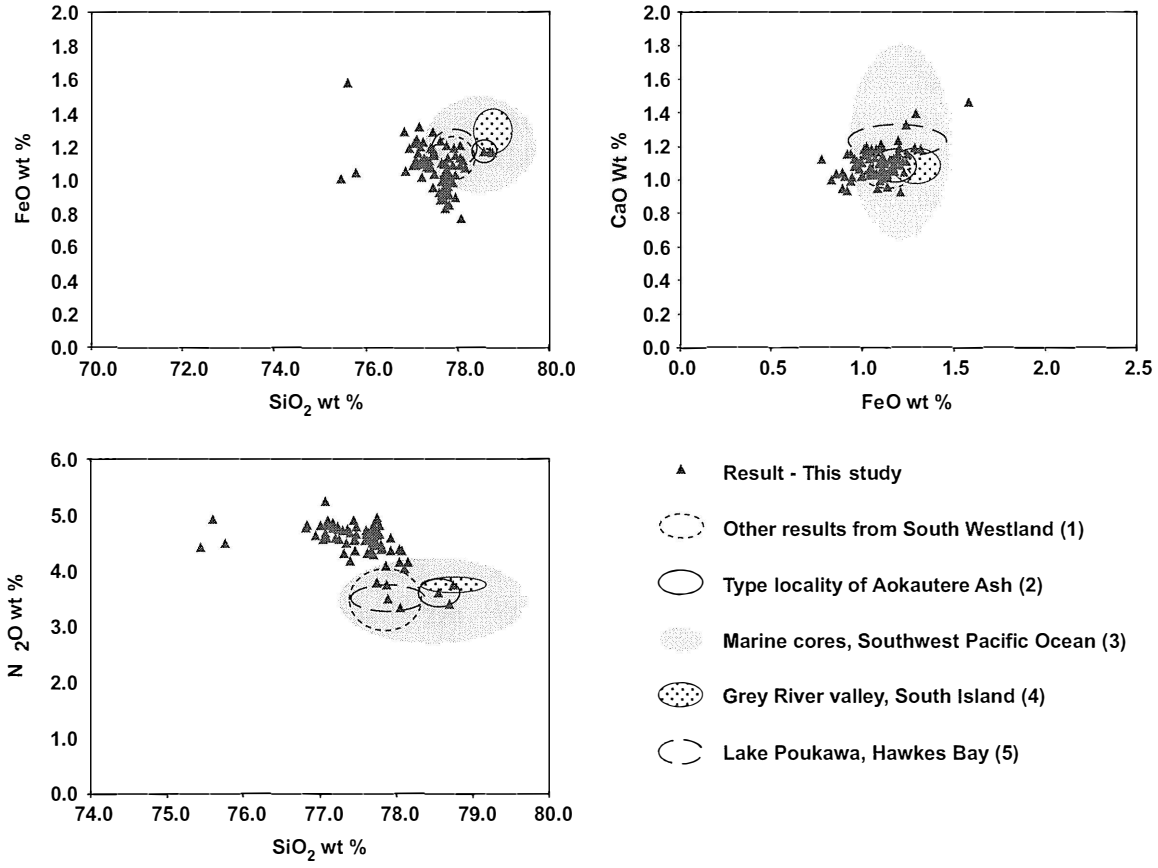

Figure 4.11: *Scatter plots of major oxides for EMP data from Core SS906. Triangle symbols show individual shard results for this study. The results from various other studies are also shown as areas representing the mean of all results plus/minus one standard deviation: (1) Previous shard analysis for glass from the study area (Newnham et al., 2006); (2) Type locality for Aokautere Ash, Aokautere (Pillans et al., 1993); (3) Kawakawa Tephra in various marine cores from the Southwest Pacific (Carter et al., 1995); (4) Kawakawa Tephra from the Grey River valley, North Westland (Mew et al., 1986); (5) Kawakawa Tephra in cores from Lake Poukawa, Hawkes Bay (Shane et al., 2002).*

The results from this study were closely grouped. The main points of note are slightly higher Na_2O content and correspondingly lower SiO_2 content when compared to previous studies. The

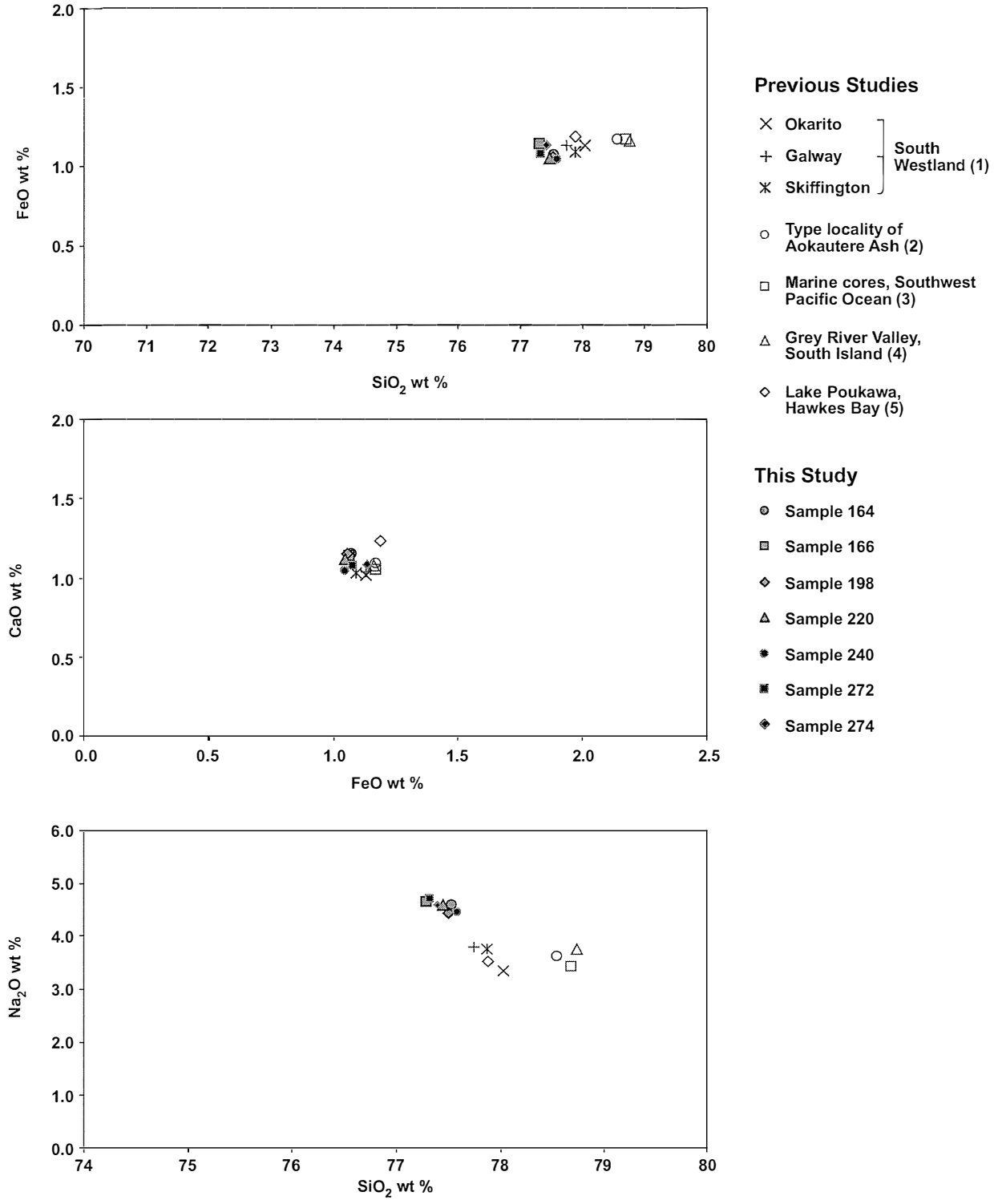

Figure 4.12: *Major oxide data for Core SS906. Solid symbols show the mean of all shards for each sample in this study. The results from various other studies are also shown (hollow symbols): (1) Previous shard analysis for glass from the study area (Newnham et al., 2006); (2) Type locality for Aokautere Ash, Aokautere (Pillans et al., 1993); (3) Kawakawa Tephra in various marine cores from the Southwest Pacific (Carter et al., 1995); (4) Kawakawa Tephra from the Grey River valley, North Westland (Mew et al., 1986); (5) Kawakawa Tephra in cores from Lake Poukawa, Hawkes Bay (Shane et al., 2002).*

variation in Na_2O and SiO_2 has probably resulted from improved probing conditions at the University of Auckland laboratory (all analyses for previous studies shown here were carried out at Victoria University of Wellington) (Lowe *et al.*, 1999).

The plot of mean results for each sample shows a close grouping with previous results. No sample shows any clear separation from the known Kawakawa Tephra distribution. Therefore, two conclusions can be made: the macroscopic tephra seen in Skiffington Swamp (Core SS906) is Kawakawa Tephra, and small peaks in glass shard counts above this tephra in the core are the result of reworking of tephra deposits from the surrounding catchment, or post-depositional mixing in the lake sediments, or both.

4.3 Correlation, Dating and Sedimentation Rates

All sample measurements were taken in centimetres (cm) from the top of each core section, and then converted to absolute depth at the site based on the original measurements recorded in field logs. The pollen data, dating and age models used in this study are from previous work in the study area (Vandergoes, 2000; Vandergoes and Fitzsimons, 2003; Vandergoes and Prior, 2003; Newnham *et al.*, 2005; Vandergoes *et al.*, 2005; M. J. Vandergoes *et al.*, unpublished data). As the pollen work and dating were carried out on different cores from those described in this study, correlation between cores was necessary. This was facilitated by identifying key stratigraphic tie-points in the two cores (for example, the Kawakawa Tephra layer) and then adjusting the depths of these points in the pollen or dating data to match the depth in the core used for this study. Depths for intermediate data points were stretched using a linear interpolation. The method and the calculations used are described in Appendix C. Ages are presented here in calibrated years before present unless otherwise stated. For ^{14}C dates, calibrated years were determined using the INTCAL98 calibration (Stuiver *et al.*, 1998). As an indicator of the sedimentation patterns at the sites studied, sample depths were plotted against ages for each site, and approximate sedimentation rates were calculated.

4.3.1 Skiffington Swamp

Pollen data for the Skiffington Swamp site were taken from Core 908, located within a few metres of Core SS906. The stratigraphy of Core 908 was very similar to that of SS906. The pollen data were correlated to the sedimentology of Core SS906 based on the stratigraphic tie-points shown in Table 4.2.

Some ^{14}C dating of material from Skiffington Swamp has previously been undertaken but the results were unsatisfactory. Many dates appeared to be far too young and exhibited age reversals with increasing depth, indicating that many Skiffington Swamp samples had been exposed to contamination by younger carbon (Newnham *et al.*, 2005). For this study, the only chronology is given by the Kawakawa Tephra, dated at c. 26,500 cal. years B.P. An approximate age/depth

Table 4.2: *Stratigraphic tie-points used to correlate the sediments of Core SS906 with pollen data from Core 908.*

Core SS906 Depth	Core 908 Depth	Description
475 cm	475 cm	Top of basal laminated silt
288 cm	282 cm	Transition from organic silt to olive-grey silt
195 cm	206 cm	Top of Kawakawa Tephra
156 cm	175 cm	Transition from olive-grey silt to fibrous sedge peat

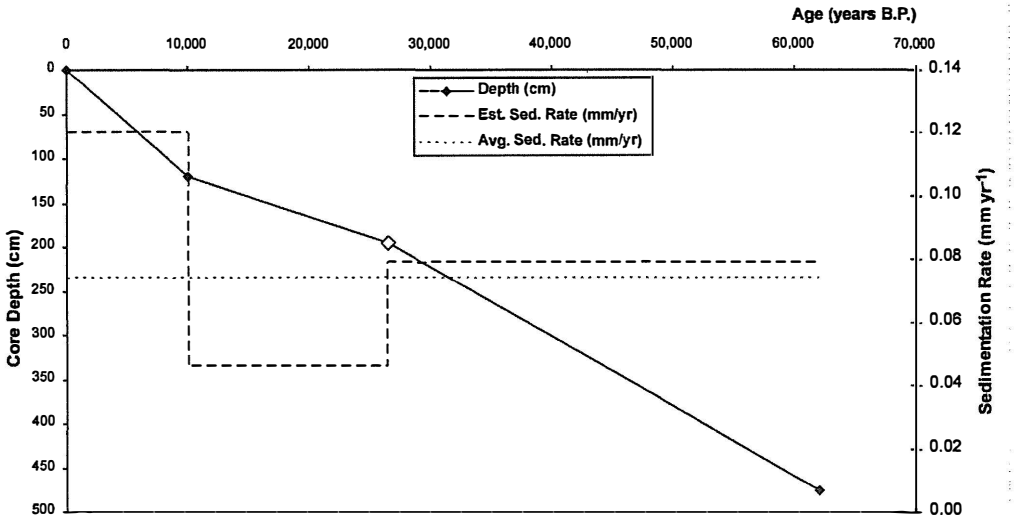

Figure 4.13: *Age/depth model for Skiffington Swamp. The hollow diamond represents the Kawakawa Tephra (196 cm depth, c. 26,500 cal. years B.P.). Other points are estimated based on the following: An approximate age of 10,000 cal. years B.P. for the establishment of dominant forest pollen in the pollen data; an approximate age for the base of the site of 62,000 cal. years B.P., based on correlation with the Okarito Pakihi site. The average sedimentation rate ('Avg. Sed. Rate') shown is for the period after the deposition of Kawakawa Tephra.*

relationship is shown in Figure 4.13, with an estimation of sedimentation rates. The pattern of lower sedimentation rate during the middle (LGM) part of the record agrees well with that from other sites.

4.3.2 Galway Tarn

Pollen data for the Galway Tarn site were taken from Core 0111. The Core 0111 site was slightly shallower than that of GT0507, but the two sites had broadly similar stratigraphies. Pollen data and dating were correlated based on the stratigraphic tie-points shown in Table 4.3. A number of ^{14}C dates were obtained from Galway Tarn samples and are shown in Table 4.4. AMS ^{14}C dating of pollen concentrates appeared to generally (but not always) give the best results, while several plant macrofossils returned anomalously young ages. A preliminary chronology for Core GT0507 was produced from ^{14}C dates of pollen separates and the Kawakawa Tephra. This was correlated along with the pollen from Core 0111 (Newnham *et al.*, 2005; M. J. Vandergoes, unpublished data).

Table 4.3: *Stratigraphic tie-points used to correlate the sediments of Core GT0507 with pollen data and dating from Core 0111.*

Core GT0507 Depth	Core 0111 Depth	Description
940 cm	897 cm	Bottom of core (impenetrable basal material)
766 cm	701.5 cm	Top of Kawakawa Tephra
658 cm	670 cm	Transition from fine reddisn-brown gyttja to peaty gyttja

The dates shown in Table 4.4 were used to construct an age/depth model for the site (Figure 4.14). An estimation of sedimentation rates suggests that the rate of sedimentation was lowest from c. 28,000–18,000 cal. years B.P. (including the LGM). Using the Kawakawa Tephra as a reference point, the average sedimentation rate has been 0.12 mm yr^{-1} for the last c. 26,500 cal. years. The Holocene sedimentation rate was higher, although this may also be influenced by increased compaction of more deeply buried sediments. The average sedimentation rate at the LGM (as defined by the Kawakawa Tephra) was c. 0.07 mm yr^{-1}.

4.3.3 Okarito Pakihi

Pollen data for the Okarito Pakihi site were taken from Core OKA1 for the Holocene and last glacial period, and Core OP913 for the earlier part of the record. Pollen data and dating were correlated based on the stratigraphic tie-points shown in Table 4.5.

Table 4.4: *Dating used for Galway Tarn, from M. J. Vandergoes (unpublished data). Depths have been adjusted to correlate with Core GT0507. Calibrated years were determined using the INTCAL98 calibration (Stuiver et al., 1998).*

Depth (cm adjusted)	Source	Lab #	^{14}C Age (yr BP)	Cal. Age (yr BP)
653	^{14}C Date	OS-37966	11,900 ± 60	13,858
678	^{14}C Date	OS-37967	12,500 ± 50	14,856
691	^{14}C Date	OS-37968	13,050 ± 60	15,395
716	^{14}C Date	OS-37969	13,550 ± 55	16,289
718	^{14}C Date	OS-42543	14,450 ± 65	17,332
721	^{14}C Date	OS-42544	14,900 ± 60	17,855
724	^{14}C Date	OS-37970	16,100 ± 110	19,231
745	^{14}C Date	OS-42541	19,150 ± 85	22,771
755	^{14}C Date	OS-42542	19,800 ± 120	23,449
766	Kawakawa Tephra		22,590 ± 230*	26,500
776	^{14}C Date	OS-42545	24,100 ± 120	28,223
777	^{14}C Date	OS-42546	24,600 ± 170	28,547
899	^{14}C Date	OS-42941	44,800 ± 770	44,900

* Froggat and Lowe (1990); Wilson et al. (1988)

A number of ^{14}C and luminescence dates have been obtained for samples from Okarito Pakihi (Table 4.6 and Table 4.7). As with other sites in South Westland, contamination of samples by younger carbon affected ^{14}C dates. AMS ^{14}C dates on pollen concentrates were found to give the oldest ages and were considered to be the most reliable. Luminescence dating was used on the lower silt layers which were beyond the c. 55,000 cal. year range of ^{14}C dating. Although large uncertainties exist in the luminescence dates, they give a broad framework for the earliest events recorded at Okarito Pakihi.

The dates were used to construct an age/depth model for the site (Figure 4.15). As with other sites, a lower rate of sedimentation was seen during the middle part of the core (encompassing the LGM), with a rise in sedimentation rate occurring after c. 18,000 cal. years B.P. The average sedimentation rate for the last c. 26,500 cal. years was 0.154 mm yr^{-1}, whereas the average between c. 60,000 and 20,000 cal. years B.P. was c. 0.05 mm yr^{-1}.

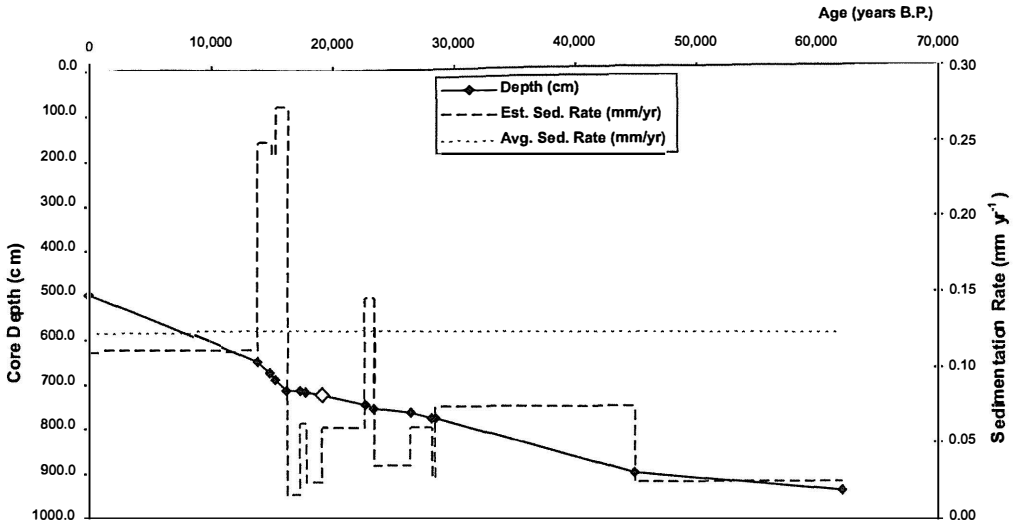

Figure 4.14: *Age/depth model for Galway Tarn. The hollow diamond represents the Kawakawa Tephra (766 cm depth, c. 26,500 cal. years B.P.). Other points based on ^{14}C dating and correlation with Okarito Pakihi (age for base of site). The average sedimentation rate ('Avg. Sed. Rate') shown is for the period after the deposition of Kawakawa Tephra. The Holocene sedimentation rate is approximate because the deposited material was unconsolidated gyttja and the upper surface was not clearly defined (the depth of 500 cm was approximate and was measured from the lake surface).*

Table 4.5: *Stratigraphic tie-points used to correlate the sediments of Core OP913 with pollen data and dating from Core OKA1. The upper part of the pollen record (100–601 cm) was derived from OKA1 and adjusted as shown below. Below 601 cm, the pollen record was derived from Core OP913 and therefore did not require adjustment.*

Core OP913 Depth	Core OKA1 Depth	Description
601 cm	550 cm	Bottom of lower silt layer in Core 913; bottom of blue-grey silt in Core OKA1
338 cm	320 cm	Transition from blue-grey silty sand to peat in both cores

Table 4.6: ^{14}C dates for Okarito Pakihi, from Vandergoes et al. (2005). Depths have been adjusted to correlate with Core OP913. Calibrated years were determined using the INTCAL98 calibration (Stuiver et al., 1998).

Depth (cm adjusted)	Material	Lab #	^{14}C Age (yr BP)	Cal. Age (yr BP)
299	Bulk Sediment (organics)	NZA 10991	9,692 ± 65	10,985
299	Bulk Sediment (organics)	NZA 11103	9,758 ± 70	11,081
299	Plant Material	NZA 11605	9,553 ± 65	10,900
299	Plant Material	NZA 11606	9,591 ± 70	10,930
299	Organic Residue	NZA 11633	9,565 ± 60	10,920
299	Organic Residue	NZA 11634	9,627 ± 60	10,940
299	Pollen Concentrate	NZA 11635	9,903 ± 65	11,368
299	**Pooled Weighted Mean (n=7)**		**9,640 ± 27**	**10,965**
317	Organic Residue > 125 μm	NZA 11200	11,215 ± 65	13,176
317	Pollen Concentrate	NZA 11076	11,975 ± 65	14,472
317	Pollen Concentrate	NZA 11075	11,802 ± 65	14,329
317	**Pooled Weighted Mean (n=3)**		**11,888 ± 46**	**14,401**
362	Pollen Concentrate	NZA 11199	14,504 ± 70	17,396
362	Pollen Concentrate	NZA 11197	14,302 ± 70	17,161
362	**Pooled Weighted Mean (n=2)**		**14,403 ± 49**	**17,272**

Table 4.7: Other dates for Okarito Pakihi, from Vandergoes et al. (2005). Depths have been adjusted to correlate with Core OP913.

Depth (cm adjusted)	Source	Age (cal. yr BP)
408	Kawakawa Tephra	c. 26,500
500	Various luminescence ages - silt layer	48,000 - 75,000
880	Luminescence age - silt layer	127,000

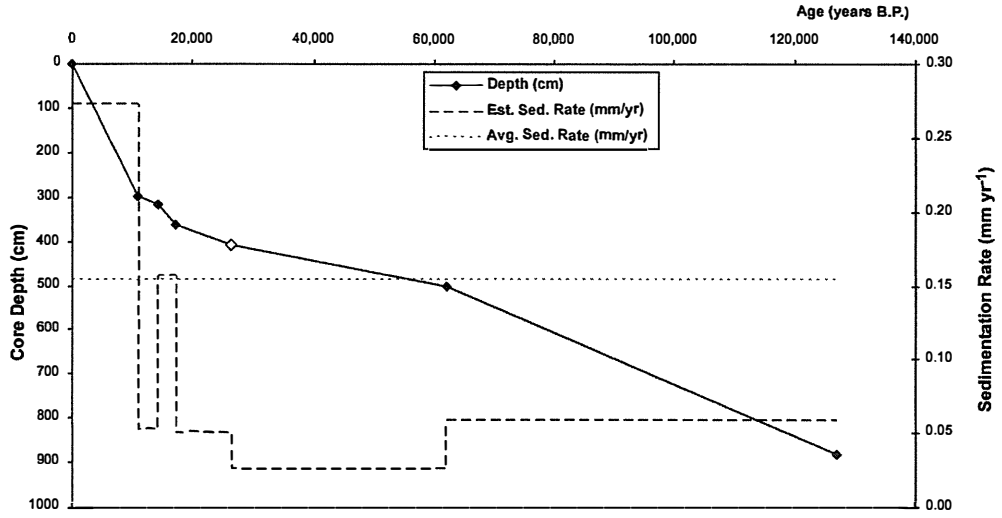

Figure 4.15: *Age/depth model for Okarito Pakihi. The hollow diamond represents the Kawakawa Tephra (408 cm depth, c. 26,500 cal. years B.P.). Other points were based on* ^{14}C *and luminescence dating. The average sedimentation rate ('Avg. Sed. Rate') shown is for the period after the deposition of Kawakawa Tephra.*

Chapter 5

Paleoclimate Proxies

In looking for a paleoclimate signal from the study area, four proxies were investigated. The first, magnetic susceptibility (MS), provided a fast and non-destructive method of examining changes in the mineralogy of the sediments. Combustible organic carbon content (COC) indicated the relative contributions to the sediment from biological and non-biological processes. Grain size was analysed for comparison with known grain-size distributions from other loess and lake sediments. Sediment mineralogy was analysed using optical microscopy and point counting methods in order to determine the mineral composition and likely sources of material.

5.1 Magnetic Susceptibility and Organic Carbon Content

MS is a measure of how easily a material is magnetised, and is essentially a proxy for the abundance of magnetic iron-bearing minerals in the sample (Dearing, 1999). COC provides a measure of the organic productivity of the site, in relation to the total sediment input. MS and COC are closely related in the environment of this study, because the MS signal is interpreted to result from the input of magnetic mineral grains from aeolian dust, whereas the COC reflects the total proportion of inorganic sediment grains. Hence, higher MS values are associated with lower COC values which relate to a general decrease in organic material and corresponding increase in the inorganic mineral content of the core. Figure 5.1 shows the MS and COC for Cores SS906 and GT0507, and the MS for Core OP913. The location of the Kawakawa Tephra has been marked for correlation purposes.

The most notable feature of the MS record from all three cores is the presence of high values during the LGM (as marked by the occurrence of the Kawakawa Tephra). More high-frequency variability is also seen during the LGM than in the earlier part of the record, although this is less obvious in Core SS906. All cores show a distinct drop in MS values after they reach a peak at some time after the deposition of the Kawakawa Tephra.

MS measurements from the base of Core SS906 below 480 cm core depth show significantly higher MS values than the rest of the core (Figure 5.2). This part of Core SS906 was fine

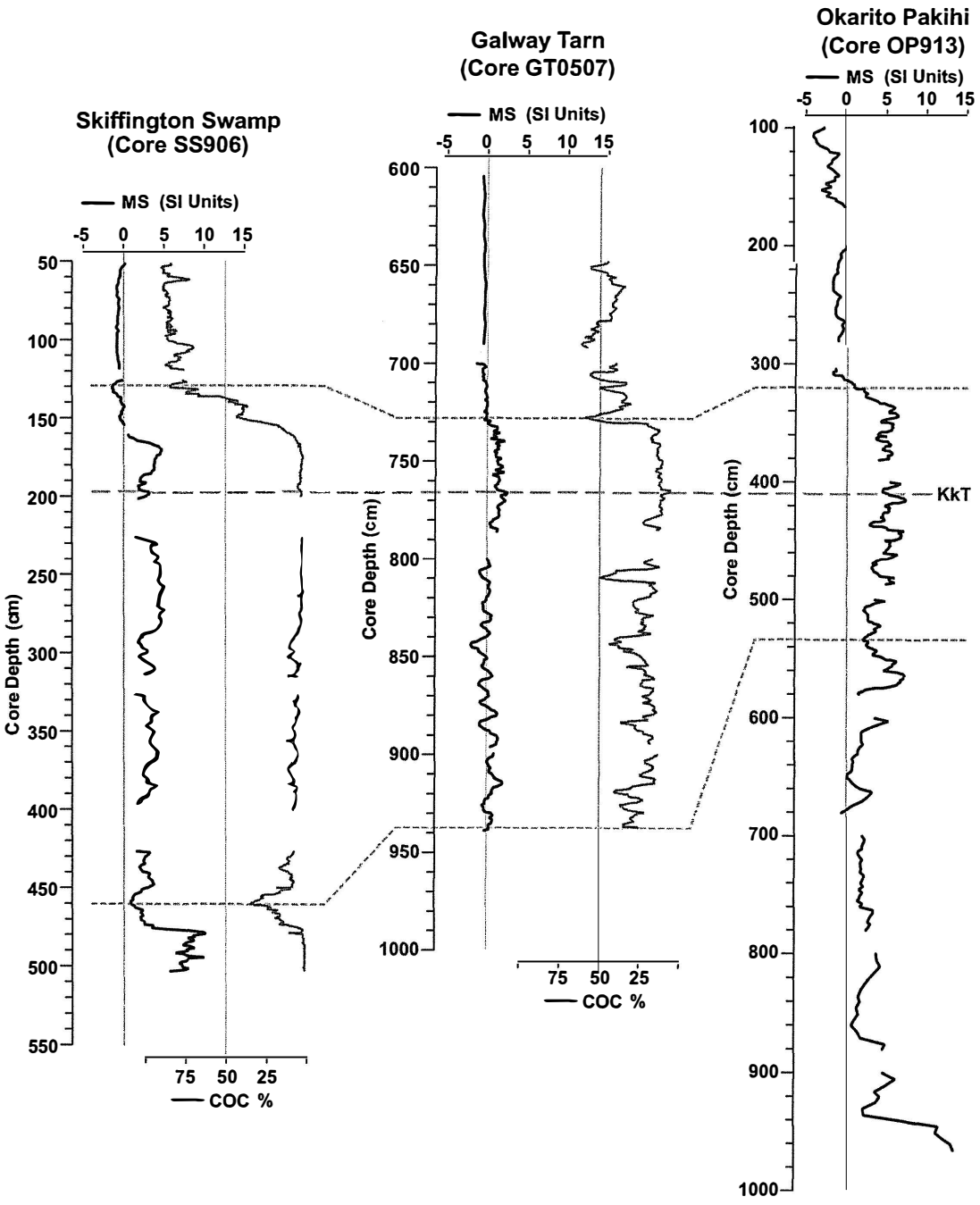

Figure 5.1: *Magnetic susceptibility (MS) as measured with the Bartington MS2 meter, and combustible organic carbon content (COC) for cores from the study area. The dashed line on the figure (marked KkT) indicates the location of the Kawakawa Tephra for correlation purposes. Dotted lines indicate possible additional correlation points, based on a visual comparison.*

laminated silt which was interpreted to have been deposited by glacial melt-water. Core OP913 also had laminated basal silt below 940 cm, and shows a similar pattern.

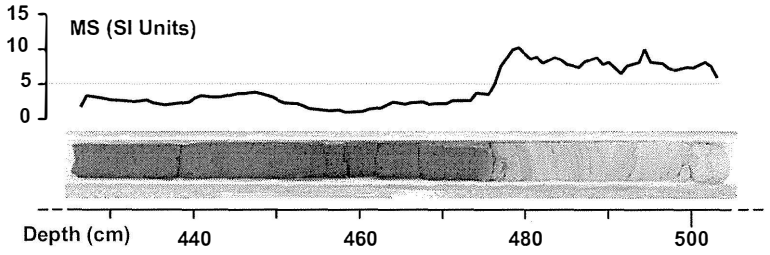

Figure 5.2: *MS measurements for the base of Core SS906 (section T5), with a photo of the core section showing the change from laminated silt to organic silt, and the associated drop in MS values.*

Figure 5.3 and Figure 5.4 show the geomorphic features of the Galway Tarn and Skiffington Swamp sites (Core SS906 and Core GT0507, respectively). Both sites are interpreted to have formed at roughly the same time, within moraine deposits of a glacial advance during MIS 4 (Loopline Moraine) (Vandergoes *et al.*, 2005). Both records show a period of generally variable MS values between the base of the core and a general rising trend prior to the deposition of the Kawakawa Tephra. It is notable that Core GT0507 contains an early peak in MS values at around 915 cm which is not seen in Core SS906. In Core SS906 the Kawakawa Tephra (196 cm depth) occurs at a time of relatively lowered MS values, whereas it is associated with a peak in MS values in Core GT0507. Figure 5.5 shows the sections of each core containing the Kawakawa Tephra in more detail.

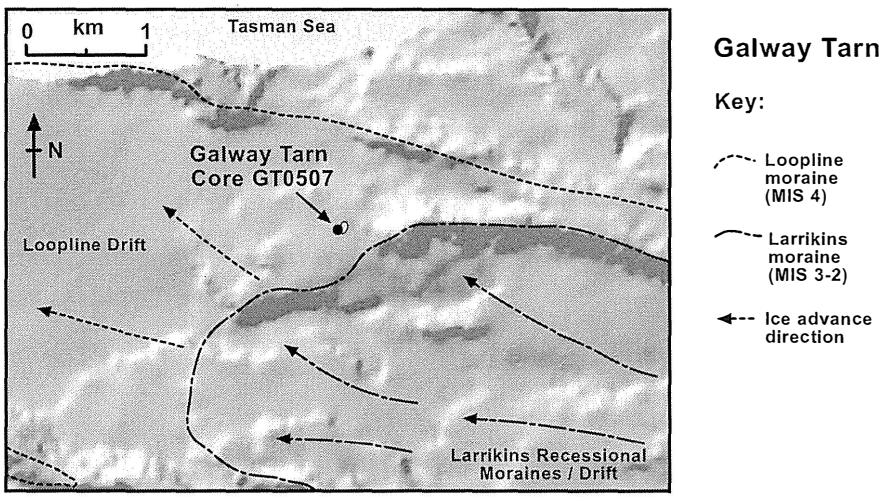

Figure 5.3: *Geomorphology of the Galway Tarn study site. The site is located just beyond the extent of the Larrikins glacial advance (MIS 3-2).*

Core OP913 is from the Okarito Pakihi site, shown in Figure 5.6. This bog formed within a moraine system deposited during MIS 6 or earlier. Subsequent advances during MIS 4–2

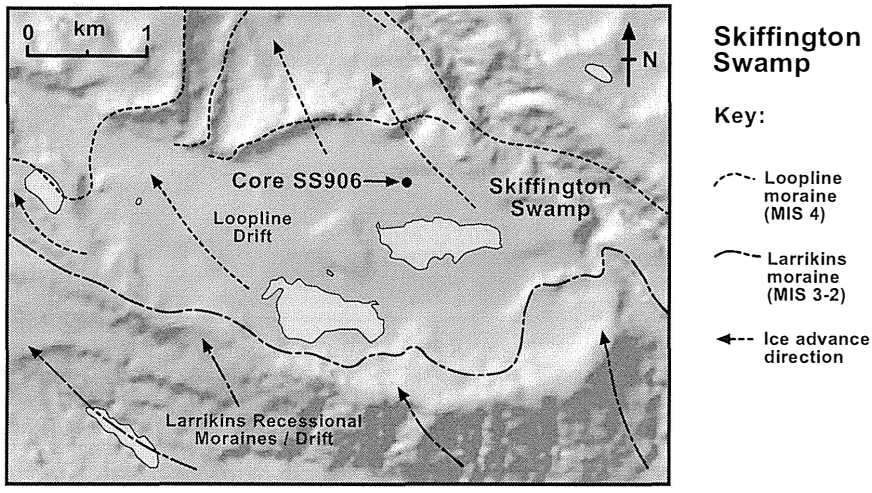

Figure 5.4: *Geomorphology of the Skiffington Swamp study site. The site formed in an area of drift or recessional moraine within the Loopline moraine system (MIS 4) and just beyond the extent of the Larrikins glacial advance (MIS 3-2).*

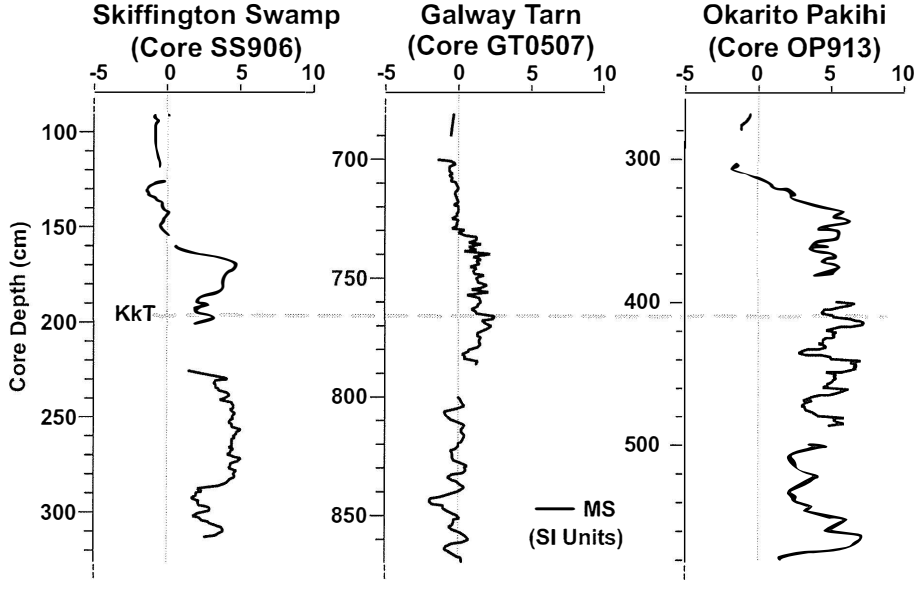

Figure 5.5: *MS measurements for the section of each core spanning the LGM (as indicated by the presence of the 26,500 cal. year B.P. Kawakawa Tephra). The dashed line marks the location of the tephra in each core.*

(associated with the Loopline, Larrikins and Moana moraines) came close to the site but did not overrun it (Vandergoes *et al.*, 2005). The basal portion of the core (below 940 cm) is laminated silt with very high MS values. Immediately above the laminated silt, the core consists of organic silt with lower MS values. However, a significant peak in MS values occurs between 930 and 880 cm. This is followed by a long interval of generally low MS values between 880 and 590 cm. More variable results are seen in the upper part of the core, which is consistent with MS records from the other sites. A drop in MS values to modern levels is seen between 340 and 310 cm,

corresponding to a compositional change from silt to peat.

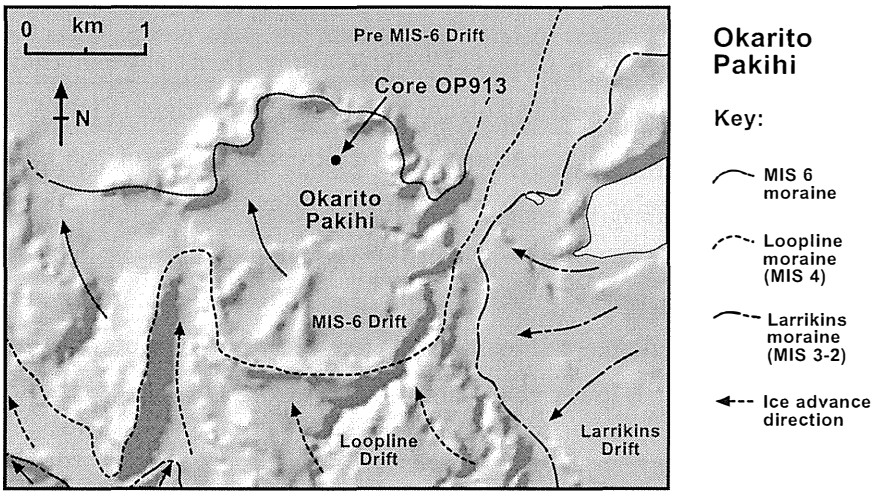

Figure 5.6: *Geomorphology of the Okarito Pakihi study site. The site formed in an area of drift or recessional moraine within a moraine system of MIS 6 or earlier age. Later ice advances came close to the site but did not overrun it.*

The COC results for Core SS906 and Core GT0507 show a similar pattern to the MS results. Note that COC data were plotted on a reverse scale for easier comparison with MS data. COC results for the base of Core SS906 (below 480 cm) and for much of the middle part of the core (400-160 cm) are saturated at close to zero (i.e. 100 % inorganic material). This result is consistent with the inorganic silt composition of the base and middle sections of Core SS906, as observed during core logging. The saturated basal section of Core SS906 corresponds to the laminated silt deposited by melt-water inwash. Above this basal section, a section of greater organic content is seen between 480 and 450 cm. This probably correlates with the basal part of Core GT0507, which lacks any basal silt unit. For both cores, the COC falls from this early value.

For Core SS906, the COC signal quickly falls to low values with little variation, and appears to be saturated for a significant portion of the core above and below the tephra layer. Above the tephra layer, a sharp rise in COC is seen (160 cm depth) which corresponds to a fall in MS. Several minor reversals are seen in this fall, until relatively high modern values of COC are reached.

The COC results for Core GT0507 are higher than those of Core SS906 throughout most of the core, consistent with the high peat and gyttja content of this core. The results also show a lot more variability than the results from Core SS906, and do not appear to be saturated at any point. From an initial moderately high value, the COC follows a general declining trend, to reach a minimum around the time of deposition of the Kawakawa Tephra. The tephra layer appears as a small spike in the COC results. Within this declining trend, there is significant variability, with a number of strong positive peaks in COC. These peaks correlate well with the MS data. From 780–730 cm, the COC data show much less variability, and minimum values are

reached. Above 780 cm, a very sharp rise in COC is seen. Variable, generally high values are seen for the remainder of the core.

Microscope analysis of samples from Core GT0507 (Galway Tarn) showed they were high in phytoliths, diatoms and other non-combustible material of organic origin (Figure 5.7). Therefore, the residue remaining from the COC process is not a direct measure of the inorganic mineral content for this core. In particular, the highly organic sections of the core produced COC values of 30–50 %, but the inorganic mineral content of these sections may have been as low as 20 %, with the remaining material consisting mostly of plant silicates. The more organic-rich sections of Core SS906 also contained some non-combustible material of organic origin, although the concentration of these was much lower than samples from Core GT0507.

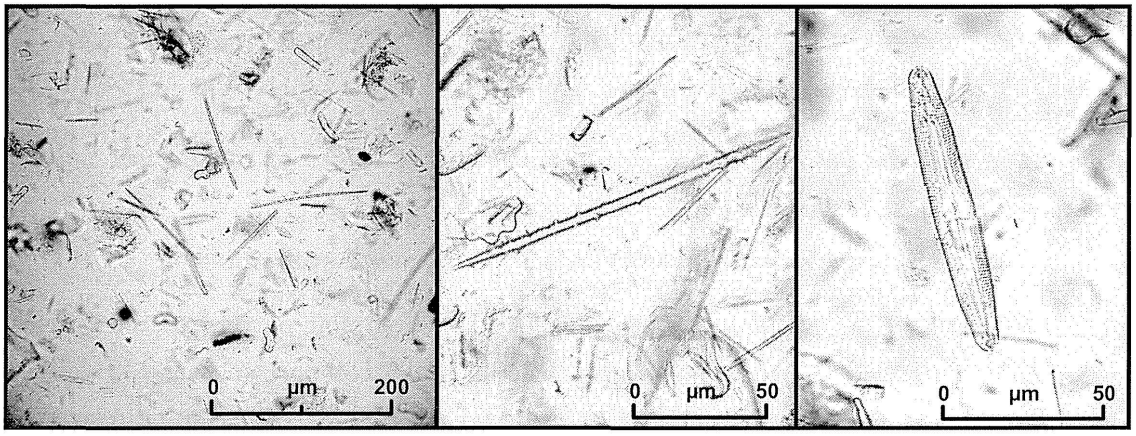

Figure 5.7: *Phytoliths and other material of organic origin from the upper section of Core GT0507. The sample was treated with hydrogen peroxide to dissolve any organic carbon, and sieved to remove grains smaller than 10 µm before being mounted on a microscope slide. The left photo shows a number of needle-like phytoliths (200 x magnification); the centre photo shows a single phytolith (400 x magnification); the right photo shows a diatom (400 x magnification).*

5.2 Grain Size Analysis

Figure 5.8 shows the grain size results for Core SS906 and Core GT0507. The finest mean grain size for samples from Core SS906 occurs in the basal laminated silt (< 20 μm). The peat and organic silt above the laminated unit is marked by a distinct change to a coarser grain size. A general coarsening upwards trend occurs from the bottom of the core until a peak is reached at a core depth of 160 cm, coinciding with the peak in MS and COC data. Prior to this peak, a significant variability is superimposed on the general coarsening upwards trend, with prominent episodes of finer grain size occurring at depths of 295 cm, 275 cm, 230–210 cm, 185 cm and 160 cm. The latter two fine intervals are particularly notable. In order to test the validity of the results from the laser sizer, samples from the prominent fine/coarse transition at 160–150 cm

were checked with an optical microscope as noted in Chapter 3. The maximum dimension of mineral grains was measured using the microscope eyepiece scale. The results are compared with those obtained from the Malvern laser sizer in Table 5.1. Note that the samples had been sieved to remove material smaller than 10 μm prior to mounting on microscope slides, so the mean grain size measured by microscope should be slightly coarser than the measurement produced by the laser sizer. However, the microscope measurements of grain size are broadly consistent with those obtained from the laser sizer.

Table 5.1: *Comparison of the grain size as measured by Malvern laser sizer and optical microscope.*

Depth (cm)	Malvern Laser Sizer		Microscope	
	Mean (μm)	SD (μm)	Mean (μm)	SD (μm)
154	97	124	108	50
156	107	141	72	22
159	35	54	37	24
160	38	50	48	31

The mean grain size measured for Core GT0507 is generally significantly finer than that of Core SS906. A weak coarsening upwards trend is seen around the time of deposition of the Kawakawa Tephra, with significant variability. No obvious correlation with other records is visible.

5.3 Mica and Organic Content

Mica content was determined by counting mineral grains in the sample. Chlorite, biotite and muscovite micas are common in samples from the study area. The source of these micas is the metamorphic rocks of the Southern Alps to the east of the Alpine Fault. The total of these three micas as a percentage of all inorganic grains is shown in Figure 5.9. 'Organic content' is also shown for Core GT0507. This core had a very high content of phytoliths, diatoms and other biological remnants. The organic material in Core GT0507 was counted separately from the mineral grains. The data have been normalised to a mineral count of 100, so that the totals expressed are 'organic material count per 100 mineral grains'.

Mica content for Core SS906 is typically around 20–30 % for samples below the Kawakawa Tephra, although only very limited data are available for this part of the core. More detailed results from depths of 200–130 cm reveal a very significant peak in mica content at a depth of 160–175 cm, reaching a value of 40 %. Above c. 165 cm, the mica content drops until values of 0–5 % are reached at a depth of 140 cm. The mica content for Core GT0507 is higher, varying

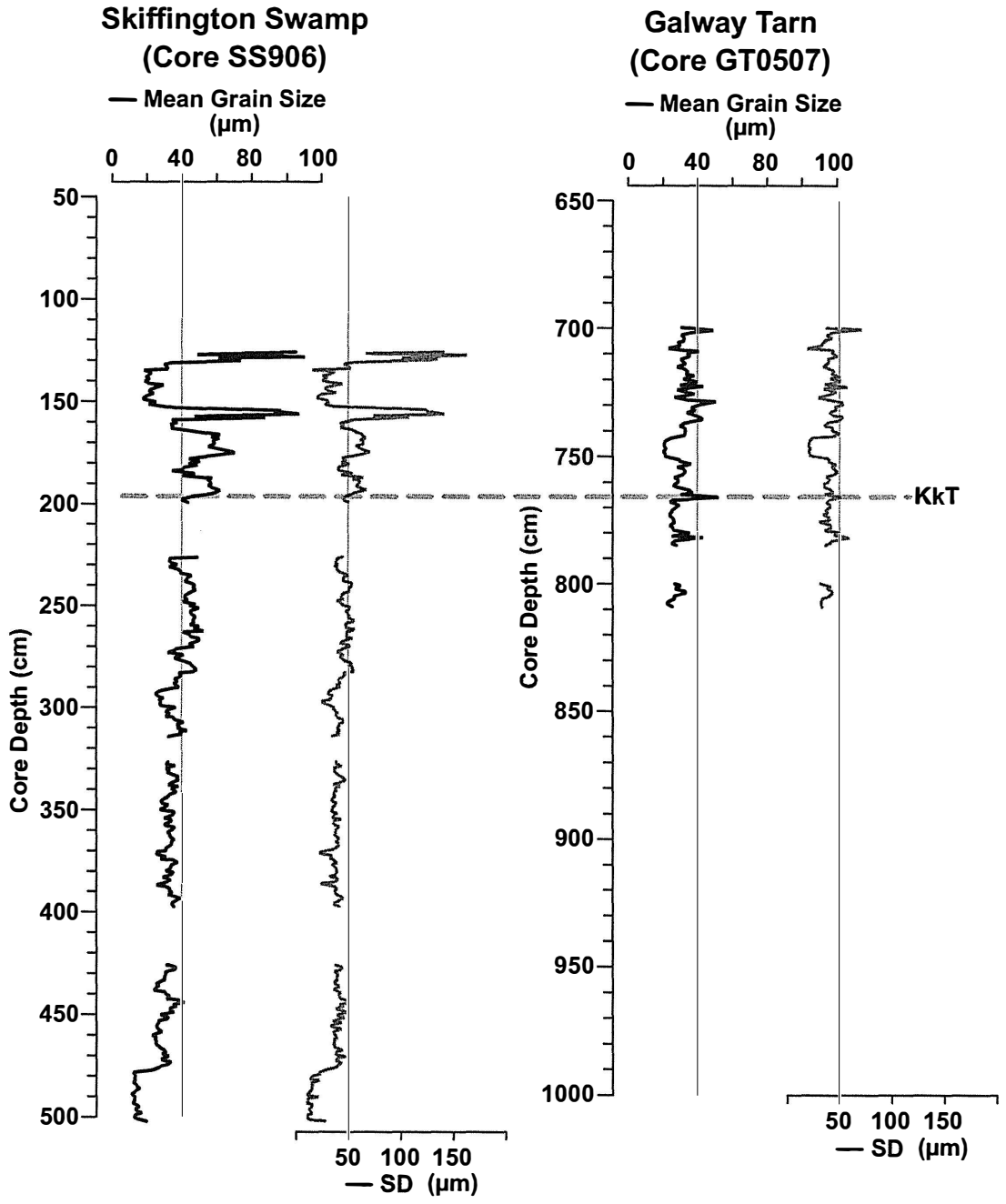

Figure 5.8: *Grain-size distributions for Core SS906 and Core GT0507. Mean and standard deviation are displayed. The dashed line on the figure indicates the location of the Kawakawa Tephra for correlation purposes.*

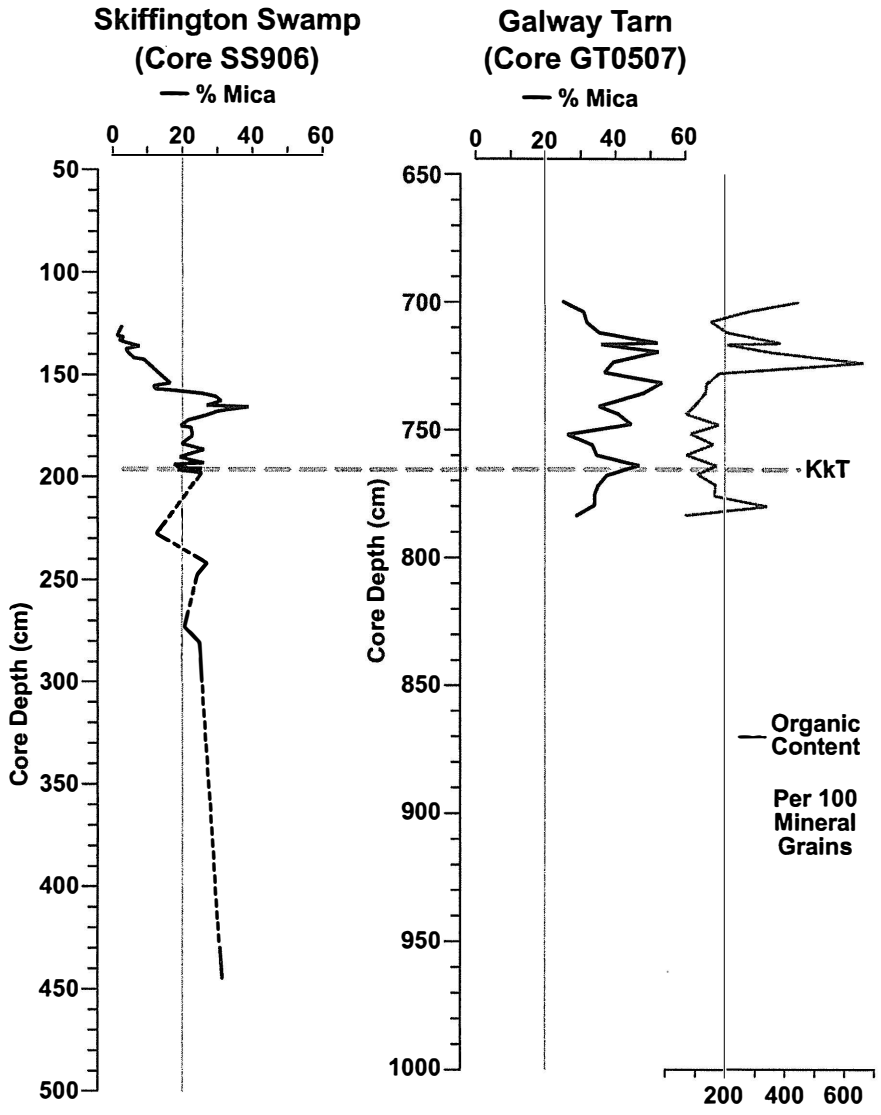

Figure 5.9: *Mica and organic content for Cores SS906 and GT0507. 'Organic Content' is the count of material of organic origin (e.g. phytoliths and diatoms) per 100 mineral grains. The dashed line on the figure indicates the location of the Kawakawa Tephra for correlation purposes. Dotted lines represent depths where no data were available.*

between 30 and 60 % for most of the core section that was studied. Also, Core GT0507 does not show the distinctive peak in mica content that is seen in Core SS906. However, there is a possible trend to higher values after the deposition of the Kawakawa Tephra, and a decline in mica content is seen above a depth of 715 cm. No samples had mica content lower than 20 %.

5.4 Correlation and Chronology of Results

Figure 5.10 shows a summary of data for the three cores used in this study. Pollen data have been correlated with the results from this study using the procedures outlined in Chapter 4. The dashed line on the figure indicates the location of the Kawakawa Tephra in each core, which provides a tie-point for correlation. Dates from ^{14}C and luminescence dating are displayed where available. ^{14}C dates have been calibrated using INTCAL98 (Stuiver *et al.*, 1998).

Dating information was used to construct a summary of data on a time scale (Figure 5.11). The existing dating information was correlated to core depth, and ages for intervening depths were approximated based on sedimentation rates.

5.5 Australian Dust Flux

Deposition of Australian dust in Westland has been documented on several occasions, generally following dust storms in Australia, and at times when wind conditions favoured dust transport across the Tasman Sea. These dust events are usually identified by reports of red colouration of snowfields on the Southern Alps due to deposited dust (McGowan *et al.*, 2000). Input of Australian dust is important to this study since it would tend to dilute the signal produced by local dust flux changes. Some recent studies have used trace elements to identify the provenance of dust collected in New Zealand and determine the proportion of dust sourced from Australia. Marx *et al.* (2005) found that red dust collected from the Franz Josef gacier contained up to 70 % material of Australian origin. However, this result represents an extreme event of Australian dust deposition rather than an average deposition rate. Marx *et al.* (2005) estimated a mean atmospheric dust concentration in Westland of 5.3 μgm^{-3}, but the rate of deposition was not known. A more realistic estimate of Australian dust content in South Westland was given by samples collected near the Haast River. These contained 11 % Australian dust, a figure which represents an average deposition rate over a 10 month collection period (Marx *et al.*, 2005).

The results of these studies indicate that dust derived from Australia may contribute to aeolian sediments in South Westland. However, there are few estimates of the deposition rates of Australian dust. While deposition rates may be high during events when dust transport across the Tasman Sea is favoured, the mean rate of Australian dust deposition in South Westland is probably relatively low. Dust derived from Australia is likely to contribute to the finer fraction of sediments, due to down-wind sorting effects removing coarser grain sizes. McGowan *et al.*

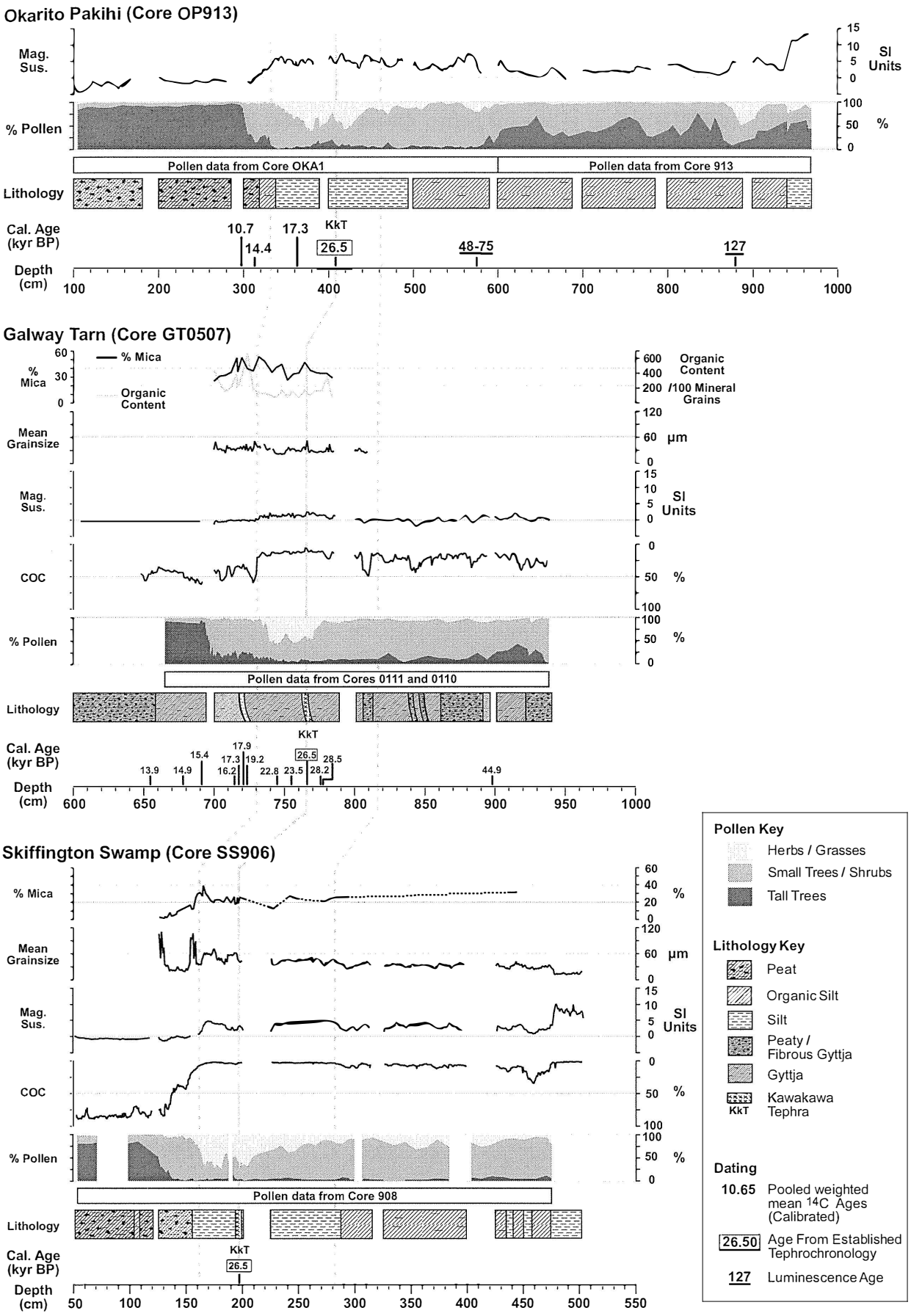

Figure 5.10: *Summary of all data for Cores SS906, GT0507 and OP913. The dashed line on the figure (marked KkT) indicates the location of the Kawakawa Tephra. Dotted lines indicate possible additional correlations.*

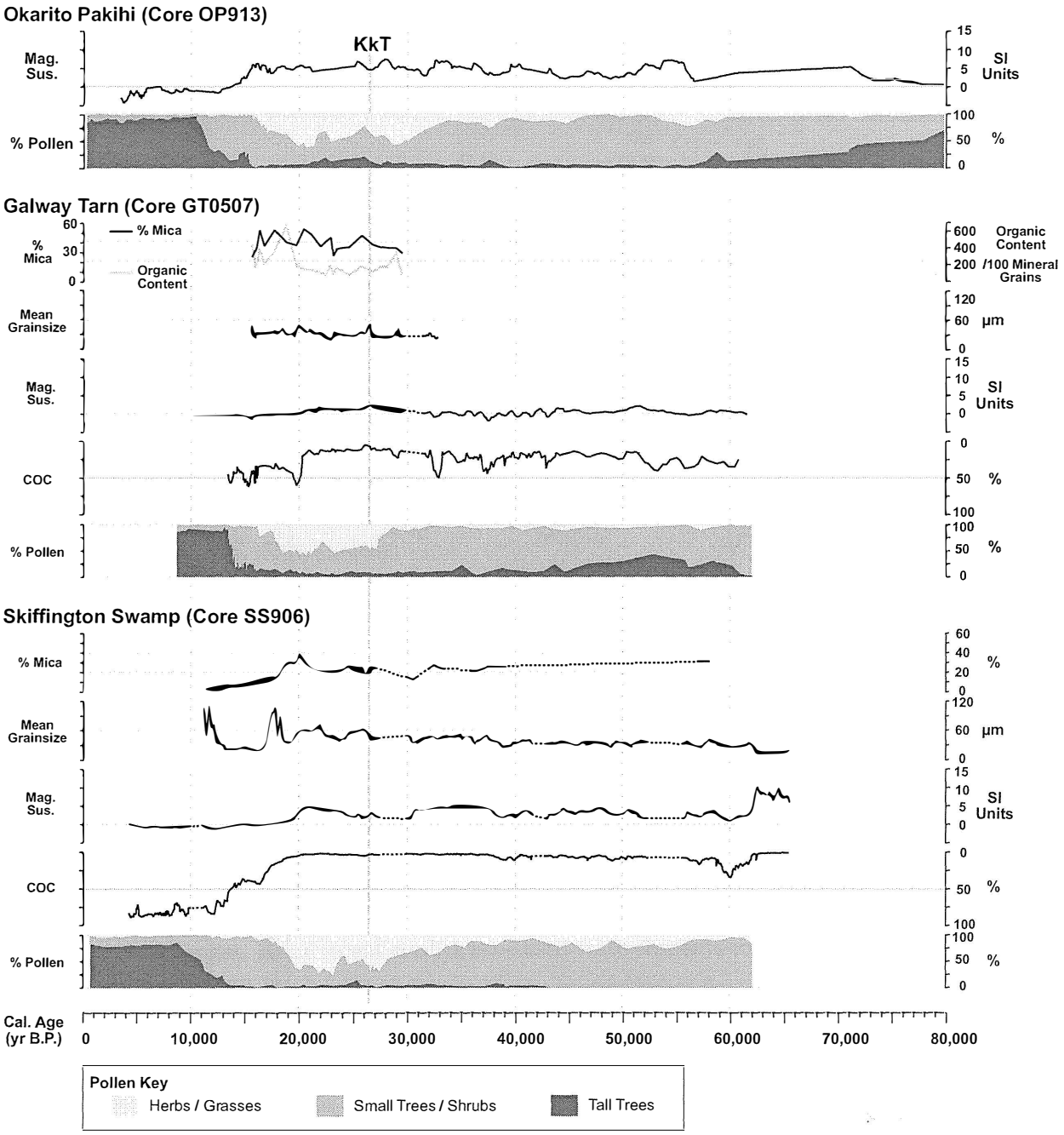

Figure 5.11: *Summary of all data for Cores SS906, GT0507 and OP913, plotted on a time scale. Ages are based on existing dating and estimates from sedimentation rates. The dashed line on the figure (marked KkT) indicates the location of the Kawakawa Tephra for correlation purposes. Dotted sections of the graphs represent depths where no data was available.*

(2000) found that red dust collected from Franz Josef glacier, with a predominantly Australian origin, had a mean grain size of 14.03 μm. This is considerably finer than the mean grain size of 27 μm for dust collected over a 10 month period from sites in South Westland (Marx and McGowan, 2005).

The sites used in this study were chosen due to their close proximity to sources of local dust entrainment from outwash plains. Marx and McGowan (2005) have shown a strong relationship between dust deposition rates and the proximity of nearby sources of dust entrainment, especially with respect to predominant wind direction. Therefore, it seems likely that the sites used for this study were most strongly influenced by local dust sources.

Chapter 6

Paleoclimate Reconstruction

This chapter comprises an interpretation of the data collected in this study in terms of paleoclimate reconstruction. Particular focus is given to the LGM period and the glacial/interglacial transition (LGIT). Vandergoes *et al.* (2005) suggested that maximum cooling in South Westland extended from c. 30,500 to 17,300 cal. years B.P., indicating an earlier onset of the LGM period than is evident in Northern Hemisphere records. In this study, 'LGM' refers to the period of maximum cooling, c. 30,000–18,000 cal. years B.P. The Kawakawa Tephra serves as a marker for the LGM period in the cores used in this study.

6.1 Limitations of the Age Model

The Kawakawa Tephra provides a stratigraphic marker in all the cores used in this study and has been dated at c. 26,500 ± 230 cal. years B.P. (Wilson *et al.*, 1988). Other dates used in this chapter are based on the age/depth models discussed in Chapter 4 and hence are subject to the uncertainties introduced by the use of sedimentation rates and limited ^{14}C dating.

^{14}C dates for this study are typically ± 60 to ± 120 years, except for dates near the limits of the ^{14}C dating technique, which have much larger uncertainty. Uncertainty in the calibration of ^{14}C dates mean the calibrated ages used in this study typically contain an uncertainty of ± 200 to ± 300 years. For intermediate samples, the age model assumes a constant sedimentation rate between dated samples. Changes in sedimentation rate are evident in the cores (e.g. Figure 4.14 and Figure 4.15 in Chapter 4), so the assumption of constant sedimentation rate between datum points is a possible source of uncertainty. For Galway Tarn and Okarito Pakihi, the possible variation in sedimentation rate is constrained by the number of ^{14}C dates available, which give a detailed picture of the age/depth relationship at these sites. Model ages are probably no more than 200 years different from the true ages for the LGM section of these cores.

The age/depth model for Skiffington Swamp contains more uncertainty since it is constrained only by the Kawakawa Tephra, and sedimentation rate changes over shorter time intervals are unknown. As an example, allowing for a 30 % variation in sedimentation rate in the period

between 26,500 and 10,000 cal. years B.P., a model age of 20,000 years at Skiffington Swamp could represent a true age between 16,600 and 21,600 cal. years B.P. This uncertainty is greatest at intermediate points which are mid-way between points of known age.

6.2 Magnetic Susceptibility

6.2.1 MS of Glacial/Interglacial Sequences

Many studies have illustrated the usefulness of magnetic properties as a paleoclimate proxy. Much of this work has been carried out on loess/paleosol sequences in China (Kukla, 1987; Xiao *et al.*, 1999). The Chinese loess/paleosol sequences show higher MS during interglacial times compared to glacial times. Studies of loess/paleosol sequences in Rotorua and Marlborough (Froggatt, 1988) and Wanganui (Palmer and Pillans, 1996) also show higher MS during interglacial times. Several mechanisms are proposed for this MS signal, including authigenic formation of magnetic minerals in soil formation processes, or the swamping of background magnetic mineral input by high volumes of quartz and feldspar grains during glacial times. Palmer and Pillans (1996) suggested that the high interglacial MS signal in Wanganui loess/paleosol sequences resulted from a continual input of magnetic minerals from the active andesitic volcanoes in the region. This background input led to the aggradation of high-MS soils during warm interglacials, but was swamped by low-MS loess rich in quartz and feldspar during cold glacial times.

A different interpretation is required for MS results from the cores used in this study. The MS signal arises from the presence of magnetic minerals in the sample. The source for these minerals is either aeolian dust, sediment derived from inwash, or volcanic material. Most material available for aeolian entrainment by wind in the study area is supplied by the rivers and glaciers at present, and would have been predominantly glacial outwash material during times of glaciation. Glaciers and rivers in the area transport a large volume of loose material with a wide distribution of grain sizes (Marx and McGowan, 2005). This material is eroded from the rapidly uplifting Southern Alps to the east of the Alpine Fault, which are composed of weakly to strongly metamorphosed quartzo-feldspathic schist, greenschist, chlorite schist and schist bearing biotite, garnet and oligoclaise (Gair, 1967). These source rocks contain abundant quartz and feldspar, with chlorite, biotite and some muscovite micas depending on the degree of metamorphism. Other minerals include garnet, amphibole, epidote and sphene. The opaque minerals ilmenite (common) and pyrite (rare) are also seen (Bishop, 1972).

Of the minerals contributed from the schists of the Southern Alps, ilmenite and biotite are the most likely source of the MS signal. Although ilmenite is not abundant in samples from the study area, it exhibits a relatively high MS. Biotite is much more common and also gives moderate MS values. Amphibole and epidote may have contributed to the MS signal, but this effect would have been small due to the very low concentrations of these minerals. Dominant

minerals such as quartz and feldspar are diamagnetic and exhibit weakly negative MS values. Ferrimagnetic minerals such as magnetite and titanomagnetite give much higher values for MS but are rare or absent in the source rocks of the Southern Alps. Table 6.1 summarises typical MS values for minerals commonly found in South Westland sediments.

Table 6.1: *The magnetic susceptibility (MS) of some common minerals. MS values from Dearing (1999); Mineral densities from Mottana et al. (1978).*

Mineral	Type of magnetism	Mass specific MS ($10^{-6}m^3kg^{-1}$)	Density (gcm^{-3})
Magnetite	Ferrimagnetic	513–1116	5.2
Titanomagnetite	Ferrimagnetic	169–290	5
Ilmenite	Paramagnetic	1.7–2.0	4.5–5.0
Pyrite	Paramagnetic	0.3	5.0–5.2
Biotite	Paramagnetic	0.05–0.95	2.8–3.2
Amphibole	Paramagnetic	0.16–0.69	3.08–3.7
Epidote	Paramagnetic	0.25–0.31	3.3–3.5
Quartz	Diamagnetic	-0.0058	2.65
Alkali-feldspar	Diamagnetic	-0.005	2.55–2.76

Another source of magnetic minerals may be from volcanic ash (Froggatt, 1988). However, volcanic material was rare in the South Westland region during the late Quaternary, and was derived from North Island rhyolitic volcanic centres. The distal tephra deposits which occur in the cores in this study are composed entirely of rhyolitic glass shards, which do not produce a measurable MS signal. Rhyolitic tephra beds in the Wanganui region were associated with minimum values for MS (Palmer and Pillans, 1996). In this study, no clear change in MS was associated with the visible Kawakawa Tephra layers, supporting the conclusion that this tephra has low MS values, and that volcanic sources have not been important as a source of magnetic minerals.

The MS signal from the study sites gives a measure of the abundance of magnetic minerals in the sediment. An increase in MS values indicates either an increase in the abundance of inorganic grains or an increase in the proportion of magnetic minerals as a fraction of the inorganic grains. The former would occur where either the supply of inorganic sediment to the site increased, or the amount of organic material generated in the environment decreased. The proportion of magnetic grains in the sediment could be changed in several ways. The mineral composition of sediments being supplied to the system from erosion of the Southern Alps could alter, although this would require significant changes in the catchment of the glaciers or rivers in the region of the sites (for example through uplift and erosion of valleys into different source rocks). Such a change is unlikely to have occurred over the relatively short time interval covered by cores

from these sites. A more likely cause for changes in magnetic mineral abundance is a change in the transport pathways by which inorganic sediment enters the sites. Changes in the transport regime have the potential to affect sediment makeup through sorting processes and weathering of sediment.

6.2.2 MS Results from the Study Area

Changes in sediment transport mechanisms are clearly visible in Skiffington Swamp (Core SS906). Below 480 cm, this core consists of fine strongly laminated silt, interpreted as a deposit formed by direct inwash of glacial melt-water. The COC results for this portion of the core are virtually 0% organic material (100% inorganic grains). However, MS results for Core SS906 below 480 cm are much higher than for other sections of the core with similarly high inorganic mineral content. Therefore, the proportion of magnetic mineral grains in the lower portion of the core must be significantly higher. This can be explained if the transport pathways of the deposited material are considered. Direct inwash of melt-water supplied sediments into a lake during the initial stages of sedimentation, so grains were transported by the action of water. After the site was abandoned by glacier retreat and isolated by later moraine deposits, the supply of sediment by fluvial processes was greatly reduced and aeolian dust became more prevalent. The minerals which provide the greatest contribution to the MS signal (ilmenite, pyrite, amphibole and epidote) have considerably higher density than quartz, feldspar and micas and are less easily entrained and transported by wind action. This sorting effect led to lower levels of these minerals in the lake sedimentation at Skiffington Swamp, and correspondingly lower MS values. A similar effect was seen in Core OP913 (Okarito Pakihi).

MS results are therefore linked to the glacial history and hence the climate at the sites used in this study by the abundance and composition of inorganic minerals in the sediments. Colder climates, associated with ice advance, lowered sea levels, vegetation loss and greater sediment availability, lead to higher MS values because of increased input of mica and heavy minerals to the site.

6.2.3 LGM Climate Changes from the MS Record

A close comparison of the MS results between the three sites for the LGM period is of particular interest. In Core GT0507 and Core OP913 (Galway Tarn and Okarito Pakihi, respectively), the LGM period is marked by high MS values showing a small degree of variability. In Core GT0507 this period of high MS values extends from 805–730 cm, corresponding to the time interval 32,500–21,000 cal. years B.P. In contrast, the same period in Core SS906 (Skiffington Swamp) contains a distinctive trough in MS values at depths of 225–180 cm, coinciding with the deposition of Kawakawa Tephra. This trough would correspond to the time interval 31,000–24,000 cal. years B.P., and is followed by a subsequent rise to a peak which marks the maximum of MS values for the core (excluding the laminated silt at the core base). The peak value of MS

is reached at 160 cm, giving a date of 20,000 cal. years B.P., and is followed by a sharp decline in MS values. Taking into account the differences in the location and morphology of the three sites, several possibilities for the different patterns of MS results exist.

The rising MS signal in Core SS906 towards the end of the LGM period might correspond to increased fluvial activity and associated sediment inwash. If the sediment supplied from the catchment contained a mineral assemblage with lower MS, the MS signal would have been reduced. However, increased fluvial activity is not evident in the results from Okarito Pakihi, despite that site having a considerably larger catchment area. There is also no change seen in the data for Core GT0507, although the very small catchment of the Galway Tarn site might mean it was less affected by changes in precipitation and fluvial activity. The small scale of the Skiffington Swamp catchment leaves little room for any catchment disturbance (such as major erosion) which could have contributed to fluvial sediment supply to the lake on the scale required.

The pollen data for the LGM period does appear to show two phases of climate cooling during the LGM, separated by a slightly warmer interval (as recorded by peaks in grass pollen concentration). However, these pollen peaks do not show any close correlation with the MS or COC results. An examination of the position of the three sites in relation to the glacial moraines provides an alternative explanation. Galway Tarn and Okarito Pakihi are both located a few kilometres from the estimated terminal positions of LGM ice advance (see Figure 2.7 in Chapter 2). In contrast, the Skiffington Swamp site is located on a lateral moraine some 10 km inland to the east of Galway Tarn. A wide piedmont ice-field would have extended across the Cook River valley in the vicinity of the Skiffington Swamp site, and would have lapped on to the steep lateral moraines at the valley margins, leaving little or no exposed outwash surface (Figure 6.1). Maximum glacial extent would therefore have shifted outwash areas, and hence the sources of aeolian dust entrainment, farther to the west of the Skiffington Swamp site. Given that aeolian transport has a sorting effect on sediments, heavier minerals (generally having higher MS) would be transported shorter distances and the MS for cores from a site such as Skiffington Swamp would be reduced when the source of aeolian sediments was more distal. The peak in MS values seen in Core SS906 occurred when glacial retreat caused the terminal position of the glacier to move closer to the Skiffington Swamp site, thereby exposing large outwash areas. At the same time, the MS values of Core GT0507 and Core OP913 were falling as vegetation began to stabilise abandoned outwash areas.

Extending this argument, it is interesting to note that a period of higher MS values also occurred between depths 280–225 cm in Core SS906, corresponding to the time interval of 38,000–31,000 cal. years B.P. This spans a significant proportion of MIS 3 prior to the LGM. A possible interpretation of this interval of high MS values is that glaciers were active and significant outwash areas existed in the vicinity of the Skiffington Swamp site at this time. This period is associated with low values of MS in Core GT0507 due to the greater distance of the Galway Tarn site from the ice margins.

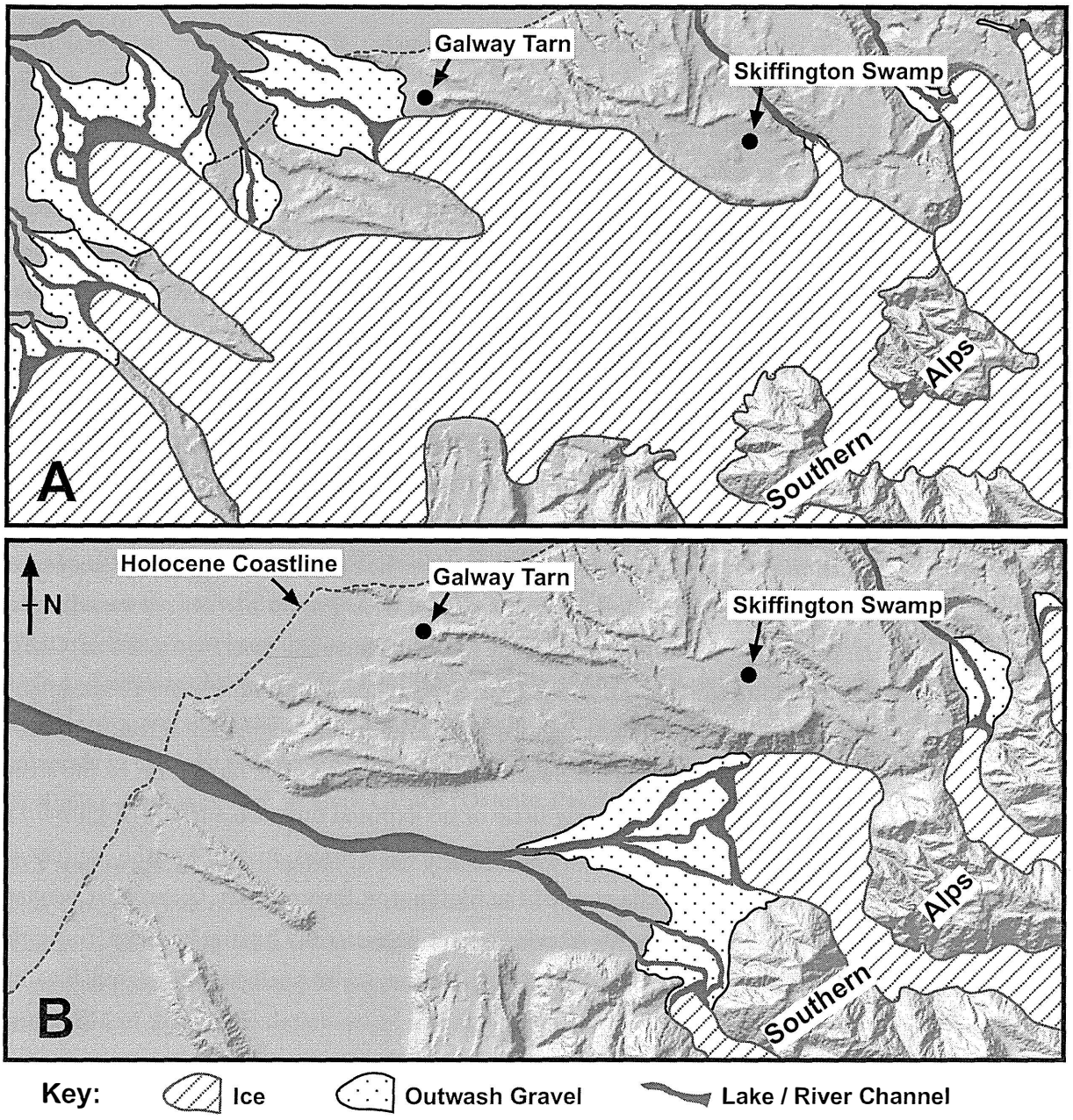

Figure 6.1: *Positions of glacier terminations and outwash gravels relative to the study sites (Cook River valley). Outwash gravels were more prevalent in the region of Galway Tarn when glaciers were extended (Diagram A). The retreat of glaciers (Diagram B) would have brought outwash areas closer to Skiffington Swamp, while vegetation would have quickly colonised and stabilised the former outwash gravels.*

The MS peak seen at 170–160 cm core depth in Core SS906 is also notable because it occurs slightly earlier than the drop in COC values which begins at 160 cm, implying a significant compositional change in the inorganic sediments while the total amount of inorganic sediment remained high. This compositional change is discussed later.

MS values for Core OP913 show an initial high peak associated with a basal laminated silt, similar to that seen at Skiffington Swamp. A second peak at a depth of 900–880 cm is interpreted to represent cold climate conditions late in MIS 6 (Vandergoes *et al.*, 2005), when inorganic sediment input to the site was higher. Between 880 cm and 590 cm, generally lower values are interpreted to represent the warm interval of the last interglacial (MIS 5e). MS values are higher during this period than those recorded for Holocene peat from the upper part of the core. There are several possible causes for this difference. The site contained a lake until the end of MIS 2, when a change occurred so that a peat bog was formed. This change would have caused an increase in the organic content of sediment from the site and a corresponding decrease in MS values, as seen in Core SS906. Greater compaction of material from deeper depths in the core would also tend to increase density and hence MS values.

A significant peak in MS values occurs at a depth of 570 cm in Core OP913, and correlates with a peak in grass pollen. This MS peak represents a cold period interpreted as occurring during MIS 4 (Vandergoes *et al.*, 2005). Lower and more variable values above this depth are consistent with cool climate during MIS 3. A general rising trend is seen over this time, culminating in a peak at a depth of 340 cm. This depth corresponds to an age of c. 15,500 cal. years B.P., which is considerably younger than similar peaks seen in Core SS906 (21,000 cal. years) and Core GT0507 (20,000 cal. years). However, the Okarito Pakihi site has several significant streams flowing into it and shows evidence of fluvial activity and aggradation of sands and silts (M. J. Vandergoes, personal communication). Therefore, changes in MS could represent changes in input of sediment from the surrounding catchment as the lake basin infilled, streams changed course, and peat bog became established. Setting aside changes in fluvial activity, the later peak in MS values may represent a later establishment of peat (and hence change from inorganic sedimentation to dominantly organic sedimentation) due to greater water depth. Measurement of combustible organic carbon content was not carried out for this core and therefore changes in composition could not be separated from changes in total inorganic percentage.

6.3 Combustible Organic Carbon

Combustible organic carbon content (COC) provides a measure of the organic productivity of the site, in relation to the total sediment input. It should be noted that this property is the combination of the organic productivity in the lake and surrounding area (leading to the deposition of organic material), the degree of preservation of organic material (which depends on the biological and chemical properties of the site) and the input of inorganic terrigenous sediment which dilutes the organic material. Thus the interpretation of organic carbon percentages should

be considered in terms of changes in one or more of these three variables.

Higher COC values seen at the base of both cores (above the basal laminated silt in the case of Core SS906) are interpreted to represent an interval of warmer climate early in MIS 3. This peak in COC values is most distinct in Core SS906 (470–450 cm), possibly because the higher altitude of the Skiffington Swamp site meant that mean temperatures were lower and the site was more sensitive to a small climate warming. Site hydrology changes (such as lowered lake level) cannot be ruled out, although these seem less likely given that the same effect is also visible at Galway Tarn. Luminescence dates on a silt layer in Core OKA1 from Okarito Pakihi gave ages of 48,000–75,000 cal. years B.P. (Vandergoes *et al.*, 2005). This silt layer is correlated with an MIS 4 cold interval and is most likely to correlate to the Loopline glacial advance. Loopline drift forms the base of the Skiffington Swamp and Galway Tarn sites, giving a maximum age for these sites. An age of c. 60,000 cal. years B.P. is therefore implied for the warm interval recorded by the organic-rich material at the base of Cores SS906 and GT0507.

The COC signal appears to be saturated for most of Core SS906 prior to the end of the LGM period, with organic content being very close to zero. However, Core GT0507 contains a higher proportion of organic material throughout and shows more detail of organic and inorganic sedimentation at the site. In particular, a number of episodes of organic enrichment are evident in the lower part of the core, below 780 cm depth. These episodes are interpreted to represent a combination of increased organic productivity and reduced input of inorganic sediment. The most likely cause of such a change is an interstadial period of warmer climate. It is notable that no obvious correlation with the pollen record is evident for these COC variations. This lack of correlation implies that the change was too short in duration to produce a significant change in the local vegetation. Alternatively, a change in the wind regime could be invoked to explain these organic-rich intervals, with the prominent wind direction or strength changing in such a way that aeolian dust transport to the site was reduced.

The most prominent of these changes occurs at a depth of 805–810 cm, which corresponds to an age of c. 32,000 cal. years B.P. The duration of this organic-rich episode is c. 1,000 years. Several similar fluctuations are seen between 40,000 and 30,000 cal. years B.P. In contrast, the COC results indicate that conditions were less variable between depths of 805 to 730 cm, corresponding to the LGM period between 32,000 and 20,000 cal. years B.P.

The cores used in this study both show a transition from low to high COC some time after the deposition of the Kawakawa Tephra. This change is interpreted to represent the effects of climate warming at the end of the LGM period, during the LGIT. In Core SS906, this occurs at a depth of 160 cm, corresponding to an age of 18,500 cal. years B.P. A minor reversal in this trend is seen between 150 and 140 cm (16,500–14,000 cal. years B.P.), and Holocene values are reached by 130 cm (12,000 cal. years B.P.). However, there is some variability in the record until 100 cm depth, which corresponds to the depth at which establishment of tall forest is complete in the pollen record (8,500 cal. years B.P.). In Core GT0507, this transition is much more abrupt. The rise in COC values begins at a depth of 731 cm, corresponding to an age of c. 20,200 cal.

years B.P. A maximum value is reached by 728 cm, which corresponds to a time interval of c. 750 years. Above 728 cm, COC values fall again, although they remain substantially higher than the low values seen during the earlier part of the record.

6.4 Grain Size

Grain size is a fundamental property of any sediment, and reflects the sediment source, transport and depositional environment (Boggs, 1995). In the case of aeolian dust, the main controls on grain size are wind strength and distance transported. Stronger winds are capable of transporting larger grains, while sorting tends to occur during transport as larger grains have more rapid settling velocities and tend to be deposited sooner than finer grains (Pye, 1987; Clemens, 1998). An increase in grain size in sediment of aeolian origin can therefore be interpreted as an increase in wind strength or a change to a more localised source area for dust entrainment.

6.4.1 Grain Size of Loess in South Westland and Other Locations

Typical loess deposits are composed of grains in the size range 10–50 μm (Pye, 1987). Table 6.2 shows grain size data for some New Zealand and international loess deposits. Considerable variation is seen, although most samples are in the range of 10–50 μm. Modern dust collected in South Westland gives mean grain sizes in the range 12.6–47.6 μm (Marx and McGowan, 2005). This provides the best indicator of the expected grain size for aeolian dust in the South Westland region. Marx and McGowan (2005) interpreted seasonal variations in grain size recorded in their data to represent seasonal variations in the strength and direction of wind, with dust entrainment being favoured by certain wind directions at each site studied, according to the location of dust source areas. Variations between sites were also explained by the proximity of source areas for dust entrainment (generally braided river channels with a high content of fine material) and the position of these source areas with respect to the dominant wind direction.

Table 6.2: *Grain size of various aeolian dust and loess samples compared.*

Source	Mean Grain Size (μm)
Typical continental loess (Pye, 1987)	10 - 50
Modern dust - South Westland (Marx and McGowan, 2005)	12.6 - 47.6 (Overall mean 27)
West Coast loess (Young, 1967)	14.7 - 17.9
Otago loess (Young, 1964)	6.2 - 25.7 (Overall mean 10.9)

6.4.2 Grain Size Changes in the Study Area

The mean grain size of samples from Core GT0507 (Galway Tarn) is generally in the range of 20–30 μm, consistent with a predominantly aeolian source for material. A general coarsening upwards trend is seen during the LGM period, interrupted by a finer interval at a depth of 750 cm (22,500 cal. years B.P.). This trend suggests dust source areas expanded and/or moved closer to the Galway Tarn site during the LGM, an interpretation which is consistent with the ice advance recorded by moraine deposits.

The interval of finer grain size at 750 cm depth could correlate to the mid-LGM climate warming which is recorded in the pollen record from all three sites. In that scenario, the finer grain size would represent either a glacier retreat (consistent with the two distinct LGM glacier advances recorded by moraine deposits) and/or a period of calmer wind conditions. Studies of grain size of Australian dust deposited in the Tasman Sea have indicated that wind strengths during the glacial intervals were not significantly different from those of the present-day (Hesse and McTainsh, 1999), although other studies have suggested that the LGM climate in New Zealand was windier than the present climate (Alloway *et al.*, 1992; Soons *et al.*, 2002). A change in wind patterns cannot be ruled out, given the strong relationship many studies have shown between wind direction, wind speed and aeolian dust transport (Clemens, 1998; McGowan *et al.*, 2000). Another notable point is that the maximum grain size recorded at this site occurred at a depth of 730 cm (19,500 cal. years B.P.), whereas evidence from glacial moraines suggests that the second LGM ice advance was less extensive than the earlier advance (see Figure 2.7 in Chapter 2). This apparent discrepancy could be explained by a more favourable position of the ice margins and outwash areas relative to wind direction during the later LGM ice advance, but the results of this study are not sufficient to confirm this as an explanation.

It should also be noted that samples from Core GT0507 are very high in phytoliths, diatoms and other material of organic origin that were not dissolved by the peroxide pre-treatment technique used. These may have produced a distorted result, especially in samples from the upper part of the core (above the LGM) where material of organic origin contributed as much as 80 % of the grains in the samples. The LGM section of the core contains the highest proportion of inorganic grains but these still contribute only c. 30 % of the sample.

In general, the grain size data from Core GT0507 are rather inconclusive, with only small variations seen. This lack of variation may be explained by the dilution of the aeolian grain size signal by the high proportion of material derived from organic processes. However, given the very small catchment of the Galway Tarn site and the very limited surface runoff into the lake, coarser grain sizes are most likely to reflect a closer source for aeolian dust being blown in to the site.

Grain size data for Core SS906 (Skiffington Swamp) indicate a more complex situation. Mean grain sizes are generally coarser than samples from Core GT0507, and are up to 60 μm during the LGM. This implies that sediment grains comprised a mix of aeolian dust and material washed in

from the surrounding catchment, because the mean grain size is too coarse for aeolian transport to be the only mechanism involved. As with Galway Tarn, there is a general coarsening-upwards trend until a peak in grain size is reached at the culmination of the LGM (170 cm depth, c. 20,000 cal. years B.P.), although there are several very coarse peaks above this point. The changes in mean grain size between these peaks (which parallel the drop in MS values and the rise in COC) show that the warmer interglacial conditions represented by the upper part of Core SS906 are associated with finer grain size. The LGM period of the grain size record (between the Kawakawa Tephra and the maximum grain size attained at 170 cm) shows a distinct interval of finer grain size. As with Core GT0507, this fine interval can be correlated to the mid-LGM climate warming recorded in the pollen record. As discussed previously, the MS and COC results do not indicate that very much recession of the glaciers occurred, and the terminal position probably remained well to the west of the Skiffington Swamp site.

Caution is required in interpretation of these grain size data because of the influence of sediment grains derived from fluvial processes in the lake catchment. A coarsening of grain size in this fraction of the sediment would most likely be in response to higher rainfall or changes in catchment vegetation, thereby recording a different signal to that of ice advance.

Significant influxes of coarse material produced peaks in grain size at 160 cm and 130 cm in Core SS906. These are interpreted as indicating changes in rainfall and/or fluvial activity within the Skiffington Swamp catchment. The peaks in mean grain size of these coarse episodes (c. 100 μm) are significantly coarser than those of any other samples for Core SS906, and indicate a significant input of coarser sediment from the catchment surrounding the lake. It is also notable that there is no correlation between these coarse grain size peaks and the MS and COC records. This lack of correlation indicates that the input of sediment causing the peak in grain size was low in magnetically susceptible minerals, and was low enough in concentration that the MS signal from other sediment grains was not diluted, while the COC values were similarly uneffected. Taken together, these changes suggest the inwash of a (relatively) small proportion of coarse grains consisting mostly of quartz and feldspar.

The earlier of these coarse intervals appears to have lasted c. 1,500 years (18,500–17,000 cal. years B.P.), which makes a single incident of catchment erosion (e.g. a slope failure) unlikely as the cause, unless significant reworking of the material had occurred. Such reworking was seen from the spread of glass shards of the c. 2-cm-thick Kawakawa Tephra in Core SS906, but the extent of that reworking was limited to c. 0.5 cm above and below the tephra. The same tephra layer has a thickness of 1 cm in Core GT0507. In comparison, the coarse interval recorded in the grain size data covers c. 5 cm. A more probable explanation is an increase in precipitation leading to increased runoff and stream erosion.

It is notable that the coarse interval in Core SS906 at 160 cm depth correlates with a thin grey silt layer in Core GT0507 at a depth of 722 cm, which also occurs at c. 18,500 cal. years B.P. This silt layer is 2 mm thick, which implies a single event or an interval of very short duration (c. 25 years at the average sedimentation rate for Galway Tarn). However, it is difficult to

determine whether this event was part of the same interval of environmental change recorded by the grain size changes in Core SS906.

6.5 Mica and Organic Content

The metamorphic rocks of the Southern Alps are rich in biotite, chlorite and muscovite, which are rapidly eroded in response to the high rates of uplift and high rainfall in the region. Large volumes of these micas are transported by glaciers and rivers in the area. A close examination of modern glacial outwash and braided river channels in South Westland reveals that they contain high proportions of fine mica grains. This provides a readily available source of micas and other minerals for transport by wind.

LGM values for total mica content in Core SS906 are typically 20–30 %. The most notable feature of the mica content is the distinct peak which occurs at 170–160 cm, corresponding to c. 20,000 cal. years B.P. This peak is followed by a steady decline to values close to zero by 130 cm. The low value for mica content in the upper part of Core SS906 indicates that little mica was input into the site during times of warm climate, either from the catchment surrounding the site or by aeolian transport. This change to a more quartz-dominated composition is consistent with the interpretation that as glaciers retreated and aeolian dust played a lesser role at the site, inwash of material with a much lower mica content became dominant.

Although the data were limited, the mica content appeared to be reduced at a depth of 230 cm, which would be consistent with the lowered MS values at that time. This lower mica content, together with the peak in mica content seen at the end of the LGM, is consistent with the interpretation of MS values (discussed in Section 6.2.3) that input of aeolian dust into the Skiffington Swamp site was greatest during the recession of the glaciers when large outwash areas were exposed close to the site.

The mica content in Core GT0507 is generally higher than that of Core SS906, which is consistent with the interpretation that aeolian dust transport was the primary source of inorganic grains in the Galway Tarn environment. There is a slight increase in mica content during the LGM between depths of 780 and 730 cm. There is considerable variability during this period, possibly due to changes in prevailing wind direction, but no clear correlation with other records. It is also notable that mica percentage remains high after the rise in the COC record (730 cm or 20,000 cal. years B.P.) which is interpreted as representing the retreat of the glaciers from near to the site. In combination, these two records show that the volume of aeolian dust entering the site was reduced, but the composition remained similar. A reduction in aeolian dust transport rates would be expected as ice retreated from the area and vegetation stabilised outwash areas. Some dust transport continued from the wide braided river channels in the area. However, because of the very small amount of fluvial activity surrounding the Galway Tarn site, aeolian dust remained the dominant source of inorganic material in the lake and the mica content remained relatively high.

6.6 Chronology of the Last Glaciation in South Westland

The chronology of the last glaciation and early Holocene in South Westland, as indicated by this study, is illustrated in Figure 6.2. The moraines within which the Skiffington Swamp and Galway Tarn sites are located were most likely to have formed during a glacial advance in MIS 4. The advance was beyond the range of ^{14}C dating, but luminescence dates gave a range of 48,000–75,000 cal. years B.P. (Vandergoes *et al.*, 2005). This glacial advance is correlated with a reduction in tall forest pollen at Okarito Pakihi and a small peak in grass pollen. The grass peak recorded in pollen data was not as significant as the later LGM peaks, suggesting that the climate did not cool as much during this MIS 4 event as during MIS 2. However, the moraine produced by the earlier advance (the Loopline Moraine) is generally higher and extends further than the LGM moraines in South Westland, indicating a more extensive glacial advance in MIS 4 (Vandergoes *et al.*, 2005).

The MS and COC data for Skiffington Swamp and Galway Tarn show a relatively warm interval following the retreat of ice, which reached a peak at c. 60,000 cal. years B.P. based on the age estimates used in this study. Climate warming was also indicated by a minor recovery of forest pollen in the Okarito Pakihi record, although full interglacial conditions were never reached. Conditions had deteriorated again by c. 58,000 cal. years B.P., with shrub and small tree pollen becoming dominant in the Okarito Pakihi pollen data. However, grass pollen remained at a low level, and Vandergoes *et al.* (2005) interpreted the MIS 4–2 period to have been cool, with lowered treelines and vegetation dominated by subalpine taxa. MS and COC values from the Galway Tarn core indicate the climate was variable during this time, with 1,500–3,000 year fluctuations in temperature and/or precipitation causing changes in the organic productivity of the lake. Variations in the MS record for Skiffington Swamp, located closer to the Southern Alps, may record several small cycles of glacial advance between 52,000 and 39,000 cal. years B.P. However, any physical evidence for small ice advances at this time has been removed by the later advances of the LGM.

A rise in MS values in the Skiffington Swamp core occurred at c. 38,000 cal. years B.P., and was followed by a period of high, relatively stable values. Mean grain size also rose at this time, and COC fell to virtually zero. A rise in grass pollen at both Skiffington Swamp and Okarito Pakihi at this time suggests that the climate had begun to cool significantly. The rise in MS values at Skiffington Swamp is interpreted to indicate that some ice advance was occurring in the vicinity of the site as early as c. 38,000 cal. years B.P. This is substantially earlier than the onset of maximum LGM cooling (c. 28,500–32,500 cal. years B.P.) noted by Vandergoes *et al.* (2005), and somewhat earlier than c. 34,000 cal. years B.P. recorded by Suggate and Almond (2005). However, MS values at Galway Tarn remained low and variable at this time, and any ice advance was probably of limited extent. COC values at Galway Tarn were still relatively high. A peak in COC values in the Galway Tarn core at c. 32,500 cal. years B.P. may represent a brief interstadial warm period, but this event is not represented by any significant change at the Skiffington Swamp site.

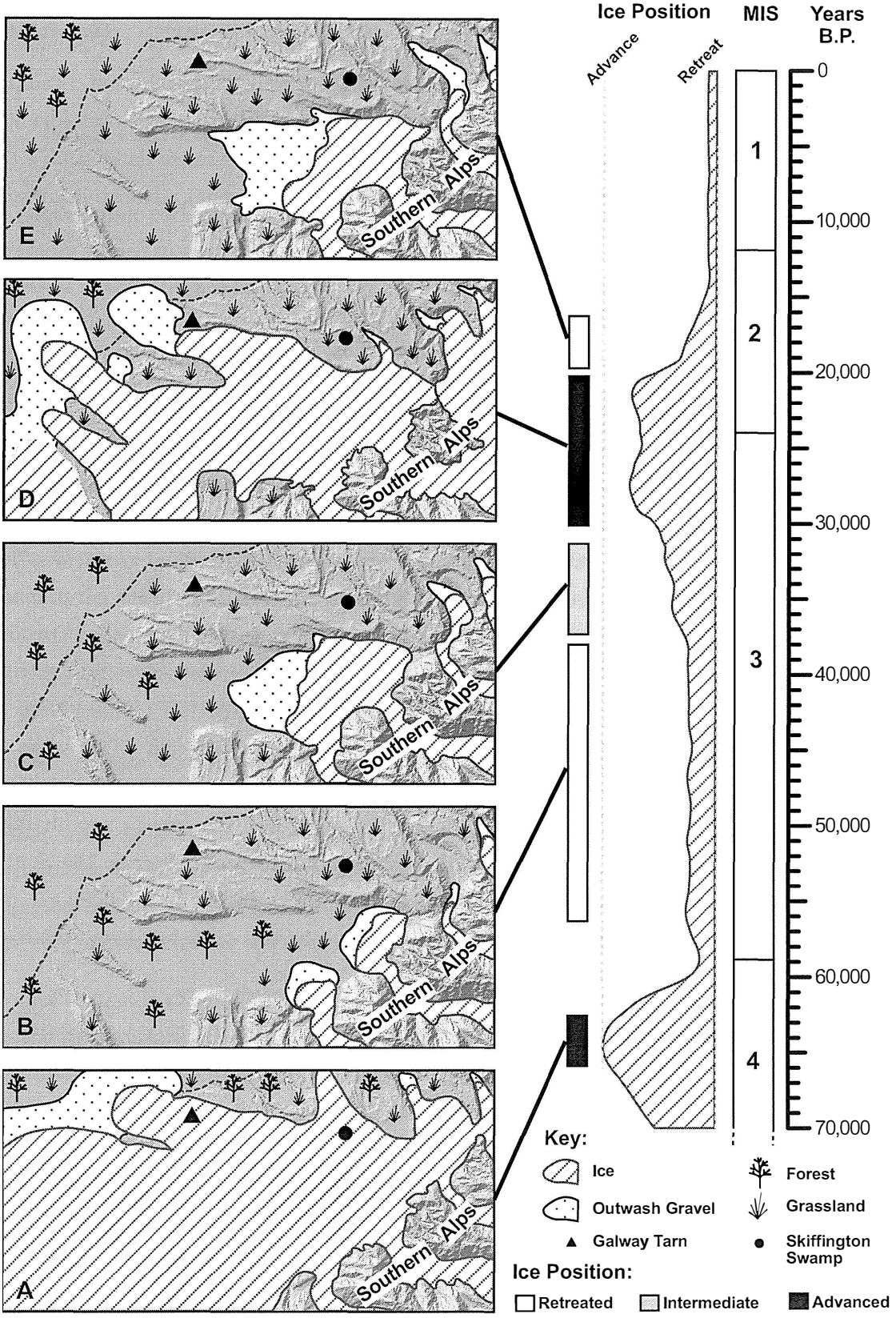

Figure 6.2: *(See next page for explanation).*

Figure 6.2 (Previous page): *Chronology of the last glaciation in South Westland. An extensive glacial advance (A) during MIS 4 deposited the moraine and drift deposits within which the Galway Tarn and Skiffington Swamp sites are located. Pollen data indicate that some forest remained during this glacial advance. Glaciers retreated during MIS 3 (B), but the climate remained cool and forest pollen never reached interglacial levels. Renewed glacial advance during the latter part of MIS 3 (C) led to increases in MS values at Skiffington Swamp, but did not affect Galway Tarn. Forest declined as the climate cooled and shrubs and grassland expanded. Glaciers reached their maximum extent during MIS 2 (D), and there may have been several glacial advances during this period. Outwash areas were located well to the west of Skiffington Swamp, and MS values were correspondingly reduced, while they reached a maximum at Galway Tarn. Grass pollen was dominant, and forests retreated to isolated patches. Glacier retreat at c. 20,000 cal. years B.P. lead to the exposure of outwash areas closer to Skiffington Swamp (E), while vegetation colonised and stabilised abandoned outwash areas near to Galway Tarn.*

After 32,000 cal. years B.P., COC at Galway Tarn fell to low values, while MS rose to a peak at c. 26,000 cal. years B.P. At Skiffington Swamp, MS values were lowered from 30,000 to 22,000 cal. years B.P. These changes suggest that between 32,000 and 30,000 cal. years B.P., ice advanced to a point near to the Galway Tarn site, at the same time moving outwash areas further from Skiffington Swamp.

The pollen records for the three sites have two major peaks in grass pollen, which have been correlated with the two distinct glacier advances represented by the Larrikins and Moana moraines. However, there is no clear correlation of these peaks with the MS, COC or grain size data from this study. An alternative to the interpretation given above is that the two periods of higher MS values at Skiffington Swamp correlate to these two glacial advances. In this scenario, other sources for aeolian dust entrainment were dominant at the Galway Tarn site, and the glacier advances did not produce a detectable signal there. However, the timing of variations seen in the Skiffington Swamp data from this study do not appear to match the changes in the pollen data, and it is difficult to explain how significant glacial advance would be recorded by the Skiffington Swamp site but not by the Galway Tarn site. In either scenario, there does not appear to be a good correlation between the pollen data and the results of this study for the early and middle parts of the LGM. This lack of correlation suggests that the ice advances seen in South Westland were not directly related to the same climate signal that caused changes in the vegetation of the area. The difference between the records could be explained if precipitation levels changed somewhat independently of temperature, given the sensitivity of South Westland glaciers to both temperature and precipitation (Hooker and Fitzharris, 1999).

A sharp rise in COC values at 20,000 cal. years B.P. in the Galway Tarn core indicates the onset of climate warming, and declining MS values may indicate that ice was already receding in the

area at that time. A peak in MS and mica content at Skiffington Swamp at 20,000 cal. years B.P. may represent the time at which receding glaciers led to a maximum amount of outwash material being exposed in the region of the Skiffington Swamp site. The age of c. 20,000 cal. years B.P. derived for this warming and glacial recession is significantly earlier than the established age of c. 17,500 cal. years B.P. for widespread retreat of Westland glaciers (Suggate, 1990). However, it is only slightly earlier than the age of c. 19,000 cal. years B.P. given by Suggate and Almond (2005) for glacial recession.

The peak in MS and mica content at Skiffington Swamp was followed by a decline in these indicators, followed by a rise in COC values. The difference in timing between the MS and COC records is reasonable if the MS signal responded to the presence of heavy minerals supplied from proximal outwash regions by aeolian transport, while the COC signal responded to climate warming and increased organic productivity in the vicinity of the site. A later response in the Skiffington Swamp COC record may also be expected due the higher altitude, and hence cooler climate, of the Skiffington Swamp site.

There is no evidence for significant late-glacial advance after c. 18,000 cal. years B.P., although an event between c. 18,500 and 17,000 cal. years B.P. did produce a peak in mean grain size in the Skiffington Swamp site. This event is interpreted as a period of higher precipitation, and may correlate with a thin grey silt layer in Core GT0507 from Galway Tarn. By c. 12,000 cal. years B.P., MS and COC at all sites had reached levels similar to the modern (Holocene) values, and the pollen record indicates that extensive forest was established at all sites by c. 10,000 cal. years B.P.

The glacial chronology for South Westland proposed by Almond *et al.* (2001) and Suggate and Almond (2005) is shown in Table 2.1 in Chapter 2 for comparison. They identified glacial advances which occurred at 50,000–40,000 cal. years B.P. and 34,000–28,000 cal. years B.P., and two which occurred between 24,500 and 19,000 cal. years B.P.

The M4 advance (c. 50,000–45,000 years B.P.) occurred at a time when results from this study record some fluctuation in glacier extent, although there is no evidence for a significant glacier advance. The MS and COC results from Skiffington Swamp suggest that major glacier advance began at c. 38,000 years B.P. The $M5_1$ advance (c. 34,000–28,000 years B.P.) could correspond to the maximum extent of this phase of advance, but evidence is not seen for any significant retreat of glaciers between c. 32,000 and c. 20,000 years B.P. which would separate the $M5_1$ advance from the later $M5_2$ advance (c. 24,500–21,500 years B.P.). Similarly, there is no evidence from this study of a significant glacier recession between the $M5_2$ and M6 advances.

Chapter 7

Conclusions

High resolution sedimentology data for cores from several sites in South Westland was investigated with the aim of identifying climate change signals and in particular a signal derived from aeolian dust input. The data from this study were compared with existing pollen data for the sites. Changes in ice extent in the region were inferred for a period from the end of MIS 4 until the early Holocene, based on the inorganic content, mineralogy and grain size of samples. These changes were compared with changes in climate inferred from pollen data. Tephra found in the study sites was analysed using electron microprobe techniques to confirm the eruptive source.

- The various indicators examined show significant changes over time, which were predominantly driven by changes in climate and/or ice extent. Using the chronology of this study (derived from tephra, luminescence, and ^{14}C dating), the inferred timing of ice advance and retreat is broadly consistent with the established glacial chronology of South Westland.

- Electron microprobe data showed that all glass shards recovered from the study area were derived from the Kawakawa Tephra. This tephra provides a useful marker for correlating cores from different sites and has been dated at 26,500 cal. years B.P. Other peaks in glass shard count in the cores were the result of reworking of the tephra and inwash of glass shards from the surrounding catchment. No other tephras were detected.

- The three sites used in this study formed on moraine and drift deposits of MIS 4 age (Galway Tarn and Skiffington Swamp) or MIS 6 age (Okarito Pakihi). The geomorphology of the area indicates that the MIS 4 advance was more extensive than subsequent advances of MIS 3 and MIS 2.

- A period of cool climate with some fluctuations in glacier extent was inferred for most of MIS 3, from c. 58,000 cal. years B.P. until c. 38,000 cal. years B.P. During this time, ice advance probably occurred within a few kilometres of the Southern Alps, in the vicinity of Skiffington Swamp site. Glacier advance was recorded at Skiffington Swamp between 38,000 and 32,000 cal. years B.P., indicating climate cooling. This is earlier than the onset of LGM cooling noted in previous studies.

- Results from the most distal site (Galway Tarn) suggest that maximum glacier extent was reached between 32,000 and 20,000 cal. years B.P., after which time widespread glacial retreat occurred. There is no clear evidence at these sites for any late glacial ice advance. If such an advance occurred it was of relatively small extent.

Table 7.1: *Glacial/interglacial sequences and nomenclature for Westland from Chapter 2, adapted from Suggate (1990).*

Years [1] BP	MIS [1]	Glacial / *Interglacial*	Age [2] (k yrs BP)	Moraine [2]	Formation [3]	Age [4] (k yrs BP)	Ice [4] Advance
0							
	1	*Aranui*					
12,000						11 - 14	Aurora 1
	2	Otira	19 - 20.5	M6	Moana	15 - 17	Aurora 2
			21.5 - 24.5	$M5_2$		18 - 20	Aurora 3
24,000					Larrikins		
			28 - 34	$M5_1$			
	3					40 - 41	Aurora 4
			45 - 50	M4	?	46 - 48	Aurora 5
59,000				M3			
	4		~60	M2	Loopline		
74,000						67 - 91	Aurora 6
	5	*Kaihinu*					
130,000							
	6	Waimea	?	M1	Waimea	?	Aurora 7

[1] MIS boundaries and boundary ages (Bradley, 1999)
[2] South Westland glacial chronology (Suggate and Almond, 2005)
[3] Moraine formations (Suggate, 1985)
[4] Fiordland speleothem/cave sediment record (Williams, 1996)

- The results of this study showed some differences from previous studies. In particular, significant ice advance occurred earlier in MIS 3 than had previously been shown. The timing of glacial advance and recession did not directly correlate with the climate inferred from pollen data, showing that ice advance and vegetation assemblage responded to different elements of the climate system.

- The four main glacial advances recorded by Almond et al. (2001) and Suggate and Almond (2005) for MIS 3–2 (Figure 7.1) may correlate with the pattern of glacial advance found in this study. The earlier advance (M4, c. 50,000–45,000 years B.P.) occurred at a time when results for this study showed some fluctuations in glacier extent, but there was no evidence of a significant glacier advance. Later advances ($M5_1$, $M5_2$, and M6) correlate with times of major glacier extension, but evidence is not seen for any significant glacier recession separating these glacial advances.

In conclusion, this study found that sedimentology changes in the lakes and peat bogs studied were strongly influenced by changes in the nature and amount of aeolian dust entering the sites, which in turn represented changes in the extent of glaciers and outwash areas. Major LGM glacial advance and retreat left a clear record in the clastic sediment at these sites, but smaller fluctuations in glacier extent were not significant enough to be recorded by changes in aeolian dust flux.

Appendix A: Core Logs

The following pages contain the full core logs for Core SS906 (Skiffington Swamp) and Core GT0507 (Galway Tarn). The first page for each log is a composite summary of all core sections. Subsequent pages show individual core sections in greater detail.

Core Log

Location: Skiffington Swamp, South Westland **Core Number:** SS906 (Full)

Logged by: J Cole-Baker **Core Length (cm):** 480

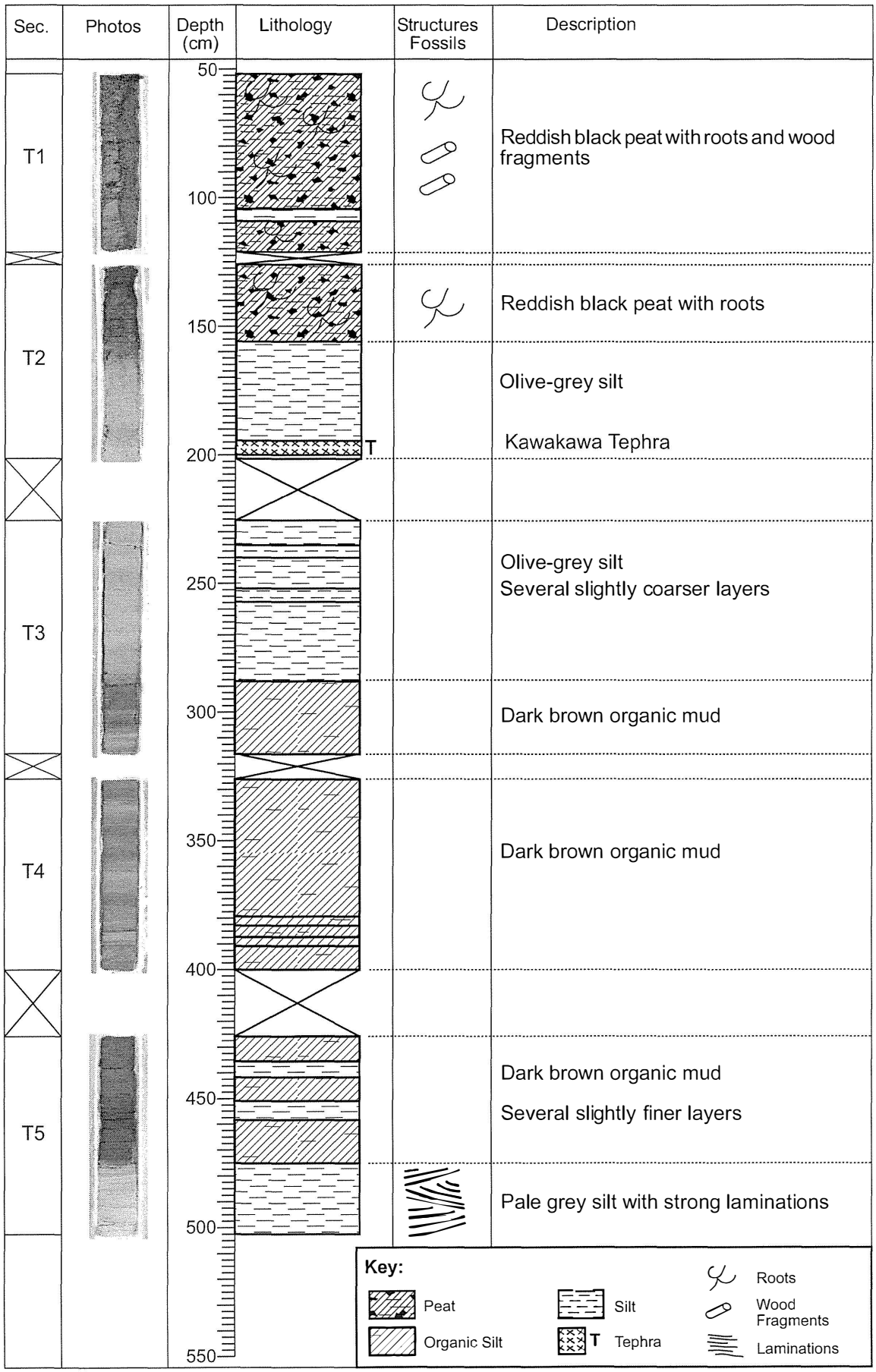

Core Log

Location: Skiffington Swamp, South Westland **Core Number:** SS906 T1

Logged by: J Cole-Baker **Core Length (cm):** 70 (52 - 122)

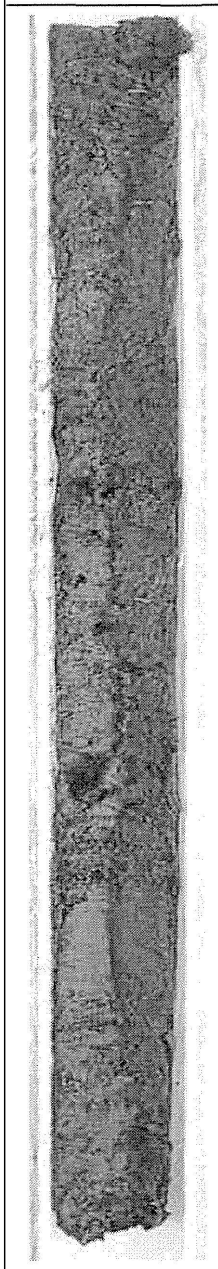

Depth (cm)	Structures Fossils	Description
0		Reddish black peat Many roots and wood fragments 2.5YR 2/1 Reddish black
10		
20		Reddish black peat with some roots 7.5R 2/1 Reddish black
30		27-29 cm Large wood fragment
40		43-45 cm Large wood fragment
50		Reddish black silty peat No root fragments 7.5R 2/1 Reddish black
60		Reddish black peat with some roots 10R 1.7/1 Reddish black
70		
80		
90		

Key:

Peat
Organic Silt
Silt
Roots
Wood Fragments
Laminations

Core Log

Location: Skiffington Swamp, South Westland **Core Number:** SS906 T2

Logged by: J Cole-Baker **Core Length (cm):** 75 (126 - 201)

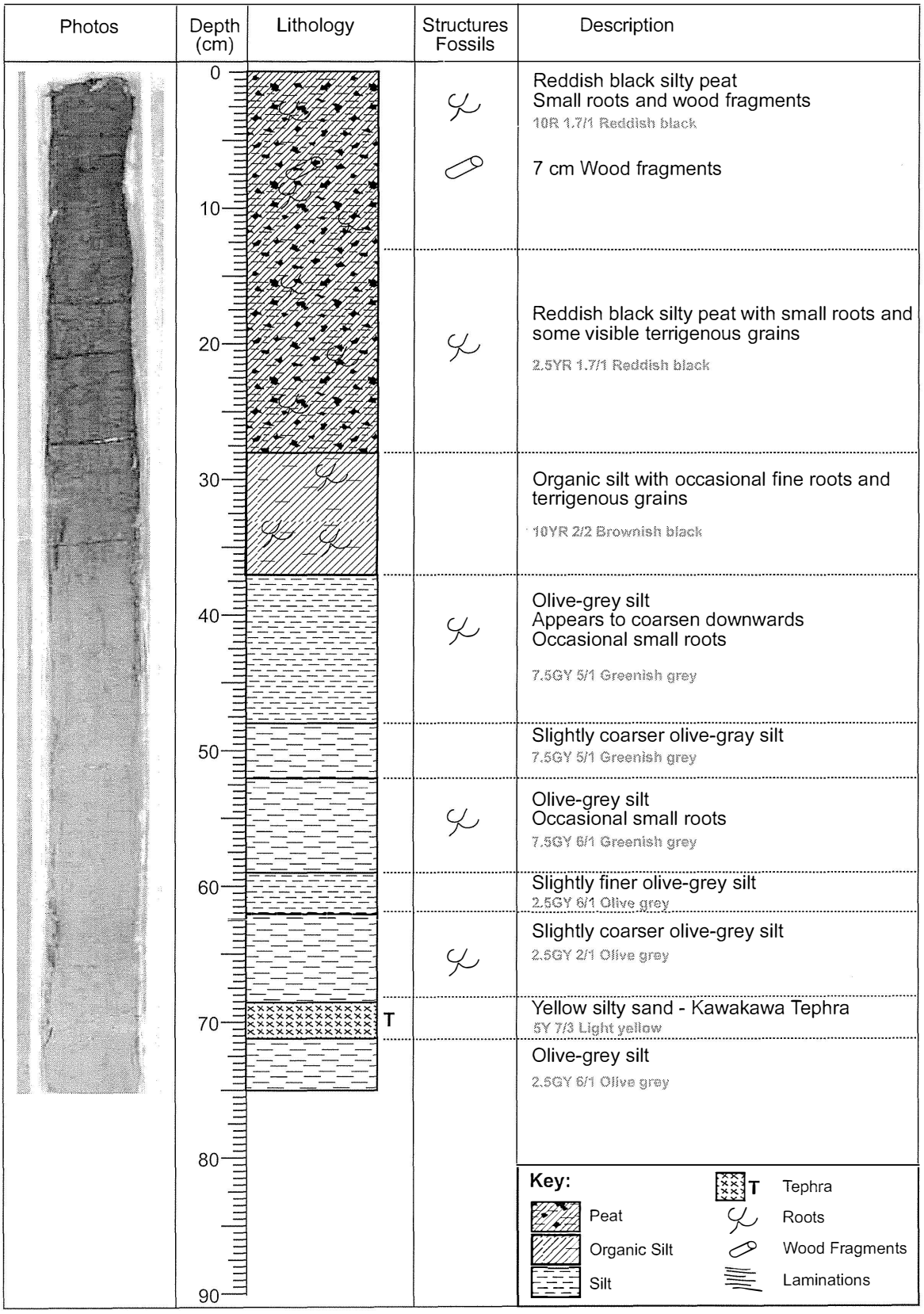

Core Log

Location: Skiffington Swamp, South Westland **Core Number:** SS906 T3

Logged by: J Cole-Baker **Core Length (cm):** 88.5 (226 - 314.5)

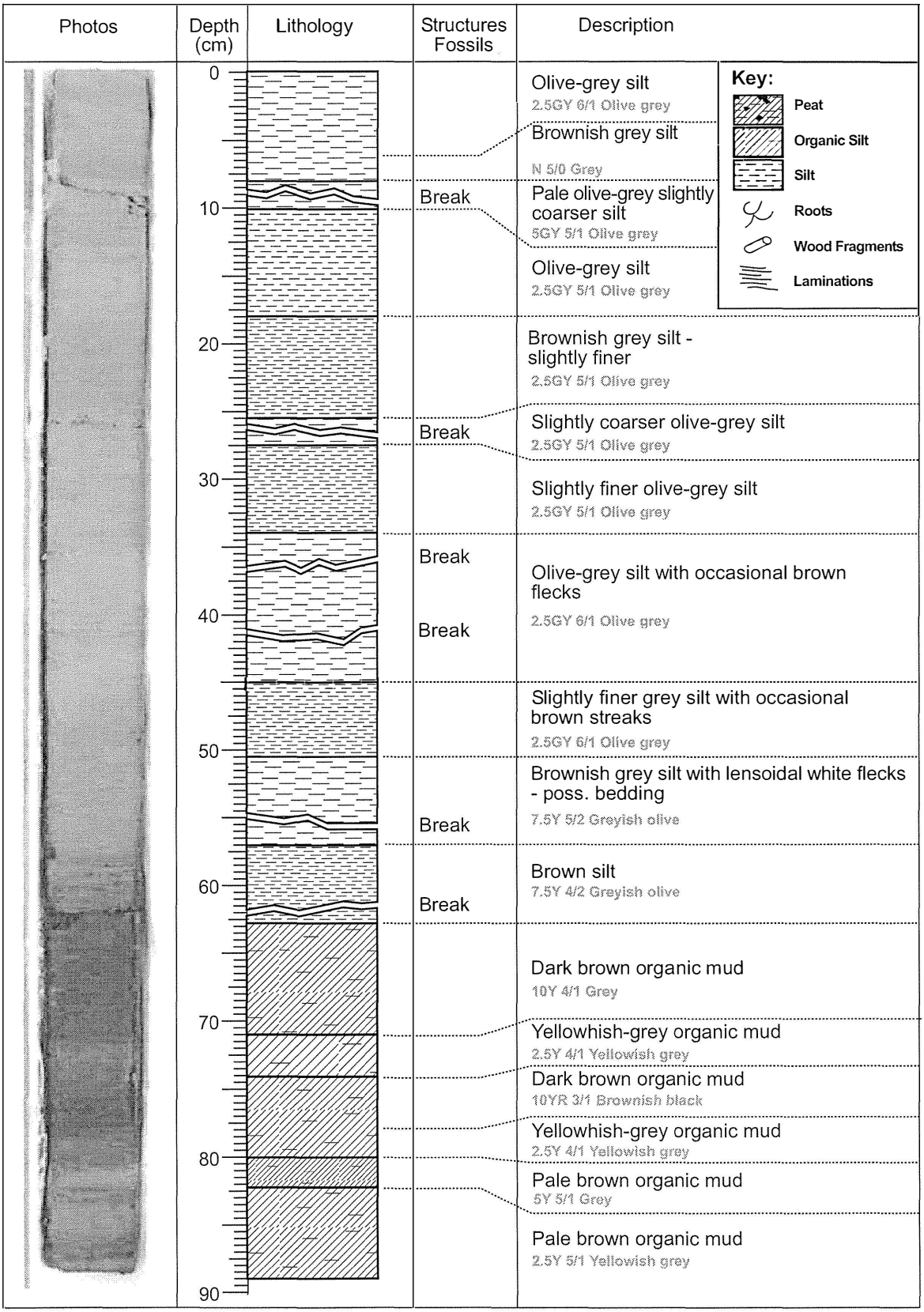

Core Log

Location: Skiffington Swamp, South Westland **Core Number:** SS906 T4

Logged by: J Cole-Baker **Core Length (cm):** 73.5 (326 - 399.5)

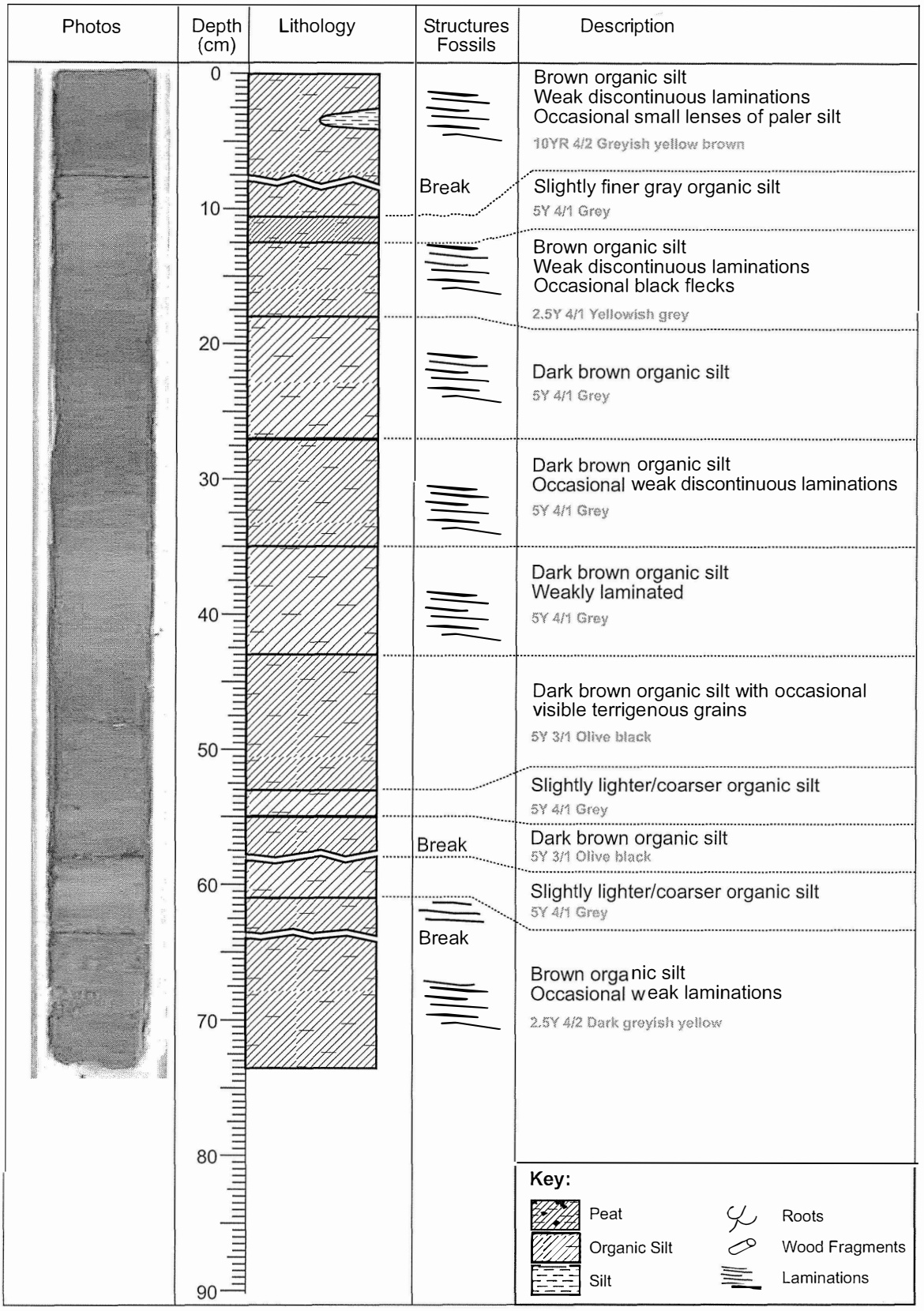

Core Log

Location: Skiffington Swamp, South Westland **Core Number:** SS906 T5

Logged by: J Cole-Baker **Core Length (cm):** 77 (426 - 503)

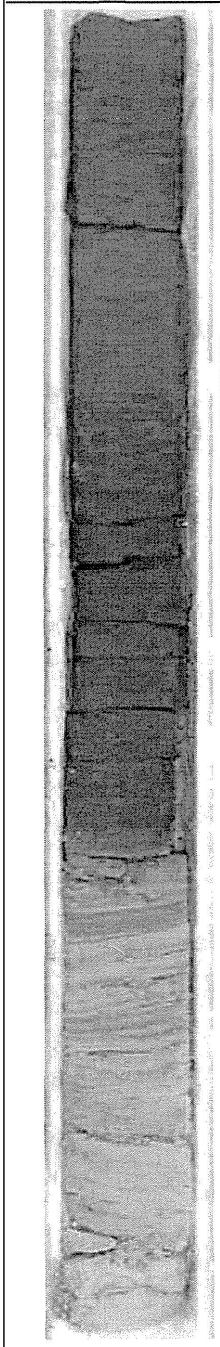

Depth (cm)	Structures Fossils	Description
0		Dark brown organic silt 7.5YR 3/1 Brownish black
		Very dark brown organic silt 2.5YR 3/1 Dark reddish grey
10	Break	Dark brown organic silt 7.5R 2/1 Reddish black
		Dark brown organic silt 7.5YR 3/1 Brownish black
20		
	Break	Dark brown organic silt 7.5R 2/1 Reddish black
30	Break	
	Break	
	Break	
	Break	Dark brown organic silt 7.5YR 3/1 Brownish black
40	Break	
	Break	
	Break	Light brown silt 10YR 3/1 Brownish black
50		Pale brownish grey silt 5Y 4/1 Grey
		Blue grey laminated silt 2.5GY 4/1 Dark olive grey
60		Pale blue grey laminated silt Strong angled laminations 2.5GY 6/1 Olive grey
	Break	Pale grey silt with weak laminations 5GY 6/1 Olive grey
70	Break	
	Break	Pale grey silt 5GY 7/1 Light olive gray
80		
90		

Key:

Peat
Organic Silt
Silt
Roots
Wood Fragments
Laminations

Core Log

Location: Galway Tarn, South Westland **Core Number:** GT0507 (Full)

Logged by: J Cole-Baker **Core Length (cm):** 340

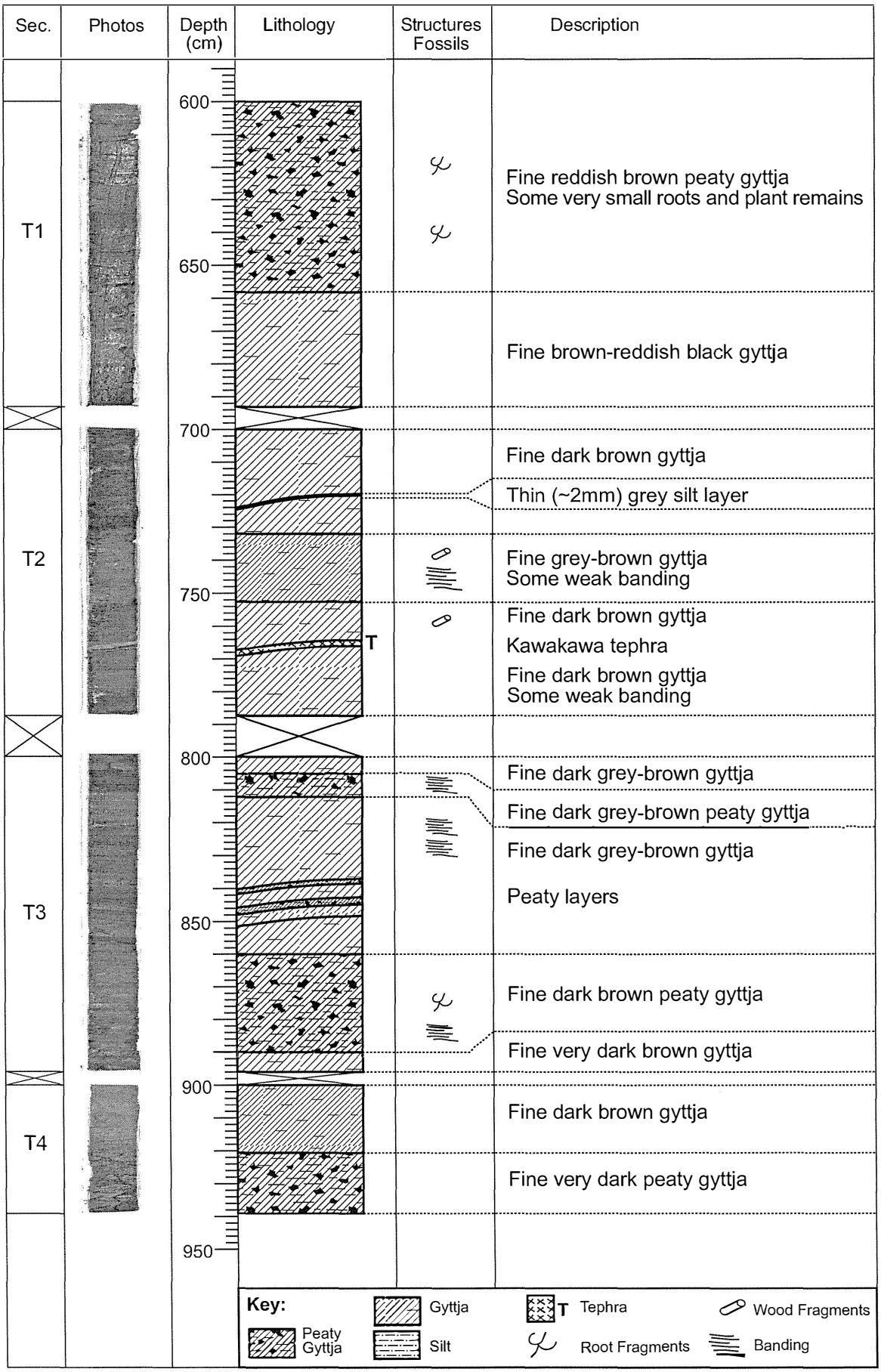

Core Log

Location: Galway Tarn, South Westland
Logged by: J Cole-Baker

Core Number: GT0507 T1
Core Length (cm): 93.5 (600 - 693.5)

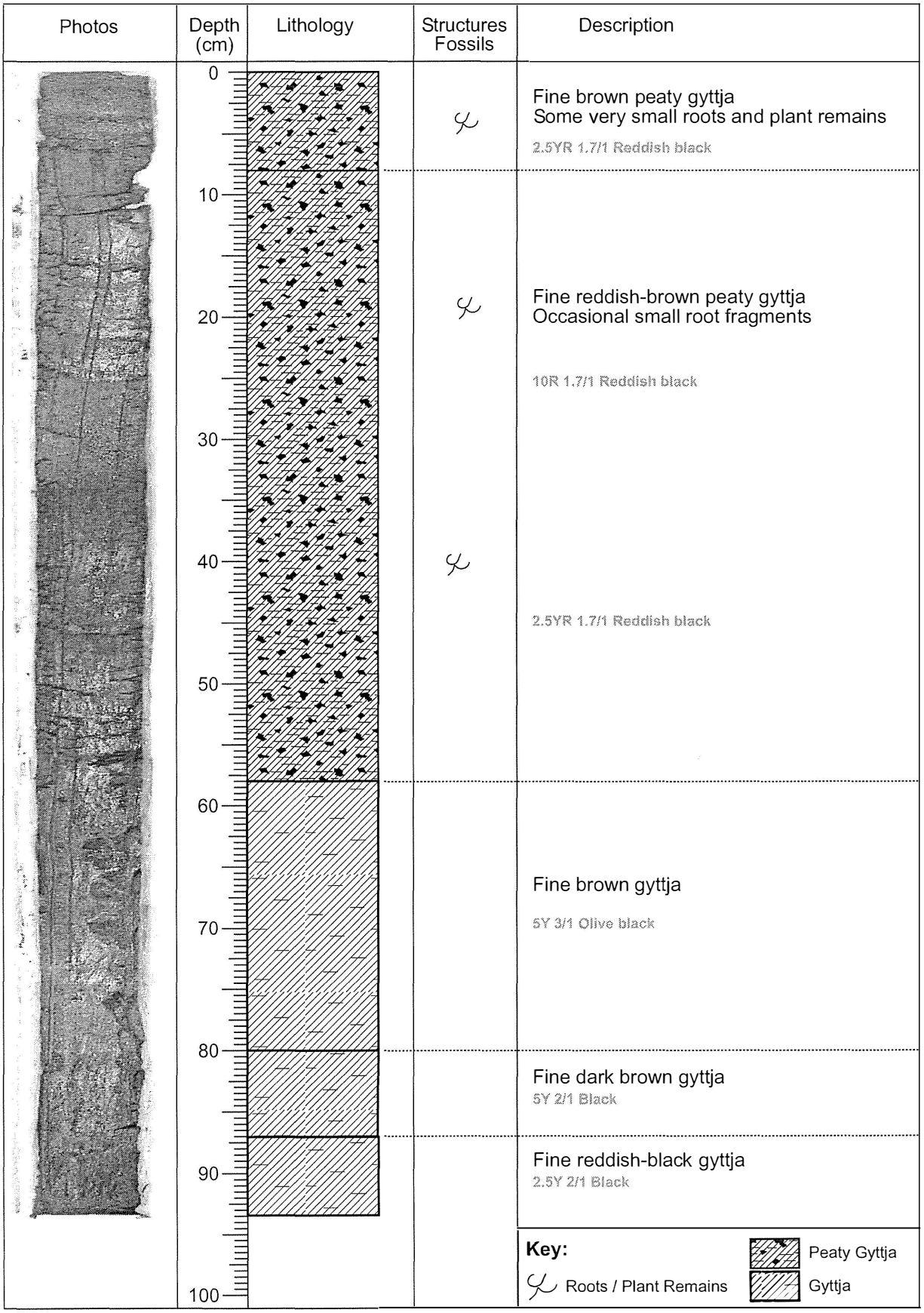

Core Log

Location: Galway Tarn, South Westland **Core Number:** GT0507 T2

Logged by: J Cole-Baker **Core Length (cm):** 87.5 (700 - 787.5)

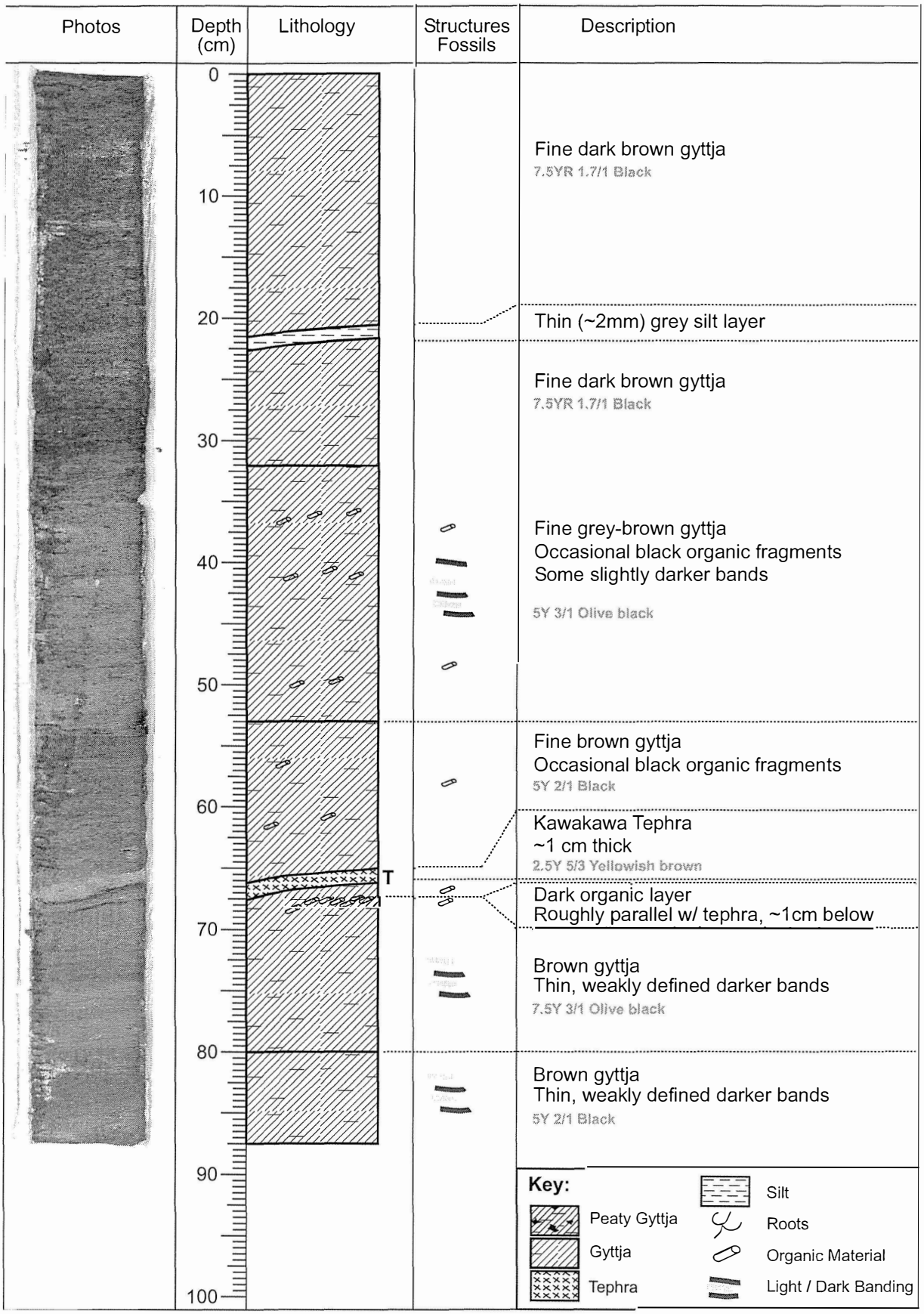

Core Log

Location: Galway Tarn, South Westland **Core Number:** GT0507

Logged by: J Cole-Baker **Core Length (cm):** 96 (800 - 896)

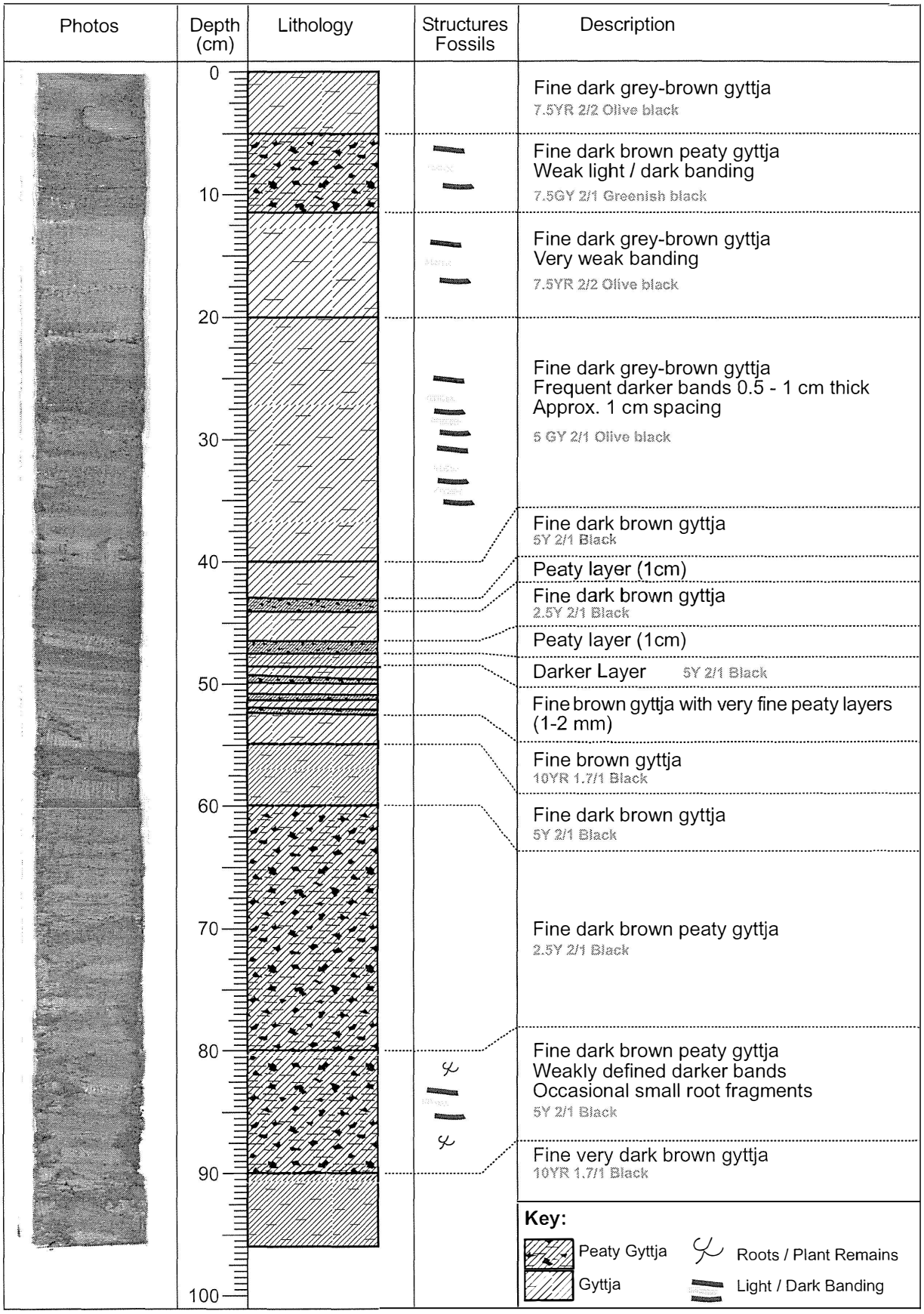

Core Log

Location: Galway Tarn, South Westland **Core Number:** GT0507 T4

Logged by: J Cole-Baker **Core Length (cm):** 39 (900 - 939)

Photos	Depth (cm)	Lithology	Structures Fossils	Description
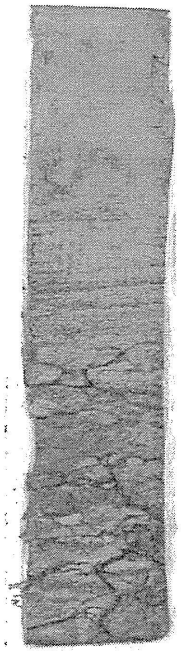	0 10 20 30 40 50 60 70 80 90 100			Fine dark brown gyttja 7.5Y 2/2 Olive black Fine dark brown slightly peaty gyttja 5Y 2/1 Black Fine dark brown peaty gyttja Several clean breaks N1.5/0 Black Fine very dark peaty gyttja 2.5YR 1.7/1 Black

Key: Peaty Gyttja Gyttja

Appendix B: Electron Microprobe Data

The following pages contain electron microprobe data (raw analysis) for glass shards from Core 906 (Skiffington Swamp). *Probe No.* refers to the sequential identifier recorded for each probe result. *Sample No.* refers to the sample from which shards were taken. Total iron is expressed as FeO.

Electron Microprobe Data (Core 906)

Probe No.	Sample No.	Probe Data														
		SiO_2	TiO_2	Al_2O_3	FeO	MnO	MgO	CaO	Na_2O	K_2O	P_2O_5	SO_3	Cl	Cr_2O_3	NiO	TOTAL %
11588	274	72.26	0.17	11.68	1.12	0.05	0.14	1.05	4.35	2.89	-0.11	-0.01	0.15	-0.03	0.21	93.92
11588	274	72.26	0.17	11.68	1.12	0.05	0.14	1.05	4.35	2.89	-0.11	-0.01	0.15	-0.03	0.21	93.92
11589	274	72.45	0.21	11.46	0.99	0.03	0.24	0.97	4.55	3.11	-0.10	0.05	0.18	0.03	0.12	94.29
11590	274	72.32	0.05	11.39	0.83	0.08	0.07	0.95	4.06	3.01	-0.17	0.00	0.15	-0.03	0.10	92.81
11591	274	72.15	0.14	11.25	1.12	0.12	0.04	0.86	4.37	2.93	-0.26	-0.02	0.17	-0.04	-0.02	92.81
11592	274	72.51	0.18	11.17	0.96	0.02	-0.02	1.05	4.50	2.91	-0.18	0.06	0.19	-0.01	-0.02	93.32
11593	274	71.37	0.16	11.41	1.00	-0.02	0.03	1.09	4.36	2.99	-0.20	-0.08	0.17	0.10	-0.05	92.33
11594	274	72.21	0.15	11.30	1.15	0.04	-0.02	1.03	4.40	2.84	-0.25	-0.02	0.16	-0.06	0.13	93.06
11595	274	72.92	0.09	11.63	1.21	0.01	0.17	1.12	4.11	2.92	-0.20	-0.11	0.16	0.07	0.05	94.15
11596	274	72.06	0.14	11.17	1.03	0.09	0.03	1.01	3.74	3.08	-0.12	-0.08	0.15	-0.06	0.04	92.28
11597	274	72.48	0.20	11.58	1.15	-0.08	0.08	0.98	4.46	2.89	-0.15	-0.04	0.16	-0.01	0.15	93.85
11599	274	73.12	0.07	11.33	1.05	0.10	0.20	1.00	4.60	3.06	-0.14	0.00	0.17	0.06	0.13	94.75
11600	274	72.08	0.12	11.42	1.04	0.17	0.20	1.02	4.02	3.00	-0.11	0.01	0.12	0.03	0.12	93.24
11601	240	71.42	0.16	11.34	1.03	0.20	0.14	0.97	4.33	3.02	-0.14	0.00	0.17	0.00	0.02	92.66
11602	240	72.25	0.07	11.35	0.99	0.08	0.01	0.96	3.85	2.97	-0.17	-0.06	0.10	0.00	0.05	92.45
11604	240	71.22	0.09	11.31	0.86	0.07	0.02	0.93	4.01	2.99	-0.20	0.10	0.20	0.01	0.10	91.71
11605	240	72.44	0.06	11.37	1.02	0.05	0.01	0.99	4.40	2.86	-0.12	0.00	0.24	-0.01	-0.07	93.24
11606	240	71.91	0.01	11.60	1.04	0.16	0.04	1.03	4.19	2.87	-0.23	0.05	0.20	-0.04	0.14	92.97
11607	240	71.63	0.16	11.33	1.06	0.15	0.09	1.03	4.23	2.95	-0.30	-0.03	0.08	0.03	0.07	92.48
11608	240	72.06	0.22	11.23	0.92	0.10	-0.03	0.95	4.24	3.01	-0.23	-0.01	0.15	0.08	0.14	92.83
11609	240	71.18	0.25	11.27	1.01	0.02	0.09	0.92	4.07	2.86	-0.16	-0.05	0.18	-0.02	-0.03	91.59
11610	240	72.06	0.01	11.37	0.93	0.11	0.06	1.06	4.20	2.99	-0.16	-0.07	0.17	-0.05	0.06	92.74
11611	240	71.35	0.08	11.27	0.76	0.11	0.07	0.92	3.94	3.11	-0.14	-0.02	0.12	0.05	0.21	91.83
11612	240	70.96	0.21	11.13	0.99	0.04	0.25	0.87	3.84	3.46	-0.26	-0.04	0.18	0.00	0.06	91.69
11613	220	73.01	0.20	11.39	1.00	0.12	0.16	1.06	4.18	2.90	-0.14	-0.03	0.14	0.04	-0.12	93.91
11615	220	71.34	0.18	11.28	1.10	0.06	0.09	1.07	4.31	2.91	-0.24	0.00	0.15	0.00	-0.07	92.18
11616	220	71.93	0.23	11.23	0.86	0.07	0.10	1.07	4.21	2.88	-0.18	-0.04	0.09	-0.01	0.27	92.71
11618	220	72.24	0.16	11.36	0.97	0.02	0.13	0.96	4.47	2.82	-0.06	-0.05	0.19	0.04	0.00	93.25
11619	220	72.12	0.13	11.24	0.82	-0.01	-0.05	0.97	4.34	3.04	-0.09	0.01	0.17	0.01	0.23	92.93
11620	220	71.45	0.04	11.52	1.11	0.09	0.06	1.10	4.42	2.81	-0.13	0.07	0.16	0.00	-0.11	92.59
11621	220	71.53	0.22	11.30	1.09	0.08	-0.07	1.04	4.20	2.92	-0.18	-0.11	0.17	0.01	0.16	92.36
11622	220	72.50	0.16	11.56	0.96	0.02	0.00	0.99	4.27	3.10	-0.28	-0.06	0.16	-0.07	-0.01	93.30
11623	220	72.30	0.22	11.38	1.01	0.07	0.10	1.02	3.85	2.88	-0.15	-0.11	0.09	-0.03	0.03	92.66
11624	220	71.35	0.07	11.11	0.90	0.04	-0.18	0.98	4.55	2.96	-0.17	-0.04	0.19	0.01	0.01	91.78
11626	220	70.34	0.21	13.27	0.97	0.06	0.01	1.10	4.17	2.79	-0.12	-0.07	0.14	-0.03	0.01	92.85
11627	220	71.55	0.10	11.36	0.84	0.10	0.01	1.06	4.04	2.91	-0.14	-0.09	0.08	-0.04	0.20	91.98
11628	198	71.59	0.14	11.15	0.84	0.03	0.20	0.86	3.98	3.51	-0.22	0.04	0.20	-0.03	-0.06	92.23

Electron Microprobe Data (Core 906) - Continued

Probe No.	Sample No.	Probe Data														
		SiO_2	TiO_2	Al_2O_3	FeO	MnO	MgO	CaO	Na_2O	K_2O	P_2O_5	SO_3	Cl	Cr_2O_3	NiO	TOTAL %
11629	198	72.73	0.20	11.44	0.95	-0.04	-0.13	1.12	4.13	2.85	-0.12	-0.06	0.15	0.09	0.17	93.48
11630	198	71.85	0.20	11.42	1.15	0.13	0.04	1.24	4.28	2.88	-0.20	-0.03	0.19	0.07	-0.02	93.20
11640	166	71.75	0.15	11.08	0.95	0.08	0.05	1.07	4.23	2.97	-0.24	-0.02	0.18	-0.04	-0.13	92.08
11642	166	68.93	0.16	13.23	0.92	-0.01	0.07	1.08	4.04	2.85	-0.16	0.00	0.11	0.02	0.13	91.37
11643	166	71.86	0.21	11.33	0.92	0.08	-0.06	1.02	4.27	2.89	-0.16	-0.03	0.15	-0.03	0.12	92.57
11645	166	71.96	0.21	11.23	0.79	0.24	0.18	0.96	4.14	2.90	-0.17	-0.06	0.14	-0.02	0.00	92.50
11646	166	72.00	0.04	11.32	0.91	0.02	0.24	1.03	3.79	3.10	-0.23	-0.05	0.16	-0.04	0.18	92.47
11647	166	71.97	0.07	11.30	0.86	0.10	0.15	0.92	4.46	2.79	-0.17	-0.06	0.19	-0.05	0.01	92.54
11648	166	72.48	0.01	11.47	1.24	0.01	0.22	1.11	4.52	2.87	-0.16	-0.01	0.13	-0.04	0.11	93.96
11650	166	72.40	0.06	11.64	1.03	0.06	0.01	1.06	4.37	2.80	-0.28	-0.02	0.13	0.09	-0.08	93.27
11651	166	72.34	0.24	11.25	0.89	0.14	0.00	1.01	4.58	2.97	-0.16	0.04	0.17	0.04	-0.09	93.42
11652	166	72.11	0.16	11.49	1.16	0.00	-0.01	1.08	4.59	2.93	-0.24	0.00	0.14	0.01	0.11	93.53
11653	166	71.64	0.17	11.46	1.01	0.05	-0.02	1.02	4.35	3.25	-0.21	-0.06	0.21	-0.05	0.14	92.96
11654	166	71.64	0.22	11.71	1.20	0.09	0.05	1.30	4.45	2.71	-0.23	-0.02	0.15	-0.04	0.04	93.27
11655	164	72.16	0.19	11.36	1.03	0.05	-0.02	1.12	4.52	2.98	-0.09	0.05	0.14	0.09	0.02	93.60
11656	164	74.58	0.28	13.12	1.56	0.07	0.14	1.44	4.86	2.81	-0.16	-0.07	0.13	-0.03	-0.08	98.65
11657	164	71.26	0.09	11.46	0.95	0.06	0.00	0.98	4.26	2.66	-0.15	-0.12	0.15	0.00	0.02	91.62
11658	164	73.36	0.03	11.55	0.90	0.02	-0.04	1.06	4.63	3.04	-0.21	-0.11	0.16	-0.06	0.05	94.38
11659	164	73.75	0.16	11.40	0.73	0.02	0.05	1.06	4.12	3.20	-0.30	-0.01	0.09	0.09	0.12	94.48
11659	164	73.75	0.16	11.40	0.73	0.02	0.05	1.06	4.12	3.20	-0.30	-0.01	0.09	0.09	0.12	94.48
11661	164	72.15	-0.01	11.46	1.06	0.00	-0.09	0.97	4.05	2.94	-0.10	-0.06	0.17	0.00	0.05	92.59
11663	164	71.97	0.12	11.16	1.11	0.04	-0.04	1.00	4.04	2.67	-0.17	-0.03	0.13	0.00	0.23	92.23
11664	272	72.52	0.20	11.75	1.06	0.07	-0.03	0.90	4.28	2.97	-0.26	0.09	0.20	0.08	0.04	93.87
11665	272	72.07	0.12	11.34	1.08	0.04	-0.01	1.00	4.33	3.07	-0.24	-0.02	0.17	0.00	0.07	93.02
11666	272	71.39	0.14	11.42	1.01	0.16	0.18	0.92	4.46	3.06	-0.20	0.00	0.17	-0.05	0.05	92.71
11667	272	72.69	0.11	11.37	0.97	0.15	-0.05	0.98	4.31	3.24	-0.22	-0.04	0.14	0.01	-0.09	93.57
11668	272	72.38	0.13	11.54	1.05	0.11	-0.01	0.98	4.93	2.99	-0.23	-0.06	0.17	-0.07	0.01	93.92
11669	272	72.10	0.14	11.49	1.14	0.10	0.06	1.04	4.27	3.04	-0.20	0.06	0.19	0.01	0.14	93.58
11670	272	71.49	0.11	11.18	0.99	0.16	-0.04	1.09	4.40	2.96	-0.20	-0.08	0.15	0.01	0.20	92.42
11671	272	71.64	0.18	11.26	0.89	0.06	0.03	1.02	4.27	2.95	-0.22	0.02	0.11	-0.02	-0.05	92.14
11672	272	73.14	0.16	11.57	0.96	0.02	-0.02	1.10	4.34	3.17	-0.14	-0.05	0.14	0.00	0.35	94.74
11673	272	72.61	0.05	11.52	1.03	0.05	-0.03	1.14	4.51	2.95	-0.13	0.02	0.18	0.00	0.11	94.01
11674	272	72.16	0.15	11.23	1.09	0.00	0.14	1.05	4.51	3.22	-0.15	0.01	0.16	-0.02	0.02	93.57
11675	272	72.13	0.14	11.18	0.82	0.08	0.20	0.88	4.18	3.10	-0.25	0.07	0.20	0.11	0.01	92.85

Appendix C: Data Correlation Methods

Microsoft Excel was used to adjust the depths of pollen data and dates from other studies to correlate with the results of this study (See Chapter 4). Stratigraphic tie-points such as changes in lithology (as identified in original core descriptions) and tephra layers were identified and matched in the cores from this study and from previous studies. The depths of these tie-points in the pollen or dating data were adjusted to allow them to be correlated with the results of this study. Depths for intermediate points were then adjusted by a linear stretching between the tie points, as in the following example (see illustration below).

Tie-points A (change from silt to peat) and B (tephra layer) have been identified in the core used in this study, and located in pollen data from previous studies (A' and B').

The depths for points A' and B' in the pollen data are adjusted to match A and B, respectively. In order to calculate the adjusted depth d of an intermediate sample depth (d') in the pollen data, the following formula is used:

$$d = A + \left(\frac{(d' - A')}{(B' - A')} (B - A) \right)$$

The depth of position d is given by the depth of the previous tie point, plus the fraction of the distance between the tie points represented by d'.

This correlation method was applied to adjust the depths of samples in the pollen data from previous studies. To calculate the approximate age for samples, the depths associated with existing dating information were adjusted as above. Ages for intermediate points were then extrapolated based on core depth, by assuming a constant sedimentation rate between dated points.

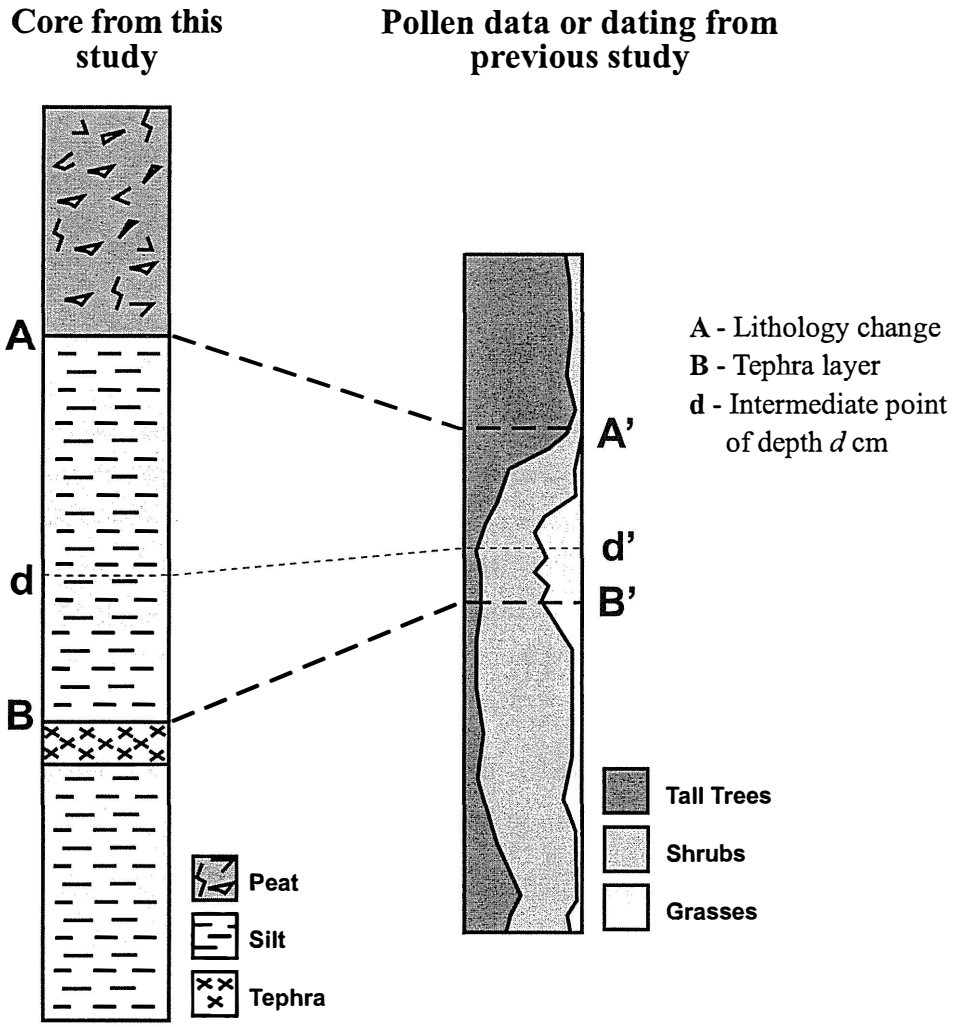
Core from this study
Pollen data or dating from previous study
A
d
B
A'
d'
B'
A - Lithology change
B - Tephra layer
d - Intermediate point of depth d cm
Peat
Silt
Tephra
Tall Trees
Shrubs
Grasses

References

Adams, J.; Maslin, M.; Thomas, E. 1999: Sudden climate transitions during the Quaternary. *Progress in Physical Geography 23:* 1-36.

Alley, R. B. 2000: The Younger Dryas cold interval as viewed from central Greenland. *Quaternary Science Reviews 19:* 213-226.

Alloway, B. V.; Stewart, R. B.; Neall, V. E.; Vucetich, C. G. 1992: Climate of the last glaciation in New Zealand, based on aerosolic quartz influx in an andesitic terrain. *Quaternary Research 38:* 170.

Almond, P. C. 1996: Loess, soil stratigraphy and Aokautere Ash on late Pleistocene surfaces in south Westland, New Zealand: Interpretation and correlation with the glacial stratigraphy. *Quaternary International 34-36:* 163-176.

Almond, P. C.; Tonkin, P. J. 1999: Pedogenesis by upbuilding in an extreme leaching and weathering environment, and slow loess accretion, south Westland, New Zealand. *Geoderma 92:* 1-36.

Almond, P. C.; Moar, N. T.; Lian, O. B. 2001: Reinterpretation of the glacial chronology of South Westland, New Zealand. *New Zealand Journal of Geology and Geophysics 44:* 1-15.

Ballinger, M. M. 2003: Developing methods for identifying cryptic tephra in peat cores from the Waikato region, North Island, New Zealand. MSc thesis, University of Plymouth.

Bard, E. 2002: Climate shock: Abrupt changes over millennial time scales. *Physics Today 55:* 32-38.

Bard, E. 2004: Greenhouse effect and ice ages: historical perspective. *Comptes Rendus Geosciences 336:* 603-638.

Berger, G. W.; Pillans, B. J.; Bruce, J. G.; McIntosh, P. D. 2002: Luminescence chronology of loess-paleosol sequences from southern South Island, New Zealand. *Quaternary Science Reviews 21:* 1899-1913.

Berryman, K.; Marden, M.; Eden, D.; Mazengarb, C.; Ota, Y.; Moriya, I. 2000: Tectonic and paleoclimatic significance of Quaternary river terraces of the Waipaoa River, east coast, North Island, New Zealand. *New Zealand Journal of Geology and Geophysics 43:* 229-245.

Bishop, D. G. 1972: Progressive metamorphism from prehnite-pumpellyite to greenschist facies in the Dansey Pass area, Otago, New Zealand. *Geological Society of America Bulletin 83:* 3177-3198.

Björck, S.; Walker, M. J. C.; Cwynar, L. C.; Johnsen, S.; Knudsen, K.-L.; Lowe, J. J.; Wohlfarth, B. 1998: An event stratigraphy for the Last Termination in the North Atlantic region based on the Greenland ice-core record: a proposal by the INTIMATE group. *Journal of Quaternary Science 13:* 283-292.

Boggs, S. 1995: Principles of sedimentology and stratigraphy. New Jersey, Prentice Hall.

Bond, G.; Showers, W.; Cheseby, M.; Lotti, R.; Almasi, P.; deMenocal, P.; Priore, P.; Cullen, H.; Hajdas, I.; Bonani, G. 1997: A pervasive millenial-scale cycle in North Atlantic Holocene and Glacial climates. *Science 278:* 1257-1266.

Bowen, F. W. 1965: Early Pleistocene glacial and associated deposits of the West Coast of the South Island, New Zealand. *New Zealand Journal of Geology and Geophysics 10:* 164-181.

Bradley, R. S. 1999: Paleoclimatology - Reconstructing climates of the Quaternary. San Diego, Academic Press.

Brauer, A.; Endres, C.; Negendank, J. F. W. 1999: Lateglacial calendar year chronology based on annually laminated sediments from Lake Meerfelder Maar, Germany. *Quaternary International 61:* 17-25.

Broecker, W. S.; Peteet, D. M.; Rind, D. 1985: Does the ocean-atmosphere system have more than one stable mode of operation? *Nature 315:* 21-26.

Broecker, W. S.; Denton, G. H. 1990: The role of ocean-atmosphere reorganisations in glacial cycles. *Quaternary Science Reviews 9:* 305-341.

Broecker, W. S. 2000: Abrupt climate change: causal constraints provided by the paleoclimate record. *Earth-Science Reviews 51:* 137-154.

Broecker, W. S. 2002: The glacial world according to wally. New York, Eldigio Press.

Burrows, C. J. 1975: Late Pleistocene and Holocene moraines of the Cameron Valley, Arrowsmith Range, Canterbury, New Zealand. *Arctic and Alpine Research 7:* 125-140.

Burrows, C. J.; Russell, J. B. 1975: Moraines of the upper Rakaia Valley. *Journal of the Royal Society of New Zealand 5:* 463-477.

Carter, L.; Nelson, C. S.; Neil, H. L.; Froggatt, P. C. 1995: Correlation, dispersal, and preservation of the Kawakawa Tephra and other late Quaternary tephra layers in the Southwest Pacific Ocean. *New Zealand Journal of Geology and Geophysics 38:* 29-46.

Chambers, F. M.; Ogle, M. I.; Blackford, J. J. 1999: Palaeoenvironmental evidence for solar forcing of Holocene climate: linkages to solar science. *Progress in Physical Geography 23:* 181-204.

Clark, P. U.; Clague, J. J.; Curry, B. B.; Dreimanis, A.; Hicock, S. R.; Miller, G. H.; Berger, G. W.; Eyles, N.; Lamothe, M.; Miller, B. B.; Mott, R. J.; Oldale, R. N.; Stea, R. R.; Szabo, J. P.; Thorleifson, L. H.; Vincent, J. S. 1993: Initiation and development of the Laurentide and Cordilleran ice sheets following the last interglaciation. *Quaternary Science Reviews 12:* 79-114.

Clayton, L. 1968: Late Pleistocene glaciations of the Waiau valleys, North Canterbury. *New Zealand Journal of Geology and Geophysics 11:* 753-767.

Clemens, S. C. 1998: Dust response to seasonal atmospheric forcing: Proxy evaluation and calibration. *Paleoceanography 13:* 471-490.

Dearing, J. A. 1999: Magnetic Susceptibility. *In:* Walden, J.; Oldfield, F.; Smith, J. P. *eds.* Environmental magnetism: a practical guide. Quaternary Research Association, London. Pp. 35-62

Delmonte, B.; Basile-Doelsch, I.; Petit, J. R.; Maggi, V.; Revel-Rolland, M.; Michard, A.; Jagoutz, E.; Grousset, F. 2004: Comparing the Epica and Vostok dust records during the last 220,000 years: stratigraphical correlation and provenance in glacial periods. *Earth-Science Reviews 66:* 63-87.

Denton, G. H.; Hendy, C. H. 1994: Younger Dryas age advance of Franz Josef glacier in the Southern

Alps of New Zealand. *Science 264:* 1434-1437.

Denton, G. H.; Heusser, C. J.; Lowell, T. V.; Moreno, P. I.; Andersen, B. G.; Heusser, L. E.; Schluchter, C.; Marchant, D. R. 1999: Interhemispheric linkage of paleoclimate during the Last Glaciation. *Geografiska Annaler Series A 81A:* 107-154.

Denton, G. H. 2000: Does an asymmetric thermohaline-ice-sheet oscillator drive 100 000-yr glacial cycles? *Journal of Quaternary Science 15:* 301-318.

Eden, D. N. 1989: River terraces and their loessial cover beds, Awatere River valley, South Island, New Zealand. *New Zealand Journal of Geology and Geophysics 32:* 487-497.

Eden, D. N.; Froggatt, P. C.; McIntosh, P. D. 1992: The distribution and composition of volcanic glass in late Quaternary loess deposits of southern South Island, New Zealand, and some possible correlations. *New Zealand Journal of Geology and Geophysics 35:* 69-79.

Eden, D. N.; Hammond, A. P. 2003: Dust accumulation in the New Zealand region since the last glacial maximum. *Quaternary Science Reviews 22:* 2037-2052.

Emiliani, C. 1955: Pleistocene temperatures. *Journal of Geology 63:* 538-576.

EPICA community members 2004: Eight glacial cycles from an Antarctic ice core. *Nature 429:* 623-628.

Erdtman, G. 1969: Handbook of palynology. Copenhagen, Munksgaard.

Frakes, L. A.; Francis, J. E.; Syktus, J. I. 1992: Climate modes of the Phanerozoic. Cambridge, Cambridge University Press.

Froggatt, M. 1988: Paleomagnetism of Last Glacial loess from two sections in New Zealand. *In:* Eden, D. N.; Furkert, R. J. *eds.* LOESS: its distribution, geology and soils. Pp. 59-68

Froggatt, P. C.; Lowe, D. J. 1990: A review of late Quaternary silicic and some other tephra formations from New Zealand: their stratigraphy, nomenclature, distribution, volume, and age. *New Zealand Journal of Geology and Geophysics 33:* 89-109.

Gage, M. 1958: Late Pleistocene glaciations of the Waimakariri Valley, Canterbury, New Zealand. *New Zealand Journal of Geology and Geophysics 1:* 123-155.

Gage, M. 1985: Glaciation in New Zealand - The first century of research. *Quaternary Science Reviews 4:* 189-214.

Gair, H. S. 1967: Geological Map of New Zealand, Mount Cook, 1st Edition, Sheet 20, 1:250,000. Department of Scientific and Industrial Research, Wellington.

Gascoyne, M. 1992: Palaeoclimate determination from cave calcite deposits. *Quaternary Science Reviews 11:* 609-632.

Hays, J. D.; Imbrie, J.; Shackleton, N. J. 1976: Variations in the Earth's orbit: Pacemaker of the ice ages. *Science 194:* 1121-1132.

Hellstrom, J.; McCulloch, M.; Stone, J. 1998: A detailed 31,000-year record of climate and vegetation change, from the isotope geochemistry of two New Zealand speleothems. *Quaternary Research 50:* 167-178.

Hendy, C. H.; Wilson, A. T. 1968: Palaeoclimatic data from speleothems. *Nature 219:* 48-51.

Hesse, P. P.; McTainsh, G. H. 1999: Last Glacial Maximum to early Holocene wind strength in the mid-latitudes of the Southern Hemisphere from aeolian dust in the Tasman Sea. *Quaternary Research 52:* 343-349.

Hooker, B. L.; Fitzharris, B. B. 1999: The correlation between climatic parameters and the retreat and advance of Franz Josef Glacier, New Zealand. *Global and Planetary Change 22:* 39-48.

Horrocks, J. L. 2000: Stratigraphy, chronology, and correlation of the Plio-Pleistocene (c. 2.2-0.8 Ma) Kauroa Ash sequence, western central North Island, New Zealand. PhD thesis, University of Waikato, Hamilton.

Huggett, R. J. 1991: Air. *In:* Climate, Earth processes and Earth history. Springer-Verlag, Manchester. Pp. 13-48

Imbrie, J.; Imbrie, K. P. 1979: Ice ages - solving the mystery. Enslow Publishers.

Imbrie, J.; Boyle, E. A.; Clemens, S. C.; Duffy, A.; Howard, W. R.; Kukla, G.; Kutzbach, J.; Martinson, D. G.; McIntyre, A.; Mix, A. C.; Molfino, B.; Morley, J. J.; Peterson, L. C.; Pisias, N. G.; Prell, W. L.; Raymo, M. E.; Shackleton, N. J.; Toggweiler, J. R. 1992: On the structure and origin of major glaciation cycles - 1. Linear responses to Milankovitch forcing. *Paleoceanography 7:* 701-738.

Imbrie, J.; Berger, A.; Boyle, E. A.; Clemens, S. C.; Duffy, A.; Howard, W. R.; Kukla, G.; Kutzbach, J.; Martinson, D. G.; McIntyre, A.; Mix, A. C.; Molfino, B.; Morley, J. J.; Peterson, L. C.; Pisias, N. G.; Prell, W. L.; Raymo, M. E.; Shackleton, N. J.; Toggweiler, J. R. 1993: On the structure and origin of major glaciation cycles - 2. The 100,000-year cycle. *Paleoceanography 8:* 699-735.

Ivy-Ochs, S.; Schluchter, C.; Kubik, P. W.; Denton, G. H. 1999: Moraine exposure dates imply synchronous Younger Dryas glacier advances in the European Alps and in the Southern Alps of New Zealand. *Geografiska Annaler 81:* 313-323.

Johnsen, S. J.; Dansgaard, W.; Clausen, H. B.; Langway, C. C. 1972: Oxygen isotope profiles through the Antarctic and Greenland ice sheets. *Nature 235:* 429-434.

Kukla, G. 1987: Loess stratigraphy in central China. *Quaternary Science Reviews 6:* 191-219.

Kukla, G. J.; de Beaulieu, J.; Svobodova, H.; Andrieu-Ponel, V.; Thouveny, N.; Stockhausen, H. 2002: Tentative Correlation of Pollen Records of the Last Interglacial at Grande Pile and Ribains with Marine Isotope Stages. *Quaternary Research 58:* 32-35.

Kukla, G. J.; Gavin, J. 2004: Milankovitch climate reinforcements. *Global and Planetary Change 40:* 27-48.

Litchfield, N. J.; Berryman, K. R. 2005: Correlation of fluvial terraces within the Hikurangi Margin, New Zealand: implications for climate and baselevel controls. *Geomorphology 68:* 291.

Litchfield, N. J.; Rieser, U. 2005: Optically stimulated luminescence age constraints for fluvial aggradation terraces and loess in the eastern North Island, New Zealand. *New Zealand Journal of Geology and Geophysics 48:* 581-589.

Lowe, D. J.; Newnham, R. M.; Ward, C. M. 1999: Stratigraphy and chronology of a 15 ka sequence of multi-sourced silicic tephras in a montane peat bog, eastern North Island, New Zealand. *New Zealand Journal of Geology and Geophysics 42:* 565-579.

Lowe, J. J.; Walker, M. J. C. 1997: Reconstructing Quaternary Environments. Essex, Longman.

Lowell, T. V.; Heusser, C. J.; Andersen, B. G.; Moreno, P. I.; Hauser, A.; Heusser, L. E.; Schluchter, C.; Marchant, D. R.; Denton, G. H. 1995: Interhemispheric correlation of late Pleistocene glacial

events. *Science 269:* 1541-1549.

Manning, M. R. 1990: The troposphere and greenhouses gases. *In:* New Zealand Climate Report 1990. Royal Society of New Zealand, Wellington. Pp. 25-28

Manville, V.; Wilson, C. J. N. 2004: The 26.5 ka Oruanui eruption, New Zealand: a review of the roles of volcanism and climate in the post-eruptive sedimentary response. *New Zealand Journal of Geology and Geophysics 47:* 525-547.

Marx, S. K.; Kamber, B. S.; McGowan, H. A. 2005: Estimates of Australian dust flux into New Zealand: Quantifying the eastern Australian dust plume pathway using tracer element calibrated 210Pb as a monitor. *Earth and Planetary Science Letters 239:* 336-351.

Marx, S. K.; McGowan, H. A. 2005: Dust transportation and deposition in a superhumid environment, West Coast, South Island, New Zealand. *CATENA 59:* 147-171.

McGlone, M. S.; Turney, C. S. M.; Wilmshurst, J. M. 2004: Late-glacial and Holocene vegetation and climatic history of the Cass Basin, central South Island, New Zealand. *Quaternary Research 62:* 267-279.

McGowan, H. A.; McTainsh, G. H.; Zawar-Reza, P.; Sturman, A. 2000: Identifying regional dust transport pathways: Application of kinematic trajectory modelling to a trans-Tasman case. *Earth Science Processes and Landforms 25:* 633-647.

Mercer, J. H. 1988: The age of the Waiho Loop terminal moraine, Franz Josef Glacier, Westland. *New Zealand Journal of Geology and Geophysics 31:* 95-99.

Mew, G.; Hunt, J. L.; Froggatt, P. C.; Eden, D. N.; Jackson, R. J. 1986: An occurrence of Kawakawa Tephra from the Grey River valley, South Island, New Zealand. *New Zealand Journal of Geology and Geophysics 29:* 315-322.

Mew, G.; Thomas, R. F.; Eden, D. N. 1988: Stratigraphy of loessic cover beds at The Lamplough, West Coast, South Island, New Zealand. *Journal of the Royal Society of New Zealand 18:* 325-332.

Moar, N. T.; Suggate, R. P. 1996: Vegetation history from the Kaihinu (Last) interglacial to the present, West Coast, South Island, New Zealand. *Quaternary Science Reviews 15:* 521-547.

Mottana, A.; Crespi, R.; Liborio, G. 1978: Guide to Rocks and Minerals. New York, Simon & Schuster.

Naish, T. R.; Field, B. D.; Zhu, H.; Melhuish, A.; Carter, R. M.; Abbott, S. T.; Edwards, S.; Alloway, B. V.; Wilson, G. S.; Niessen, F.; Barker, A.; Browne, G. H.; Maslen, G. 2005: Integrated outcrop, drill core, borehole and seismic stratigraphic architecture of a cyclothemic, shallow-marine depositional system, Wanganui Basin, New Zealand. *Journal of the Royal Society of New Zealand 35:* 91–122.

Nelson, C. S.; Hendy, C. H.; Jarrett, G. R.; Cuthbertson, A. M. 1985: Near-synchroneity of New Zealand alpine glaciations and Northern Hemisphere continental glaciations during the past 750 kyr. *Nature 318:* 361-363.

Newnham, R. 1999: Temperature changes during the Younger Dryas in New Zealand. *Science 283:* 759.

Newnham, R.; Vandergoes, M.; Garnett, M.; Lowe, D.; Prior, C. 2005: Test of AMS 14C dating of pollen concentrates using tephrochronology. *Journal of Quaternary Science, Draft*

Newnham, R.; Vandergoes, M.; Garnett, M.; Lowe, D.; Prior, C. 2006: Test of AMS 14C dating of pollen concentrates using tephrochronology. *Journal of Quaternary Science (In Press)*

Newnham, R. M.; Lowe, D. J.; Williams, P. W. 1999: Quaternary environmental change in New Zealand: a review. *Progress in Physical Geography 23:* 567-610.

Newnham, R. M.; Lowe, D. J. 2000: Fine-resolution pollen record of late-glacial climate reversal from New Zealand. *Geology 28:* 759-762.

Palmer, A. S.; Vucetich, C. G. 1989: Last glacial loess and early last glacial vegetation history of Wairarapa Valley, New Zealand. *New Zealand Journal of Geology and Geophysics 32:* 499-513.

Palmer, A. S.; Pillans, B. J. 1996: Record of climatic fluctuations from ca. 500 ka loess deposits and paleosols near Wanganui, New Zealand. *Quaternary International 34-36:* 155.

Pillans, B.; McGlone, M.; Palmer, A.; Mildenhall, D.; Alloway, B.; Berger, G. 1993: The last glacial maximum in central and southern North Island, New Zealand: a paleoenvironmental reconstruction using the Kawakawa Tephra Formation as a chronostratigraphic marker. *Palaeogeography, Palaeoclimatology, Palaeoecology 101:* 283-304.

Preusser, F.; Andersen, B. G.; Denton, G. H.; Schlüchter, C. 2005: Luminescence chronology of Late Pleistocene glacial deposits in North Westland, New Zealand. *Quaternary Science Reviews 24:* 2207-2227.

Pye, K. 1987: Aeolian dust and dust deposits. London, Academic Press.

Ruddiman, W. F. 2003: Oribital insolation, ice volume, and greenhouse gases. *Quaternary Science Reviews 22:* 1597-1629.

Salinger, J. 2001: Climate variations in New Zealand and the Southwest Pacific. *In:* Sturman, A.; Spronken-Smith, R. *eds.* The physical environment: A New Zealand perspective. Pp. 131-149

Sandiford, A.; Newnham, R.; Alloway, B.; Ogden, J. 2003: A 28 000 - 7 600 cal yr BP pollen record of vegetation and climate change from Pukaki Crater, northern New Zealand. *Palaeogeography, Palaeoclimatology, Palaeoecology 201:* 235-247.

Schmittner, A.; Saenko, O. A.; Weaver, A. J. 2003: Coupling of the hemispheres in observations and simulations of glacial climate change. *Quaternary Science Reviews 22:* 659-671.

Shackleton, N. J. 1967: Oxygen isotope analysis and pleistocene temperatures reassessed. *Nature 215:* 15-17.

Shackleton, N. J.; Opdyke, N. D. 1973: Oxygen isotope and palaeomagnetic stratigraphy of Equatorial Pacific Core V28-238: Oxygen isotope temperatures and ice volumes on a 10^5year and 10^6 year scale. *Quaternary Research 3:* 39-55.

Shackleton, N. J. 1987: Oxygen isotopes, ice volume and sea level. *Quaternary Science Reviews 6:* 183-190.

Shane, P. 2000: Tephrochronology: a New Zealand case study. *Earth-Science Reviews 49:* 223-259.

Shane, P.; Lian, O. B.; Augustinus, P.; Chisari, R.; Heijnis, H. 2002: Tephrostratigraphy and geochronology of a ca. 120 ka terrestrial record at Lake Poukawa, North Island, New Zealand. *Global and Planetary Change 33:* 221-242.

Singer, C.; Shulmeister, J.; McLea, B. 1998: Evidence against a significant Younger Dryas cooling event in New Zealand. *Science 281:* 812-814.

Soons, J. M. 1963: The glacial sequence in part of the Rakaia Valley, Canterbury, New Zealand. *New Zealand Journal of Geology and Geophysics 6:* 735-756.

Soons, J. M.; Moar, N. T.; Shulmeister, J.; Wilson, H. D.; Carter, J. A. 2002: Quaternary vegetation and climate changes on Banks Peninsula, South Island, New Zealand. *Global and Planetary Change 33:* 301-314.

Stokes, S.; Lowe, D. J.; Froggatt, P. C. 1992: Discriminant function analysis and correlation of late Quaternary rhyolitic tephra deposits from Taupo and Okatina volcanoes, New Zealand, using glass shard major element composition. *Quaternary International 13/14:* 103-117.

Stuiver, M.; Reimer, P. J.; Bard, E.; Beck, J. W.; Burr, G. S.; Hughen, K. A.; Kromer, B.; McCormac, G.; Van der Plicht, J.; Spurk, M. 1998: INTCAL98 radiocarbon age calibration, 24,000-0 cal BP. *Radiocarbon 40:* 1041-1083.

Sugden, D. E.; Bentley, M. J.; Fogwill, C. J.; Hulton, N. R. J.; McCulloch, R. D.; Purves, R. S. 2005: Late-glacial glacier events in southernmost South America: A blend of 'northern' and 'southern' hemispheric climatic signals? *Geografiska Annaler Series a-Physical Geography 87A:* 273-288.

Suggate, R. P. 1965: Late Pleistocene geology of the northern part of the South Island, New Zealand. *New Zealand Geological Survey Bulletin 77*

Suggate, R. P. 1985: The glacial/interglacial sequence of North Westland, New Zealand. *New Zealand Geological Survey Record*

Suggate, R. P. 1990: Late Pliocene and Quaternary glaciations of New Zealand. *Quaternary Science Reviews 9:* 175-197.

Suggate, R. P.; Almond, P. C. 2005: The Last Glacial Maximum (LGM) in western South Island, New Zealand: implications for the global LGM and MIS 2. *Quaternary Science Reviews 24:* 1923-1940.

Taylor, K. C.; Lamorey, G. W.; Doyle, G. A.; Alley, R. B.; Grootes, P. M.; Mayewski, P. A.; White, J. W. C.; Barlow, L. K. 1993: The 'flickering swicth' of late Pleistocene climate change. *Nature 361:* 432-436.

Turney, C.; Baillie, M.; Clemens, S.; Brown, D.; Palmer, J.; Pilcher, J.; Reimer, P.; Leuschner, H. H. 2005: Testing solar forcing of pervasive Holocene climate cycles. *Journal of Quaternary Science 20:* 511-518.

Turney, C. S. M. 1998: Extraction of rhyolitic component of Vedde microtephra from minerogenic lake sediments. *Journal of Paleolimnology 19:* 199-206.

Turney, C. S. M.; McGlone, M. S.; Wilmshurst, J. M. 2003: Asynchronous climate change between New Zealand and the North Atlantic during the last deglaciation. *Geology 31:* 223-226.

Tzedakis, C. 2003: Timing and duration of Last Interglacial conditions in Europe: a chronicle of a changing chronology. *Quaternary Science Reviews 22:* 763-768.

Urey, H. C. 1947: The thermodynamic properties of isotopic substances. *Journal of the Chemical Society:* 562-581.

Vandergoes, M. J. 2000: A high resolution record of late Quaternary vegetation and climate change, south Westland, New Zealand. PhD thesis, University of Otago, Dunedin.

Vandergoes, M. J.; Fitzsimons, S. J. 2003: The Last Glacial-Interglacial transions (LGIT) in south Westland, New Zealand: paleoecological insight into mid-latitude Southern Hemisphere climate change. *Quaternary Science Reviews 22:* 1461-1476.

Vandergoes, M. J.; Prior, C. A. 2003: Ams dating of pollen concentrates-a methodological study of late

quaternary sediments from south westland, New Zealand. *Radiocarbon 45:* 479-491.

Vandergoes, M. J.; Newnham, R. M.; Preusser, F.; Hendy, C. H.; Lowell, T. V.; Fitzsimons, S. J.; Hogg, A. G.; Kasper, H. U.; Schlüchter, C. 2005: Regional insolation forcing of late Quaternary climate change in the Southern Hemisphere. *Nature 436:* 242-245.

Veevers, J. J. 1990: Tectonic-climatic supercycle in the billion-year plate-tectonic eon: Permian Pangean icehouse alternatives with Cretaceous dispersed-continents greenhouse. *Sedimentary Geology 68:* 1-16.

Walker, M. 1995: Climatic changes in Europe during the Last Glacial/Interglacial Transition. *Quaternary International 28:* 63-76.

Walker, M. 2005: Quaternary dating methods. Chichester, Wiley.

Warren, G. 1967: Geological Map of New Zealand, Hokitika, 1st Edition, Sheet 17, 1:250,000. Department of Scientific and Industrial Research, Wellington.

Williams, P. W. 1996: A 230 ka record of glacial and interglacial events from Aurora Cave, Fiordland, New Zealand. *New Zealand Journal of Geology and Geophysics 39:* 225-241.

Williams, P. W.; King, D. N. T.; Zhao, J. X.; Collerson, K. D. 2004: Speleothem master chronologies: combined Holocene O-18 and C-13 records from the North Island of New Zealand and their palaeoenvironmental interpretation. *Holocene 14:* 194-208.

Williams, P. W.; King, D. N. T.; Zhao, J. X.; Collerson, K. D. 2005: Late Pleistocene to Holocene composite speleothem O-18 and C-13 chronologies from South Island, New Zealand - Did a global Younger Dryas really exist? *Earth and Planetary Science Letters 230:* 301-317.

Wilson, C. J. N.; Switsur, V. R.; Ward, A. P. 1988: A new 14C age for the Oruanui (Wairakei) eruption, New Zealand. *Geological Magazine 125:* 297-300.

Wilson, C. J. N. 2001: The 26.5 ka Oruanui eruption, New Zealand: an introduction and overview. *Journal of Volcanology and Geothermal Research 112:* 133-174.

Wunsch, C. 2003: Greenland-Antarctica phase relations and millennial time-scale climate fluctuations in the Greenland ice-cores. *Quaternary Science Reviews 22:* 1631-1646.

Wunsch, C. 2006: Abrupt climate change: An alternative view. *Quaternary Research (In Press)*

Xiao, J. L.; An, Z. S.; Liu, T. S.; Inouchi, Y.; Kumai, H.; Yoshikawa, S.; Kondo, Y. 1999: East Asian monsoon variation during the last 130,000 Years: evidence from the Loess Plateau of central China and Lake Biwa of Japan. *Quaternary Science Reviews 18:* 147.

Young, D. J. 1964: Stratigraphy and petrolography of north-east Otago loess. *New Zealand Journal of Geology and Geophysics 7:* 839-863.

Young, D. J. 1967: Loess deposits of the West Coast of the South Island, New Zealand. *New Zealand Journal of Geology and Geophysics 10:* 647-658.

Zachos, J.; Pagani, M.; Sloan, L.; Thomas, E.; Billups, K. 2001: Trends, rhythms, and aberrations in global climate 65 Ma to present. *Science 292:* 687-693.

Zubakov, V. A.; Borzenkova, I. I. 1990: Global palaeoclimate of the late Cenezoic. Amsterdam, Elsevier Science Publishers B.V.